Mesure de l'acidité des matériaux par l'approche des molécules sondes en RMN solide

Auteur : Scholzen, Pascal
Promoteur(s) : Job, Nathalie
Faculté : Faculté des Sciences appliquées
Diplôme : Master en ingénieur civil en chimie et science des matériaux, à finalité spécialisée
Année académique : 2017-2018
URI/URL : http://hdl.handle.net/2268.2/4550

UNIVERSITY OF LIEGE

FACULTY OF APPLIED SCIENCE

TOTAL Research & Technology Feluy

Probe molecule acidity measurements of Y zeolites by ^{31}P solid state NMR

SCHOLZEN Pascal

Thesis presented for obtaining the Master's degree in

Chemical and Materials engineering

Supervisors:

ANDREEV Andrey (TRTF)

JOB Nathalie (ULiège)

Academic year 2017-2018

Acknowledgements

First of all, I would like to express my gratitude to Mr. Andrey Andreev, my mentor and supervisor, who devoted a lot of his time to my thesis, provided me with support and information during the internship and was always open to my questions and discussions.

Special thanks go to Mr. Vincent Livadaris for giving me the possibility to do my internship in his team at Feluy.

I am also grateful to Mrs. Nathalie Job for having accepted to be my academic supervisor and her help during my thesis and its organization.

Furthermore, I would like to thank Mrs. Nancy Verkest for her guidance during the preparation and NMR analysis of the samples and to Mrs. Isabella Perotti for having carried out the ICP analysis on my samples.

Thanks to Mr. Charles Guarin, Mrs. Anne Massinon and Mr. Philippe Schouppe for performing the outgassing of the zeolites to be analyzed for me.

I am also grateful to Mr. Florian Faucher for the discussions about my results and sharing his experiences with me, and to Mr. Christophe Cucuzzella for his advice during my internship.

I wish to thank Mr. Frederik Thelen for proofreading my written work.

And last but by no means least I would like to seize the opportunity to thank the entire team of the analytical department at the Total Research and Technology center at Feluy. They have given me always good advice and made sure I had a good time during my internship.

Résumé

L'utilisation de la RMN solide du noyau ^{31}P des molécules sondes d'oxides de trialkylphosphine (R$_3$PO) par rotation à l'angle magique (MAS) de 15 kHz est une approche simple et sûre pour la caractérisation des sites acides de Brønsted des ponts SiOHAl dans les zéolites Y ultra-stables (USY), nécessaires à la catalyse des procédés d'hydrocraquage. Cette technique permet de différencier les sites de Brønsted de ceux de Lewis, de détecter leur localisation à l'aide des sondes de taille différentes, d'identifier leurs forces en fonction du déplacement chimique dans le spectre et de déterminer la concentration de chaque site. Les différentes zéolites USY à analyser sont obtenues par un traitement de désalumination plus ou moins sévère et le rapport Si /Al devient 6 (CBV712), 15 (CBV720) et 30 (CBV760), alors que la structure microporeuse n'est pas altérée. Avec le TMPO, le TEPO et le TBPO, on utilise trois molécules de sonde ayant des températures de fusion et d'évaporation, une basicité et surtout une taille différente. TMPO et TEPO distinguent 4 sites d'acide de Brønsted différents, alors que seulement 2 sont reconnus lors de l'analyse avec le TBPO, parce qu'il est considéré de ne pas pénétrer dans les supercages de la microstructure. Pour les zéolithes les plus fortement désaluminées, une concentration en site acide plus faible est mesurée. A l'exception du CBV712 à très faible mésoporosité, le TBPO détecte le plus de sites acides, taille, grâce à une forte basicité, malgré sa grande taille. Les forces mesurées des sites acides varient de faible à relativement forte, mais aucune différence significative entre les zéolithes n'est détectée.

Abstract

The use of solid state (SS) 15 kHz Magic Angle Spinning (MAS) NMR of the ^{31}P nucleus of trialkylphosphine oxides (R_3PO) probe molecules is an easy and safe approach for the characterization of the SiOHAl - bridge Brønsted acid sites of ultra-stable Y (USY) zeolites, necessary for the catalysis of hydrocracking processes. This technique is able to differentiate the Brønsted acid sites from Lewis acid sites, to detect their location using probes of a different size, to identify their strengths based on the chemical shift in the spectrum and to determine the concentration of each acid site. The different USY zeolites to be analyzed are obtained by a more or less severe dealumination treatment and the Si/Al ratio becomes 6 (CBV712), 15 (CBV720) and 30 (CBV760), whereas the microporous structure is not altered. With TMPO, TEPO and TBPO, three probe molecules with various fusion and evaporation temperature, a different basicity and especially a distinct size are used, all found out to have their advantages and disadvantages. TMPO and TEPO distinguish 4 different Brønsted acid sites, while only 2 are recognized during the analysis with TBPO, because it is considered not to enter the supercages in the microstructure. For more strongly dealuminated zeolites, a lower acid site concentration is measured and except for CBV712 with a very low mesoporosity, TBPO detects the most acid sites, despite its big size, due to a strong basicity and probing of the sites from outside the pores. Acid site strength from weak to relatively strong are measured, but no significant difference in between the zeolites is detected.

Contents

1   Introduction

Nowadays, there is a mismatch between the offer and demand of the parts of crude oil. In fact, the untreated crude oil contains too many heavy and too few light parts, such as naphtha, natural gas, diesel and kerosene. Therefore, a simple distillation is not sufficient and a big part of the distillate would not be used. A solution for this problem is a catalytic process, called *Hydrocracking*. During the hydrocracking process, acidic catalysts are used in order to attack long and heavy carbon chains and to split them up into smaller and lighter parts. During this process, double bonds occur in the smaller chains, which are eliminated by reaction with hydrogen. For this kind of process, zeolites are the perfect catalysts. Firstly, they possess strong acid sites and are therefore able to crack the long chains efficiently. Secondly, their high porosity and specific surface area is the reason for a good transportation of the different reactants and products and the presence of many acid sites inside the zeolite. Last but not least, the thermal stability of the zeolites is also a crucial property, because the cracking reactions occur at high temperatures.

In order to evaluate the performance of a zeolite as hydrocracking catalyst, the determination and characterization of its acid sites is crucial. Different properties are important: the acidity type, the strength, the location and the concentration of an acid site and various methods are used in laboratories and industries to characterize these properties. In this work, an approach using ^{31}P 15 kHz Magic Angle Spinning Solid State Nuclear Magnetic Resonance spectroscopy of trialkylphosphine probe molecules, is presented.

The aim of this work is to test this method on ultra-stable Y zeolites impregnated with different trialkylphosphine probes using a solid route. The influence of the choice of probe molecule and other parameters of the sample preparation on the results are analyzed. Peak models for the analysis of the different zeolites as function of the probe are established and the results of the acid site properties, detected by the probes, are presented.

2 Introduction to solid state Nuclear Magnetic Resonance (NMR) spectroscopy

In this section, an introduction to the principles of Nuclear Magnetic Resonance (NMR) spectroscopy is given and more precisely with regards to Magic Angle Spinning (MAS) Solid State NMR (SSNMR). Furthermore, explanations about the common experiments that have been performed during this work is provided.

The key principle of NMR is to excite the nuclear spins of a given element in presence of a strong external magnetic field by modulated radiofrequency (rf) pulses. The response to the excitation of the spins happens at a resonance frequency, which can be slightly shifted according to the environment the nucleus (physical proximity and chemical bonds to other atoms). There are two main NMR applications, i.e. liquid state NMR and solid state NMR. The main difference between those two is that SSNMR deals with strong dipolar interaction between the different nuclei in solids that does not exist in liquids due to molecular motions. Nevertheless, the basic principles are same in both cases.

2.1 Basic principles of NMR

First of all, it is important to note that in NMR theory; the nuclei are classified depending on the nuclear spin quantum number (I) of the nucleus. The simplest case are dipolar spin nuclei, which have an I equal to ½. The theory and the experiments become more complicated for nuclei with quadrupolar spins that have the I greater than ½. As shown in **Figure 1**, there are two different energy levels that the spins can occupy in dipolar nucleus, denoted -½ and ½. Therefore, only one transition in between with a specific energy can occur. In case of a quadrupolar nucleus, there are several different spin energy levels and therefore various transitions exist in between them. As a result, the analysis of those nuclei is more complicated than and not as straightforward as the dipolar ones. For reasons of simplicity and due to the fact that all nuclei analyzed in this work are dipolar, only theory of this kind of nuclei is presented hereinafter. If the nuclei are close to each other inside the bond network, their interaction can cause the appearance of smaller peaks at a certain distance to the main peak, called *J-coupling*. These effects are neglected in the following explications as they are only important when dipolar nuclei are directly bonded, which is not the case in the current studies [1].
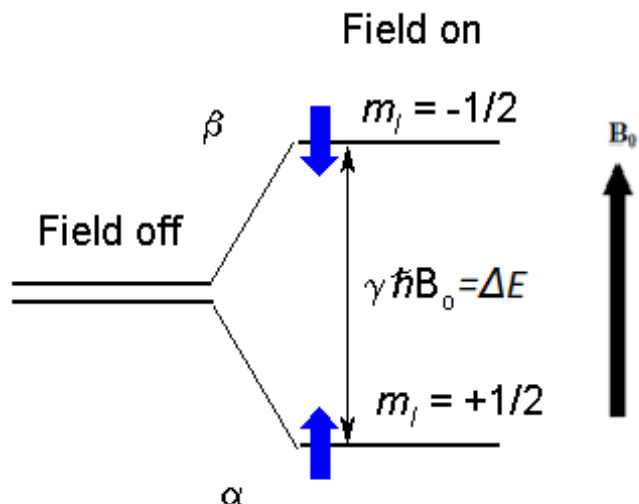
Figure 1. The different energy levels of the spins in a dipolar nucleus (adapted from [2])

2.1.1 Introduction to the quantum mechanics approach of the NMR

A simple way of understanding the NMR principles is the energy level approach. This approach is very similar to the one of other spectroscopic techniques, such as the infrared spectroscopy. For the definition of different energy levels of the nuclear spins, an introduction to the basic principles of quantum mechanics is necessary. A short introduction into SSNMR theory is done hereinafter [1].

One important feature of quantum mechanics is that observable quantities are always represented by operators. Like in mathematics, an operator is something that acts on a function in order to produce a new function, like the sinus operator or the derivative operator. Operators have been introduced by their property of transforming a certain function into another function when applied to them. However, there are some functions that do not change when certain operators are applied to them. One example is the derivative operator acting on the exponential function, as shown in equation (1). As one can see, the exponential function remains the same, except from the multiplication by the constant A. The exponential function $\exp(Ax)$ is therefore called *eigenfunction* of the derivative operator, with the constant A as its *eigenvalue*. Those principles are very important, because if one measures the value of a certain observable quantity, the result always equals one of the eigenvalues of the operator, representing this observable quantity. Therefore, the energy level of a system is necessarily equal to one eigenvalue of the operator representing the energy, with the wave function, associated to the system, as eigenfunction [1].

$$\frac{d}{dx}\exp(Ax) = A * \exp(Ax) \qquad (1)$$

One of the most important operators in quantum mechanics is the one representing an observable energy quantity, called *Hamiltonian* (H or $\widehat{H}$). Different kinds of $\widehat{H}$ are defined, as function of the system that is observed. Their construction is quite complicated and not really necessary to perform in this case. It is thus just accepted that for a nuclear spin inside a magnetic field oriented in z direction, $\widehat{H}$ represents the interaction energy between the spin and the magnetic field, given by:

$$\widehat{H}_{spin} = -\gamma B_0 \widehat{I}_z \qquad (2),$$

with γ the *gyromagnetic ratio*, the ratio of the magnetic moment to the angular momentum of a particle and a fundamental intrinsinc property of a nucleus [3]. $\widehat{I}_z$ is an operator that represents the z component of the angular momentum of a nuclear spin. Some nuclei possess an intrinsinc source of angular momentum, called the nuclear spin angular momentum, and it is its z component that interacts with the magnetic field [1].

The number of eigenfunctions and eigenvalues of $\widehat{I}_z$ is dependant on the spin quantum number I. I can be an integer or a half-integer, and there are (2*I* + 1) eigenvalues and eigenfunctions for $\widehat{I}_z$. As cited in the beginning of this chapter, this report focuses on the case of nuclei with dipolar spins, I= ½ . Each eigenfunction is represented by the quantum number *m*, -½ and ½ in the case of a dipolar nucleus. The two eigenfunctions are denoted $\psi_{+\frac{1}{2}}$ and $\psi_{-\frac{1}{2}}$ and the respective eigenvalue equations are:

$$\widehat{I}_z \, \psi_{+\frac{1}{2}} = +\frac{1}{2}\bar{h} \, \psi_{+\frac{1}{2}} \quad \text{and} \quad \widehat{I}_z \, \psi_{-\frac{1}{2}} = -\frac{1}{2}\bar{h} \, \psi_{-\frac{1}{2}} \qquad (3),$$

with $\bar{h} = h/2\pi$, h: Planck's constant. It can be deduced that the eigenvalue of the eigenfunction ψ_m is $m\bar{h}$ [1].

Due to the fact that the only difference between $\widehat{I}_z$ and $\widehat{H}_{spin}$ is a multiplication by $-\gamma B_0$, the two ψ_m are also the eigenfunctions of $\widehat{H}_{spin}$. The eigenvalues of $\widehat{H}_{spin}$ are therefore the eigenvalues of $\widehat{I}_z$ multiplied by $-\gamma B_0$:

$$-\frac{1}{2}\bar{h}\gamma B_0 \text{ for } \psi_{+\frac{1}{2}} \qquad \text{and} \qquad +\frac{1}{2}\bar{h}\gamma B_0 \text{ for } \psi_{-\frac{1}{2}}. \qquad (4)$$

Those two eigenvalues represent the two possible energy levels E_m in the case of a dipolar spin nucleus in a magnetic field B_0, also represented in **Figure 1** [2].

For practical reasons, in case of a dipolar nucleus, the energy level that corresponds to m = ½ is defined as α and the one that corresponds to m= -½ as β. As shown in **Figure 1**, α often corresponds to the lowest energy level. This corresponds to the case of a positive γ, like it is for most nuclei, for ^{1}H and ^{31}P, for example. In quantum mechanics, only transitions where m changes of +1 or -1 are permitted (single quantum excitation), so both transitions, $\alpha \to \beta$ and $\beta \to \alpha$, are possible. The transition energy of those transitions is the following:

$$\Delta E_{\alpha \to \beta} = E_\beta - E_\alpha = \frac{1}{2} \, \overline{h} \gamma B_0 - \left(-\frac{1}{2} \, \overline{h} \gamma B_0 \right)$$

$$= \overline{h} \gamma B_0$$

$$= \left(\frac{h}{2\pi} \right) \gamma B_0 = -\Delta E_{\beta \to \alpha} \qquad (5)$$

For the spectral analysis, this energy transition is transformed into a frequency. The energy of a photon of frequency ν is given by $h\nu$, therefore the transition frequency $\nu_{\alpha \to \beta}$ is given by:

$$\nu_{\alpha \to \beta} = \frac{\Delta E_{\alpha \to \beta}}{h} = \gamma B_0 / 2\pi \qquad (6)$$

The result is the appearance of a single spectral line at the frequency $\gamma B_0 / 2\pi$ [1].

Based on the previous calculations and demonstrations, for a spin in a magnetic field one defines the so-called *Larmor frequency*:

$$\omega_0 = -\gamma B_0 \; in \; \left[\frac{rad}{s} \right] \qquad or \qquad \nu_0 = -\frac{\gamma B_0}{2\pi} \; in \; [Hz] \qquad (7)$$

As one can see, the frequency is the opposite of the $\nu_{\alpha \to \beta}$ transition frequency and is proportional to the strength of the magnetic field B_0 and to γ. For that reason, the spectral line of a nucleus should be found at the opposite value of the Larmor frequency. For nuclei of the same isotope that are situated in a different chemical environment, spectral lines at a slightly different frequency can be found. This can be explained by a different value for γ for the different nuclei. A simple way to express this variation is the use of the chemical shift δ:

$$\omega_0 = -\gamma(1 + 10^{-6} * \delta) B_0 \qquad or \qquad \nu_0 = -\gamma(1 + 10^{-6} * \delta) B_0 / 2\pi \qquad (8)$$

In practice, the Larmor frequency of a reference nucleus is found experimentally and assigned to a chemical shift $\delta = 0$. The Larmor frequency/ the chemical shifts of the other components are detected with respect to this reference nucleus. The chemical shift δ has been introduced due to the fact that the Larmor frequency of a nucleus depends on the magnetic field strength B_0 of the NMR device. In order to have comparable results from one NMR device to another, this dependency should be eliminated. Aside from the detected frequency, a reference frequency ν_{ref} is needed for every nucleus and the chemical shift is given by:

$$\delta(ppm) = 10^6 * \frac{\nu - \nu_{ref}}{\nu_{ref}} \qquad (9)$$

In theory, the choice of this reference frequency is arbitrary, but there is an international agreement on what reference molecule is to be used for what kind of nucleus, in order to have the same origin for everyone and to therefore have comparable results [1]. An example for the definition of reference frequencies is given by the IUPAC recommendation [4]. In this case, the reference frequency

of the proton is found due to the ^{1}H analysis on the tetramethylsilan (TMS). The reference frequencies of the other nuclei are calculated based on this result.

In this section, the basic principles of the energy levels in case of NMR have been explained. This has been used in order to predict the spectral line of a single spin in the simplest case. This method can also be used to predict the spectral lines of more complicated cases, such as coupled spins, where the explanations can be found in [1]. More information about NMR mechanisms is given in the next part of this report.

2.1.2   The vector model (Bloch model)

A very useful and simple way of understanding the principles of NMR experiments is by means of the vector model. In order to understand the mechanisms occurring during the experiments, the use of quantum mechanics is necessary. Thanks to the vector model, details of the quantum mechanics will not have to be provided. The downside of this model is that it cannot be applied to coupled spins. However, it is still sufficient in order to understand the basic experiments and even more complicated ones such as the spin-echo experiment [1].

As cited in the previous section, there are some nuclei that possess an internal angular moment due to its spins. Associated to an angular momentum, there is always a magnetic moment that can be aligned in any direction. The representation of the spins in **Figure 1**, with only two possible states α and β is therefore too simplistic and the spin can, in reality, be described as a combination of those states. Without the presence of an external magnetic field, the orientation of the magnetic moment is totally random. In case of an NMR experiment, a very large number of nuclei is analyzed and their small magnetic fields will cancel one and another out and no net effect can be observed, as shown in **Figure 2 a)** [1].
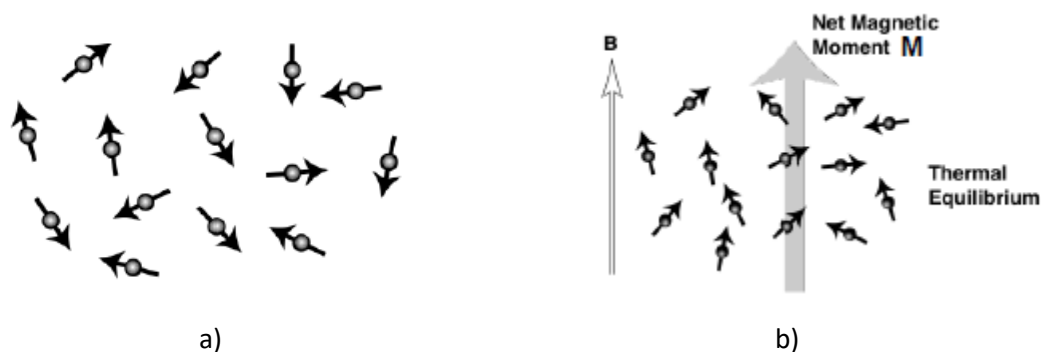

a)   b)

Figure 2. Bulk magnetization of a great number of nuclei a) in the case of no external magnetic field and b) in the case of an existing strong external magnetic field (taken from [5])

Now, when a strong external magnetic field is applied to the sample, the individual magnetic moments of the nuclei start interacting with this field as function of the angle between the moment and the field. As shown in **Figure 1**, a magnetic moment parallel to the magnetic field corresponds to the lowest energy level and therefore the most probable situation, whereas an anti-parallel magnetic moment corresponds to the highest energy level and the less probable situation. As shown in **Figure 2 b)**, the magnetic moments are still oriented quite randomly due to the thermal movement, but there is a little energetic advantage of being oriented parallel to the magnetic field. If the contributions of the magnetic moments are all added up, there is a net magnetic field alongside the direction of the external field B, but alongside the directions perpendicular to B, they still cancel one and another out. The created net magnetic moment is called *bulk magnetization* of the sample, represented by so-called *magnetization vector*. This equilibrium magnetization is not reached instantly. When the sample has just been placed into a magnetic field or when the magnetization vector is shifted from its equilibrium orientation, it takes some time until the bulk magnetization reaches its equilibrium intensity along the z-axis. This process is called relaxation and its duration depends on the nucleus, often up to several seconds. It is characterized by the time constant T_1, called *longitudinal relaxation time* [1].
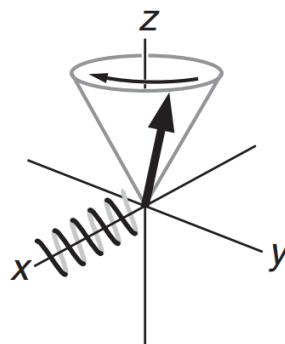
Figure 3: Precession of the magnetization vector around the external magnetic field for a nucleus with a positive γ, when tilted from its equilibrium position. Alongside the x-axis a schema of the detection coil is represented (taken from [1]).

If one supposes the external magnetic field to be along the z axis, then the equilibrium bulk magnetization is oriented in the z-direction, too. If now one manages to tilt the magnetization vector away from its equilibrium position, it starts rotating around the direction of the magnetic field with a constant angle, as shown in **Figure 3**. This happens due to the fact that the energy of interaction between the magnetic moments of the nuclei and the external magnetic field is only dependent on the angle between them and therefore also the energy of the system. On the other hand, the interaction energy does not

depend on the orientation of the magnetization vector in the x-y plane. This movement is named *precession* and happens at the Larmor frequency of the nucleus, defined in the previous section:

$$\omega_0 = -\gamma B_0 \ in \ \left[\frac{rad}{s}\right] \qquad or \qquad \nu_0 = -\frac{\gamma B_0}{2\pi} \ in \ [Hz] \qquad\qquad (10).$$

In the case of an NMR analysis, the movement is therefore called *Larmor precession*. The Larmor frequency has a negative sign in case of a positive γ and the precession is thus in the direction as shown in **Figure 3** [1].

It is the Larmor precession that is actually detected during the NMR experiment and it is its precession frequency, which is characteristic for the nucleus to be analyzed, its Larmor frequency. The precession is detected thanks to a small coil of wire around the sample, situated in the x-y plane, along the x-axis like in **Figure 3** for example. Every time the magnetization vector "cuts" the coil, a current is induced, which can be amplified and recorded afterwards. For a coil along the x-axis, the x component of the magnetization is measured, which gives an oscillating *free induction decay* (FID) signal. As represented in **Figure 4**, its intensity depends on the angle θ between the magnetization vector and the external magnetic field and the oscillation frequency equals the Larmor frequency: $M_x = M_0 \sin(\theta) \cos(\omega_0 t)$ (11). Thanks to the Fourier transformation of the signal, the spectrum is obrtained and the oscillating frequency can be deduced. More information about this is given later [1].
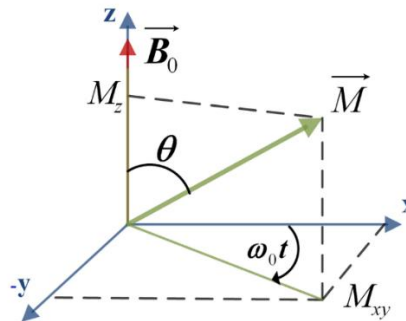
Figure 4: Evolution of the intensity of the FID signal, detected by a coil oriented along the x-axis. (adapted from [6])

One crucial step of an NMR experiment is to tilt the magnetization vector from the z axis into the x-y plane. This is performed by replacing the magnetic field alongside the z-axis by a different one situated in the x-y plane. The magnetization vector then starts the precession around this new magnetic field, as shown in **Figure 5.** In practice, it is unfortunately impossible to switch the main external rapidly and a small coil in the x-y plane is used, with a magnetic field oscillating at radiofrequency. For example by applying a small magnetic field aligned with the x axis, oscillating back and forth from +x to -x with a frequency ω_{RF}

close to the Larmor frequency of the nucleus to be analyzed, this small magnetic field is able to rotate the magnetization around the x-axis thanks to the effect of *resonance* [1].
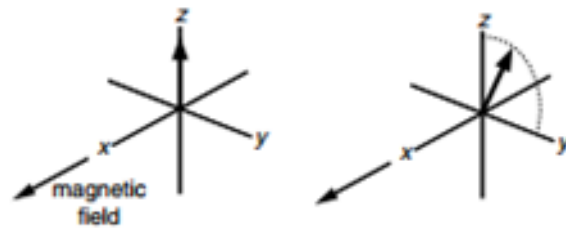
Figure 5: Rotation of the global magnetization vector into the x-y plane by a pulse along the x-axis (taken from [1])

In order to understand the principles of resonance, one has to place oneself into a *rotating frame*. The rotating frame that is used in this case has a fixed z-axis but is rotating around this axis with a frequency $-\omega_{RF}$. The radiofrequency pulse described in the previous paragraph can be subdivided into two magnetic fields B_1^+ *and* B_1^- of intensity B_1, rotating in opposite direction with frequencies ω_{RF} *and* $-\omega_{RF}$ as shown in **Figure 6**. This results in an oscillation of the magnetization exclusively along the x-axis between the two intensities $2B_1$ and $-2B_1$, because the components of the two rotating magnetic fields along the y-axis cancel each other out. If a nucleus with a positive gyromagnetic ratio γ is considered, the Larmor frequency of the precession is negative and thus rotates in the same direction as B_1^-. This results in a very strong interaction between the magnetization and this magnetic field, whereas the interaction with B_1^+, rotating in the opposite direction, is negligible. The main goal of the introduction of the rotating frame, having the same frequency as the pulse ω_{RF}, is therefore to make the magnetic field B_1^- timeindependent. The resulting magnetic field of the radiofrequency pulse appears to be static, with a constant intensity B_1 [1].
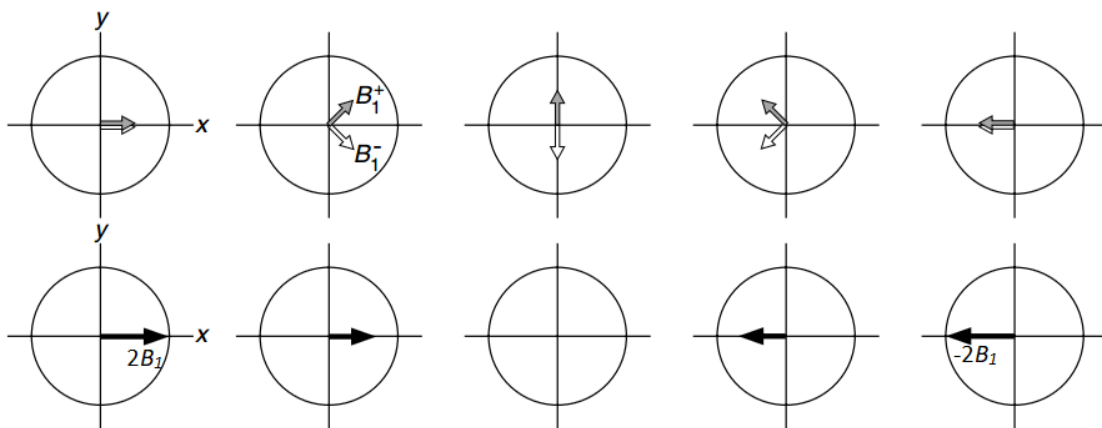
Figure 6: Representation and decomposition of the radiofrequency pulse by to anti-rotating magnetic fields (adapted from [1])

Just as the magnetic field generated by the pulse, the Larmor precession is also seen differently in the rotating frame. If the rotation frequency of the rotating frame is $-\omega_{RF}$ and the Larmor frequency ω_0, then the apparent frequency of the Larmor precession becomes $\Omega = \omega_0 - \omega_{RF}$, called *offset*. Despite the fact that one is now situated in a rotating frame, the formula $\omega = -\gamma B$, giving the precession frequency of a magnetization vector around a magnetic field, is still valid. Therefore, the apparent magnetic field ΔB in the rotating frame is given by:

$$\Delta B = -\frac{\Omega}{\gamma} \qquad (12),$$

called the *reduced field.* This represents the principle of resonance and is the reason why low intensity impulsions can overcome the much stronger external magnetic field B_0. In order to analyze the effect of the two different magnetic fields being present at the same time, the effective field B_{eff} acting on the magnetization vector is determined. Still being in the rotational frame, B_{eff} can be found by simple addition of the vectors of the two magnetic fields, as shown in **Figure 7**. The resulting intensity and the angle θ with the z-axis can be found by: $B_{eff} = \sqrt{B_1^2 + \Delta B^2}$, with the resulting precession frequency $\omega_{eff} = |\gamma| \, B_{eff}$, and $\tan \theta = \frac{B_1}{\Delta B}$. For an offset equal to zero, it can be seen that the only influence on the magnetization is the rf-pulse and it starts the precession around the x-axis [1].
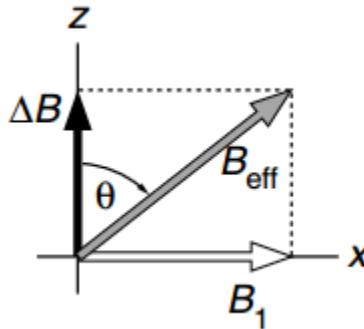
Figure 7: Determination of the effective magnetic field B_{eff} in presence of the external magnetic field B_0 and the field generated by the pulse B_1, situated in the rotational frame (taken from [1]).

Based on the offset, two different types of pulses are distinguished: on-resonance pulses and hard pulses. The on-resonance pulse corresponds to a zero offset and is the easiest case. It corresponds to a pulse with a frequency ω_1, also called transmitter frequency, exactly equal to the Larmor frequency of the nucleus to be analyzed. In this case, B_{eff} is equal to B_1 and therefore aligned with the x-axis and the magnetization vector starts precessing in the y-z plane with a frequency ω_1. If the pulse is applied for a given time t_p, the magnetization vector has been tilted by an angle $\beta = \omega_1 t_p$, called the *flip angle of the*

pulse. By adjusting t_p, different flip angles can be reached, but the most common ones are 90° and 180°. In practical NMR spectroscopy, several resonances, corresponding to different Larmor frequencies, can be found in the spectrum. Therefore, it is not possible to have an excitation in resonance with all different lines of the spectrum and some excitations with a non-zero offset necessarily occur, called hard pulses. Nevertheless, the condition that $\omega_1 \gg |\Omega|$ leads to a hard pulse. This is crucial in order to have a tilt angle θ close enough to 90° and therefore to be able to able to assume that the magnetization vector behaves similarly to the case of an on-resonance pulse [1].

After having introduced the basic principles of the global magnetization, of its precession around a magnetic field and the principles of an radiofrequency pulse, one is now able to understand the most basic pulse-acquire experiment. This experiment can be divided into three differet steps. First of all, the sample is allowed to reach equilibrium magnetization alongside the z-axis, due to the presence of the strong external magnetic field. Afterwards, the radiofrequency pulse power is turned on with the desired frequency close to the resonance frequency of the nucleus to be analyzed and kept on for long enough to rotate the magnetization by 90° into the x-y plane. When the pulse power is turned off, the magnetization vector starts precessing around the external magetic field with its significant Larmor frequency, which is detected thanks to a coil in the x-y plane. The intensity of the oscillating signal decreases exponentially due to the so-called *transverse relaxtaion* of the magnetization in the x-y plane, sometimes also called *spin-spin relaxation*. This effect is characterized by the *transverse relaxation time T_2* and describes the time taken by the nuclei spins to orient randomly in the x-y plane and to result in a zero magnetization, as shown in **Figure 8**. More information about the theory and equations of this effect is not given in this work, but can be found in Chapter 9 of the book [1]. The result of the rotation and the exponential decay is a FID signal, which can be transformed into the spectra by different mathematical treatments, as shwon in the following paragraph. It is important to distinguish between the longitudinal relaxation with its characteristic time T_1, presented at the beginning of this chapter, and the transverse relaxation with its characteristic time T_2. First of all, the value of T_2 is always much smaller than the one of T_1. In addition, whereas T_2 is proportional to the decay of the FID signal and can directly be deduced from it, T_1 is not seen in the signal and the spectrum at all. Nevertheless, T_1 can also be detected and it is important that the time between two pulses is longer than T_1, in order to be sure that the magnetization has reached its equilibrium before a pulse [1][7].
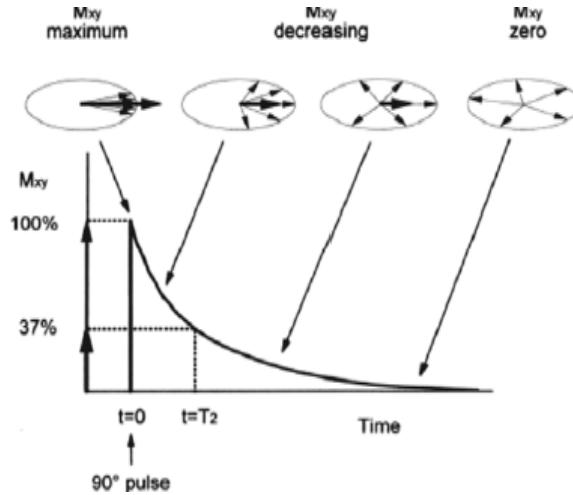
Figure 8: Exponential decay of the magnetization in the x-y plane due to the transverse relaxation with a characteristic time T_2 (taken from [8])

2.1.3 Fourier transformation and signal treatment

In this chapter, we start from the assumption that during the pulse, the magnetization has been rotated onto the x-axis and then starts rotating with its Larmor frequency in the positive direction. Detection is made in the rotating frame with its rotation frequency ω_{RF} and therefore, the detected signal has a frequency equal to the offset (Ω). Supposing that the signals are detected along the x and the y-axis, both signals are given by:

$$S_x = S_0 cos\Omega t \ and \ S_y = S_0 sin\Omega t \qquad (13),$$

with S_0 the maximum signal intensity and Ω the offset. Due to the manner in which the Fourier transformation works, it is convenient to write down S_x and S_y as the real and the imaginary part of the combined complex $S(t)$ signal. Considering the exponential transverse magnetization decay shown in the previous paragraph with a time constant T_2, the total FID signal $S(t)$ can be represented by the formula:

$$S(t) = \left(S_x(t) + S_y(t)\right) * \exp\left(-\frac{t}{T_2}\right) = S_0 \exp(i\Omega t)\ exp\left(-\frac{t}{T_2}\right)$$

$$= S_0 \exp(i\Omega t)\ exp(-R_2 t) \qquad (14),$$

with $R_2 = \frac{1}{T_2}$ the first order rate constant. The shorter the time T_2 or the bigger R_2, the faster the decay of the signal. The representation of the real and the imaginary part of the FID signal is shown in **Figure 9** [1].
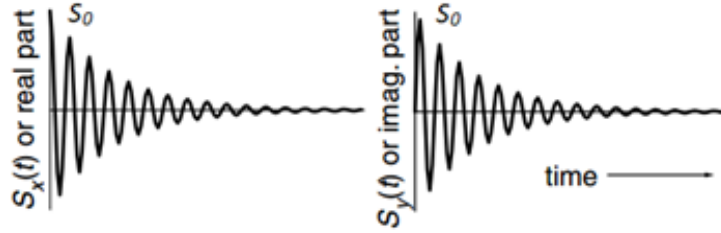
Figure 9: Representation of the real and imaginary part of a typical FID signal (taken from [1])

The Fourier transformation (FT) of a signal like the one shown in equation (14), gives the signal $S(\omega)$ in the frequecy domain, represented in the spectrum. The calculation of $S(\omega)$ for a single signal is made in Annex 1 and the result is shown in equation (15):

$$S(t) = S_0 \exp(i\Omega t) \exp(-R_2 t) \; --FT\longrightarrow \; \frac{S_0 R_2}{(\omega-\Omega)^2 + R_2^2} + i \frac{-S_0(\omega-\Omega)}{(\omega-\Omega)^2 + R_2^2} = S_0[A(\omega) + iD(\omega)] \;\; (15).$$

This shows that the signal consists of a real part $A(\omega)$ and an imaginary part $D(\omega)$ also in the frequency domain. Both parts of the signal show two typical lineshapes in the frequency domain: The real part has a so-called *absorption mode Lorentzian* lineshape in the spectrum (**Figure 10 a)**) and the imaginary part a so-called *dispersion mode Lorentzian* lineshape (**Figure 10 b)**). In general, only the absorption mode is analyzed and the dispersion mode is not represented in the spectrum, because it is larger and smaller than the absorption mode and has a negative and a positive part. Nevertheless, it is important to know of its existence when it comes to phasing. The peak of the absorption mode line $A(\omega)$ is centered at the oscillation frequency Ω of the signal, with a maximum intensity equal to $A(\omega = \Omega) = \frac{R_2}{(\Omega-\Omega)^2 + R_2^2} = \frac{1}{R_2} = T_2$. Another important property of the peak is its width at half of its maximum heigth, which is equal to $\frac{1}{\pi T_2}$ or $\frac{R_2}{\pi}$ Hz as derived in Annex 1. A faster decay of the FID (smaller T_2 and bigger R_2) therefore gives a smaller and broader peak, which is bad for the resolution of the spectrum. In the case of an FID signal representing a sum of different signals in the time domain, the signal in the frequecncy domain is simply represented by the sum of the Fourier transforms of the different signals and the spectrum is composed of different lines, due to the linear character of the FT [1].
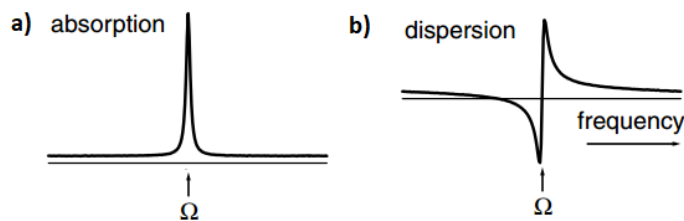
Figure 10: Representation of the absortion and dispersion mode Lorentzian lineshapes (taken from [1])

In the previous section, the perfect case was supposed, with an impulsion tilting the magnetization exactly on the x-axis. Unfortunately, the instrumental and the electronical setup is responsible that it cannot be guaranteed that the two measured signals really correspond to the signals in the defined axis system. As a result, the measured signal becomes a linear combination of the real part and the imaginary part of the signal and the spectrum is therefore a combination of absortion mode and dispersion mode Lorentzian lineshapes. The signal is said to be dephased and more details about this are explained in Annex 1. Very often during the post-acquisition data treatment, a phase correction is performed in order to obtain a purely absorption mode lineshape [1].

In the following, another post-acquisition data treatment technique is presented, which aims at enhancing the sensitivity of the signal and to increase the Signal-to-Noise-Ratio (SNR). Due to the fact that the signal intensity decreases with time and the noise intensity remains almost constant, the idea is to modify the FID and to give more importance to the early parts, while the later noisy parts are neglected. This can be done by multiplying the original FID signal with a function that starts at 1 and then decreases to 0 with time. A simple and typical example of a so-called *weighting function* is the decreasing exponential:

$$W_{LB}(t) = \exp(-R_{LB}t)$$
$$=> \ S(t) * W_{LB} = S_0 \exp(i\Omega t) \exp(-R_2 t)* \exp(-R_{LB}t)$$
$$= S_0 \exp(i\Omega t) \exp(-(R_2 + R_{LB})t) \qquad (16),$$

with R_{LB} a positive constant, increasing the value of the rate constant R to $(R_2 + R_{LB})$. The term LB stands for *Line Broadening*, which comes from the secondary, negative effect of this multiplication. In fact, the higher rate constant results in the more rapid decrease of the FID and causes the peaks to become larger (width at half maximum = $\frac{R_2+R_{LB}}{\pi}$) and smaller (maximum height = $\frac{1}{R_2 + R_{LB}}$) , which has a negative effect on the resolution. In practice, a compromise between a low SNR and a sufficiently high resolution [1].

Different other methods also exist with the aim of obtaining smoother spectra, but the ones that are used in this work have been presented [1].

2.2   Different types of experiments and the corresponding pulse sequences

In the previous sections, the theory of the general NMR principles has been introduced and it has been shown how the magnetization of the nuclei can be rotated using pulses. In addition, the precession of the magnetization and the way in which the signal has been collected and treated mathematically was

described. In this section, the principles and the pulse sequences of the different types of experiments are explained.

2.2.1 Simple *onepulse* experiment

The *onepulse* experiment is the basic NMR experiment. As shown in **Figure 11**, only a single pulse P_1 with a certain length and intensity is applied to rotate the magnetization by 90° in the x-y plane. Afterwards, the precession in the Larmor frequency and relaxation of the magnetization starts and the FID signal is detected. In between two pulses, a certain delay d_1 is important in order to ensure the magnetization equilibrium after longitudinal relaxation, as well as to have the same initial position before a pulse [2].
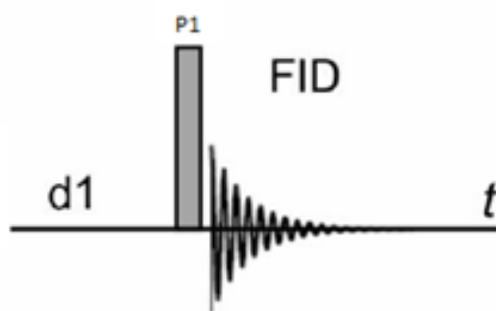
Figure 11. Pulse sequence of the *onepulse* experiment (adapted from [9])

2.2.2 A *cross polarization* experiment

The *cross polarization* experiment is an experiment used for the detection of dilute spins, to perform some spectral editing or to obtain information about the spins close in space. The problem with dilute spins is that they result in a low SNR due to their low abundance, and their relaxation time tends to be long, because not much homonuclear dipolar interaction is present that could stimulate relaxation. The solution is to transfer the magnetization to the dilute spins X from a nearby network of another, more abundant spins with a shorter relaxation time, mostly ^1H. In theory, cross polarization can be performed between every nucleus, but the coupling between the proton and another dipolar nucleus is the most common one. The very basics of this experiment is explained in the following [10].

The pulse sequence of a typical *cross polarization* experiment is shown in **Figure 12**. As one can see, the first step is a 90° pulse on the ^1H spin. Afterwards, a *contact pulse* is applied in the rotating frame of the proton in order to maintain the magnetization along the –y axis by creating the so-called *spin-lock field* $B_1(H)$ and to provide a quantization axis for the ^1H spins. The contact pulse applied in the rotating frame of the X spins, resulting in the spin-lock field $B_1(X)$, has the same effects on the X spins. As shown

in **Figure 1**, the spin state α with the lowest energy is aligned with the magnetic field B_1, whereas β has the highest energy and shows in the opposite direction. The difference in energy between these two states is given by $\Delta E = h\gamma B_1$ (5). Due to the fact that the initial magnetization in direction of $B_1(^1H)$ is of the same size as the one created by a much stronger external field B_0, $B_1(^1H)$ is too weak to sustain it and the ^1H magnetization is reduced by $\alpha \to \beta$ spin transitions. At the same time $\beta \to \alpha$ spin transitions occur in order to conserve the energy of the system, which creates a magnetization of the X spins. This energy and therefore the magnetization transfer is due to the presence of dipolar interactions between the nuclei. Variable amplitude contact pulses as shown in **Figure 12** are often used to increase the efficiency of the magnetization transfer under magic-angle spinning. The maximum signal is obtained if the amplitudes of the contact pulses are adjusted in order to achieve the Hartmann-Hahn matching condition, derived from equation (5):

$$\gamma_H B_1(^1H) = \gamma_X B_1(X) \qquad (17)$$

In this case, the energy of a $\alpha \to \beta$ spin transitions of an ^1H spin is exactly compensated by a $\beta \to \alpha$ spin transition of an X spin. After the transfer of the magnetization, the FID signal of the X nucleus is analyzed, while applying a decoupling pulse in order to prevent interaction between the proton and the X nucleus during the acquisition. From equation (17), the enhancement factor in CP can be derived, which equals $\frac{B_1(X)}{B_1(H)} = \frac{\gamma_H}{\gamma_X} = \frac{26.75}{10.84} = 2.5$ in the case of ^{31}P as X nucleus. This leads to an increased sensitivity of the ^{31}P nucleus analysis [10].
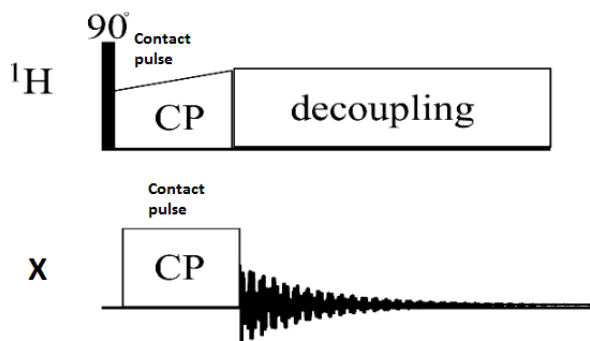
Figure 12. Pulse sequence of the *cross polarization* experiment (taken from [11])

2.3   Solid versus liquid state NMR

Most of the previous descriptions are valid for both, liquid state and solid state NMR. Nevertheless, there are some differences that notably influence the experimental setup of the analysis. The difference arises from the fact that in liquid state NMR the molecules are in a steady motion, which limits the number

of interactions due to the averaging of anisotropic NMR interactions. Beside the chemical shift interactions and the J-coupling, notably the orientation-dependent dipolar coupling influences the spectra in solid state NMR. The result of this interaction is a very broad NMR spectrum with a much lower resolution compared to liquid state NMR spectrum containing only very sharp transitions.
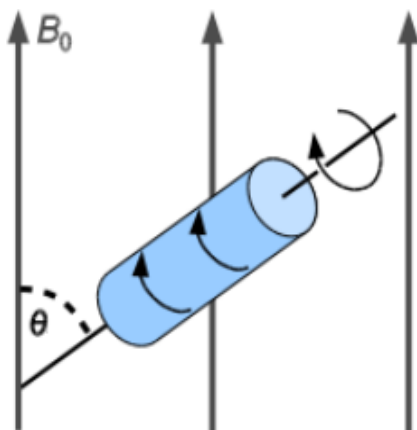
Figure 13. Principle of magic angle spinning of a sample inside an external magnetic field (adapted from [12])

The dipolar coupling arises from the interaction through space of the magnetic moments of the nuclear spins. This coupling has to be distinguished from the already cited scaler J-coupling, because this is an indirect coupling of the nuclear spins mediated by electrons. In order to understand and afterwards reduce the effect, the interaction energy of the dipolar coupling between a spin pair is evaluated. For the case of a homonuclear spin-pair interaction of a sample rotating at high speed with an angle θ to a strong external magnetic field B_0 as shown in **Figure 13**, the interaction dipolar interaction energy is represented by the Hamiltonian:

$$\hat{H}_{dd}^{homo} = -\left(\frac{\mu_0}{4\pi}\right)\frac{\gamma_I\gamma_S\bar{h}}{r^3}(3cos^2\theta - 1)[\hat{I}_z\hat{S}_z - \frac{1}{2}(\hat{I}_x\hat{S}_x + \hat{I}_y\hat{S}_y)] \qquad (18),$$

with $\boldsymbol{\mu_I} = \gamma_I\bar{h}\boldsymbol{I}$ and $\boldsymbol{\mu_S} = \gamma_S\bar{h}\boldsymbol{S}$ the magnetic moment of the two spins I and S, r the distance between the spins, γ the gyromagnetic ratio and $\bar{h}$ Planck's constant. The development of this equation is not shown in this work, but can be seen in the chapter 1.4.2 of the book [10]. As one can see, there is only one term that can be influenced, namely the spinning angle θ. For a θ equal to 54.74°, called the *Magic Angle*, the interaction energy becomes 0 and therefore the dipole-dipole coupling should be removed. This is the principle of *Magic Angle Spinning (MAS)* SSNMR. The necessary rotation speed to be completely effective depends on the intensity of the dipolar coupling and can take up to >150 kHz for strongly coupled protons. However, there is also has a big effect for lower rotational speeds. In order to get SSNMR spectra

with better resolution, there is a continuous effort to reach faster MAS spinning speed. It has to be noted that the dipolar interactions can also be used in a positive way and can serve as source of information. The previously shown *cross-polarization* can only be performed in solid state NMR, for example. Lastly, some other differences between liquid and solid-state NMR can be cited. One difference is that devices with higher power and larger free space inside the magnet have to be used, in order to excite the spins and to have space for the specialized MAS probes [10].

3   Background of the used methods

In this chapter, the principles of the analysis of the acidity of zeolites by R_3PO probe molecules are explained. In order to get a better understanding of this, the different zeolites that have been analyzed are presented in a first step before their production and properties are explained.

3.1   Description of the used zeolites

The different zeolites that have been analyzed in this work are the aluminosilicates of faujasites family (FAU). Faujasites are zeolites with the structure represented in **Figure 14 a).** As highlighted on the graph, there are different cages and channels that are formed by the structure: hexagonal prisms, sodalite cages and supercages, cited in order of increasing size. The size of the different cages and channels are shown in **Figure 14 b)**, which helps imagine the pathway that the probe molecules accomplish, before they can reach the active sites of the zeolite.
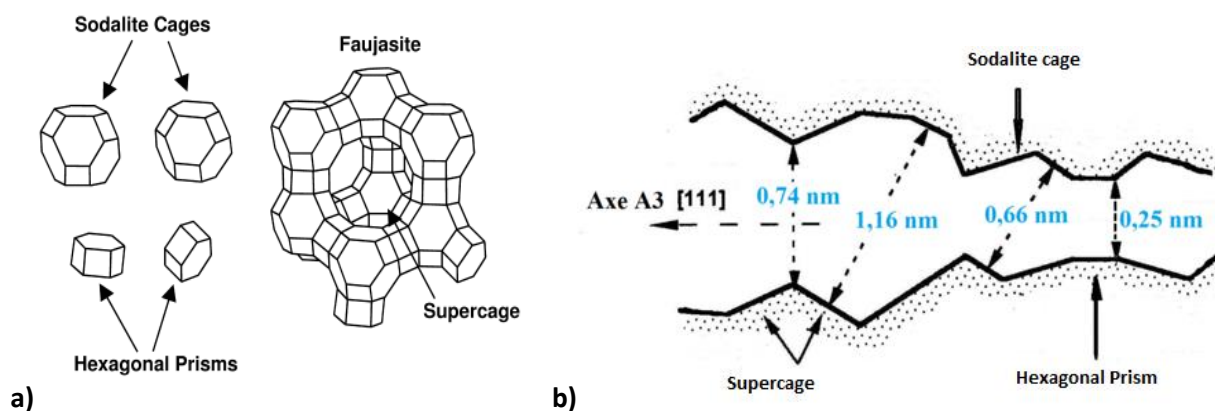
Figure 14. a) Basic structure and cage and **b)** channel size of faujasite zeolites (**a)** Adapted from [13]; **b)** Adapted from [14])

Various types of faujasites exist depending on their Si/Al ratio. With a Si/Al=1-1.5, the zeolite X is the faujasite with the lowest ratio. It is very acidic and has a large cation exchange capacity, but unfortunately it is unstable in catalysis. Due to its Si/Al of about 2.5, the zeolite Y is less acidic but more stable than the zeolite X. By changing the hydrothermal synthesis, one can decide which of both zeolites is produced, but if a higher Si/Al is needed, post-synthetic modifications are necessary. Possible post-treatments are ion exchange, hydrothermal treatment/ steaming, acid treatment and base treatment, which theoretically allow tuning the Si/Al to infinity. Faujasites with framework Si/Al of about 6 or higher are called USY (ultra-stable Y) zeolites and they possess an improved catalytic and hydrothermal stability. In this work, commercial USY zeolites CBV 712, CBV 720 and CBV 760 from the company *Zeolyst International* company are used and analyzed. Some properties of those zeolites are represented in **Table 1** [15].

Table 1. Major properties of the different USY zeolites used in this work ([15][16])

Zeolite	CBV 712	CBV 720	CBV 760
Bulk Si/Al ratio (mol/mol)	6	15	30
Cation	H^+	H^+	H^+
Surface area (m²/g)	730	780	720
Na$_2$O weight %	0.05	0.03	0.03
Dealumination treatments	Ion exchange Moderately steamed Acid treated	Ion exchange Severely steamed Acid treated	Ion exchange More severely steamed Acid treated

As shown in **Table 1**, the first post-synthetic treatment is an ion exchange for all three zeolites. The new cation is whether NH_4^+ or H^+ and from the initial sodium cation only a small fraction is left. An advantage of this exchange is that the zeolites become a more reactive to aqueous acid treatments. The second treatment is steaming, during which the zeolite is treated with a hot steam flow for several hours. The result of this treatment is a dealumination of the zeolite framework. However, the bulk Si/Al ratio remains constant and extra framework aluminum (EFAl) species are generated. The severity of the steaming determines the quantity of framework aluminum removed and the amount of EFAl produced. Unfortunately, a too large amount of EFAl can reduce the catalytic properties of the zeolite and reduce the accessibility of the pores. In addition, the degree of agglomeration of those EFAl species increases that are more difficult to remove afterwards. In order to remove the EFAl species, an acid treatment with

different mineral or organic acids is often used. This treatment improves the pore accessibility, as well as the acid properties and the overall bulk Si/Al ratio is increased. A secondary outcome is the further dealumination of the framework, without altering the crystallinity and microporosity. Beside the stabilization, a positive side effect of those dealumination treatments is the mesoporisation of the zeolite structure. This secondary pore system facilitates the mass transport inside the zeolite and gives access to bigger molecules. On the other hand, the overall microporosity and acidity are only minimally altered, so the micropore structure shown in **Figure 14** is still correct for USY zeolites [15][17]. A schematic presentation of the post-synthetic treatments is shown in **Figure 15**.
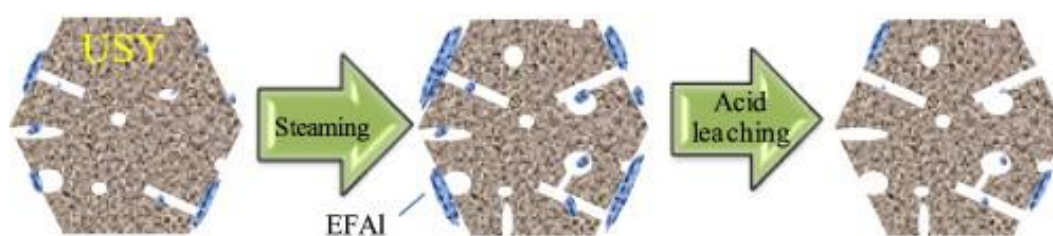
Figure 15. Graphical abstract of the post-synthetic dealumination treatments of Y zeolites (Taken from publication [17])

Faujasites are one of the most used catalysts for petrochemical applications. Due to their strong acidity, they are used for several hydro-conversions and for hydrocracking, in particular. Their main acid properties arise from Brønsted bridge SiOHAl sites. Their acidity varies as a function of the structure and the size of the cage. Other possible acid sites could be terminal SiOH or AlOH groups, as well as the ones generated by EFAl [15].

3.2 Principles of the approach of trialkyl phosphine oxides (R$_3$PO) as probe molecules

The determination of different acid properties of zeolites is crucial in order to understand and determine their activity and selectivity during the catalytic reactions. Different properties of acid sites are important such as the acidity type (Lewis or Brønsted acid site), the acidity strength, location (internal or external site) and the concentration of each site. To get more information about these properties is beneficial for the improvement and development of those zeolites and to create zeolites more adapted to the specific reactions. For the determination of those properties, lots of different analytical techniques can be used. Beside ammonia Temperature Programmed Desorption (TPD), calorimetry, titration and

various Infrared spectroscopy techniques (IR), SSNMR, especially on ^{31}P nucleus, has been applied in the past [18].
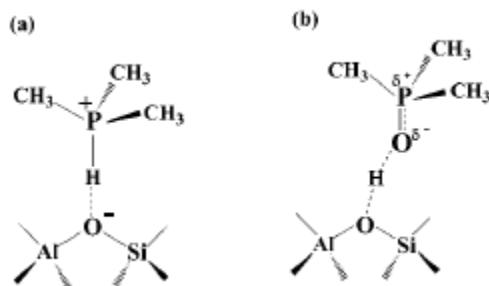
Figure 16. Graphical representation of the junction between (a) TMP and (b) TMPO and the zeolitic Brønsted acid sites (Taken from [19])

SSNMR of ^{31}P can be applied by the use of phosphorus containing basic probe molecules. There are two different types of probe molecules that are commonly used: trialkylphosphine (mostly trimethylphosphine TMP) and trialkylphosphine oxides (R_3PO). Contrary to different other techniques, it is capable to simultaneously detect the acidity type, the acid site location, the acid site strength as well as to quantify them [18]. The downside of the use of TMP are the toxicity, the inflammability, the air-sensitive nature and the fact that it is gaseous at ambient temperature, making the sample preparation more difficult. In addition, during the reaction with Brønsted acid sites, the molecule forms $TMPH^+$ complexes, as shown in **Figure 16 (a)** with resulting resonances between -2ppm and -5ppm as function of the acid site strength. The resulting ^{31}P chemical shift range is therefore very narrow and the differentiation between the acid sites with various strength seems unlikely. For the distinction between different Lewis type sites, the TMP molecule is more appropriate, but for most catalytic applications the Brønsted acid sites are more important [19].

In the case of trialkylphosphine oxides, hydrogen bonded complexes are formed during the reaction of the probe molecule with Brønsted acid sites, as shown in **Figure 16 (b)**. As a result, the P=O bond length of the probe molecule increases and the ^{31}P NMR shows low field line shift, if the probe molecule is bonded to stronger Brønsted acid sites. The chemical shift range corresponding to Brønsted acid sites is much higher (>50 ppm) than in the case of TMP and allows a more easily distinction between the sites of various strength [20].

In addition, the R_3PO approach is also suitable for the detection of Lewis acidity, being less straightforward than based on TMP usage. Due to the fact that Lewis acid sites only weakly interact with trialkylphosphine oxides and easily react with water, the probe molecules are dissociated, if the sample is

in contact with water. In contrast, the bond between Brønsted acid sites and the R_3PO probe molecules are strong enough to remain during hydration. Thus, only the intensity of the ^{31}P signal corresponding to probe molecules bonded to Lewis acid sites is decreased upon hydration, which allows to distinguish between both acid types. Similarly to the case of Brønsted acid sites, the higher the chemical shift in the ^{31}P spectrum, the stronger the Lewis acid sites where the R_3PO molecule is bonded to [18].

During its application as catalysts, molecules of various sizes have to enter the zeolite through different channels and pores of different sizes. According to their size, they will therefore be able or not to bind to acid, which makes it indispensable to distinguish between the acid sites situated at different positions. As shown in **Figure 14**, the size of the micropores and microchannels of the USY zeolites CBV 712, CBV 720 and CBV 760 that are used in this work are quite small and can therefore be selective for molecules of various sizes. During dealumination treatments, some larger pores are created facilitating the overall mass transport, without altering the structure of the micropores containing the Brønsted acid sites. The use of different types of trialkylphosphine oxides with different R_3 chain lengths, thus having a different kinetic diameter, can be used to sperate the acid sites into larger and smaller channels. In the literature, trimethylphosphine oxide (TMPO), triethylphosphine oxide (TEPO), tributylphosphine oxide (TBPO) and trioctylphosphine oxide (TOPO) are the most often used probe molecules, with kinetic diameters of 0.55 nm, 0.60 nm, 0.82 nm and 1.10 nm respectively. Therefore, the two larger molecules are not considered to access the supercages, whereas the two smaller ones have to. This can provide the information regarding the acid site location [18].

Lastly, it is important to note that by means of the method using trialkylphosphine oxides as probe molecules the amount of the different acid sites, distinguished in the previous paragraphs, can be detected. To do so, two assumptions are made. Firstly, it is considered that the intensity of a peak in the NMR spectra is proportional to the quantity of the probe molecule bonded to the specific acid site. Secondly, it is assumed that the signal of each probe molecule added to the zeolite sample can be seen in the spectrum afterwards, even if it is not bonded to an acid site, but physisorbed or in its crystalline form. By doing a deconvolution of the spectrum, the concentration of the respective acid site in the zeolite can be calculated. The precision of this measurement strongly depends on the accuracy of the masses of the zeolite sample and of the probe molecule added. According to literature, ICP tests are often performed in order to control the quantity of phosphorus added, since the mass of added R_3PO is not measured precisely [21].

In the literature, two main methods are discussed for the adsorption of the R_3PO probe molecules on the zeolites. The first one is a wet route. For that, a known amount of the probe molecule is dissolved

into a solvent, mostly anhydrous dichloromethane (CH_2Cl_2), which is then added to a vessel containing the dehydrated zeolite. The choice of solvent is extremely important, as it can interact with the acid sites as well. Afterwards, the solvent is evacuated under primary vacuum, followed by heating the sample up to a temperature superior to the probe molecule's melting point for a relatively short time in order to ensure its uniform distribution inside the channels. Then, the loaded zeolite is transferred into the rotor under the glovebox [18]. The second method is a solid route. The zeolite is mixed with the pure probe molecule inside or outside the rotor and then treated above the melting temperature of the probe molecule for a longer time. The drawback of this method is that the distribution of the probe molecule is less controlled and a longer heat treatment is necessary [22]. In this work, the second method has been used due to its simplicity. Moreover, there is no risk of residual solvent and the use of toxic solvents is avoided. CH_2Cl_2, for example, causes skin, eye and respiratory irritations, as well as dizziness. In addition, it is suspected of causing cancer and can damage organs [23]. Another point is its purity, because it is very likely to adsorb water and therefore can cause water to remain in the sample. Finally, it is important to note that there are various articles in literature describing the wet route, but only very few can be found that make use of the solid route. Moreover, the sample preparation of the solid route is often only poorly described, like in [22] for example. For those reasons, this method needs to be developed.

4 Experimental Section

In the following sections, information and explanations are given about the preparation and execution of the NMR experiments. The different steps are highlighted in details and the principles of the treatment and analysis of the results are also explained.

4.1 Preparation of the zeolites

Three different zeolites are analyzed in this work. These are commercial USY zeolites delivered by the company *Zeolyst* and denoted as CBV 712, CBV 720 and CBV 760. The most important difference between these zeolites is the bulk Si/Al ratio, which is 6, 15 and 30, respectively. Some features of the zeolite production have already been mentioned in section 3.1, as well as some other properties in **Table 1** [16].

The zeolites can principally be used directly as they arrive from the supplier, the only treatment that has to be performed is a dehydration. Due to their porous structure and high specific surface area (SSA), they are very sensitive to humidity in the air and adsorb water very rapidly, which can occupy the

Brønsted acid sites. This feature requires dehydration of the zeolite under vacuum and high temperature. After dehydration, the zeolite should not get in contact with humidity, therefore this process is done in a hermetic recipient that can be kept closed directly afterwards. All information about the vacuum outgassing program of the zeolite is represented in **Figure 17**. Afterwards, the tubes containing the zeolites are transferred to the glovebox under N_2 atmosphere (less than 10 ppm O_2), where they are opened and the zeolites can be manipulated.
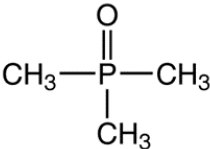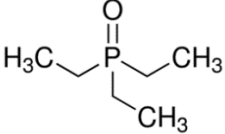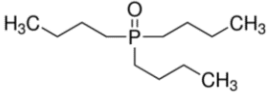
Evacuation Phase			Heating Phase		
Temperature ramp rate:	10.0	°C/min	Ramp rate:	10.0	°C/min
Target temperature:	30	°C	Hold temp:	350	°C
Evacuation rate:	10.0	mmHg/s	Hold time:	300	min
Unrestricted evac. from:	10.0	mmHg			
Vacuum setpoint:	500	µmHg	Evacuation and Heating Phases		
Evacuation time:	10	min	Hold pressure:	100	mmHg

Figure 17. Conditions of the vacuum outgassing program for the zeolites

4.2 Preparation and properties of the trialkylphosphine oxides

During the experiments, different trialkyl phosphine oxides have been used in order to measure the number of acid sites that occur in the different cage sizes of the zeolites. In this work, trimethylphosphine oxide (TMPO), as well as triethylphosphine oxide (TEPO) and tributylphosphine oxide (TBPO) is used. The three molecules have been purchased by *Alfa Aesar*. The main properties of these molecules are summarized in **Table 2**.

Table 2. Some important properties of the different probe molecules

Molecule	TMPO	TEPO	TBPO
Fusion temperature at 1 atm, °C	141	48-52	64-69
Evaporation temperature at 1 atm, °C	194	243	347.7
Kinetic diameter, nm	0.55 [20]	0.6 [20]	0.82 [20]
Molecular mass, g/mol	92	134	218
Relative basicity	Low [20]	Middle [20]	High [20]
Molecular structure			

The preparation of the probe molecules is straightforward. The molecules can be used directly as they arrive from the supplier, the only treatment that has to be performed is a dehydration. Due to their basicity, the probe molecules react with the humidity in the air and form their conjugated acids, which would lead to an underestimation of the acid sites of the catalysts. Dehydration in a drying oven of the probe molecules is performed at 65 °C for 2 h under nitrogen atmosphere for TMPO and TBPO and at 25 °C under vacuum atmosphere for TEPO, due to its low melting point. Afterwards, the probe molecules are placed into a glovebox to avoid their exposure to the air humidity.

4.3 Rotor preparation

For the experiments, rotors with 4 mm external diameter made of zirconium oxide (ZrO_2) have been used, supplied by the *Coretecnet* company. The advantage of those rotors is their hardness and their resistance to temperature. They can be treated in the oven up to temperatures above 600 °C, without being damaged. For those rotors, different kinds of caps made of various materials are produced, with different advantages and disadvantages. The first kind of caps is made of *Kel-F* polymer. Their advantages are a low price, as well as good rotational properties inside the NMR device. In addition, they are quite easy to remove from and to put on the rotor and they can be reused many times. Unfortunately, they do not resist to high temperatures (more than 70 °C) and therefore cannot be used for samples that have to be heated. The second kind of caps are made of ZrO_2, like the rotors and come from the supplier *Coretecnet* Their advantage is a very good heat resistance, which makes them suitable for samples, where a severe heat treatment is necessary. Unfortunately, they are very expensive (around 10 times the price of the other caps), they are quite difficult to remove from the rotor and their rotation stability is not as good as of the previous cap type. Due to the fact that their part entering the rotor consists of fingers with gaps in between and the material is very hard, this kind of caps break quite easily when removing them from or inserting them into the rotor. During the experiments, several caps of this type brake and sometimes the results had not to be considered. The last type of caps is made of other types of ceramics, called *Vespel* and *Torlon*. They exist in two different models: with and without a polymer O-ring. They resist to heat treatments in the oven up to 210 °C, are easier to put in and remove and less fragile than ZrO_2 caps and they have the same price as polymer *Kel-F* caps. A downside is that they do not have such a good rotation stability as the polymer cap. For the model without O-Ring, a too high temperature can cause a contraction of the cap during the heat treatment due to the difference in thermal dilation between the cap and the rotor. The model with O-Ring is remarkably easy to put and remove, but the state of the O-Ring has to be checked visually before every heat treatment and the stability of the cap on the rotor

has to be checked afterwards, because of its degradation due to the high temperature. On average after 5 treatments at around 200 °C, the O-Ring has to be exchanged. A picture of a 4 mm ZrO_2 rotor and the different kinds of caps are shown in **Figure 18**. Of ZrO_2 caps, a broken example is shown, due to their very brittle character.

Figure 18. Picture of a 4 mm ZrO_2 rotor and four different kinds of suitable caps, made of Torlon (yellow, with O-Ring), Kel-F polymer (transparent), Vespel (brown, without O-Ring) and ZrO_2 (white, broken). The tip of a ball pen is shown, in order to indicate the small size of the devices.

Due to the small rotor size, it is complicated to fill them up with the zeolite and the probe molecule. In addition, it is not easy to put the cap on it, especially in the glovebox where the sensitivity of the hands is reduced by the thick gloves. In order to resolve this problem, two different types of filling tools have been designed by the *Bruker* company and adapted precisely to this kind of caps and rotors. One filling tool has two openings, with the upper one being smaller so that the rotor does not fall through, that allows the easy filling. The other one has only one opening and helps to put the rotor straightly on the cap. Inside the rotor, the added materials have to be compacted to ensure a stable rotation and to avoid the formation of a hole in the center during rotation because of centrifugal forces. The packer has the adapted diameter to compact the zeolite and the probe molecules inside the rotor. In addition, it helps to remove the excess of the product in the rotor and to measure the height up to which the rotor can be filled to put the caps correctly. For the opening of the rotors also special equipment has been designed by the company *NMR – service* that works quite well for all kind of caps, beside for the ones made of ZrO_2. Pictures of the different kinds of filling and caps removal tools are shown in Annex 2.

Before the rotor filling, its empty mass has to be measured. The empty rotor with the adapted cap on is weighed. This step has been done outside of the glovebox. Afterwards, the rotor with the cap, appropriate filling tools and packers, nitrile gloves and different cleaning devices are put into the glovebox. Firstly, the necessary quantity of the probe molecule is added to the rotor and weighed. Then, the zeolite is added gradually while compacting the content inside the rotor regularly, until it reaches the adapted height. Attention has to be paid during the filling due to the electrostatic charging of the devices inside the glovebox, which causes the powder of the zeolites to stick to the borders of the filling tools, to the tube containing the zeolite and to the gloves of the glovebox, therefore nitrile gloves are put over these gloves before manipulating. When the rotor is filled up to the suitable height, the remaining inner wall of the rotor has to be cleaned from zeolite sticking to it. This zeolite could hinder putting the cap on or make the removal more difficult. As a next step, the cap can be inserted into the rotor. Especially for the caps made of ZrO_2 this has to be done carefully and it is important to insert them straightly so that they do not tilt. One particularity of the caps with O-Ring is that they have to be inserted with a screwing motion, which makes the use of a supporting device unnecessary. Finally, the filled rotor is cleaned from the outside, removed from the glovebox together with all the devices to be cleaned and is then ready for the heat treatment. The rotor is positioned in a crucible containing a granulated powder with the cap to the bottom or to the top, whether the probe molecule should be liquid or gaseous at the treatment temperature. After the treatment, the cooled down rotor is weighed to calculate the added zeolite mass.

4.4   Information about NMR device and sample analysis

The NMR spectra of the samples were acquired using a Bruker Avance III HD 500 MHz (magnetic field of 11.7 T) device. A broad band MAS probe was used, designed for 4mm outer diameter rotors and capable to spin them up to a spinning speed of 15 kHz. The probe installed in the NMR device has two different entering channels: an entrance H for the analysis of the proton (^{1}H) and an entrance X for the analysis of other nuclei. The H entrance is a narrow band entrance, which is optimized for the ^{1}H detection. The operating frequency can only be varied by about 25 MHz around the general operating frequency for ^{1}H (500.13 MHz), but therefore has a very high sensitivity. The X entrance is a broad band entrance that allows working with operating frequencies between approximately 50 MHz (inferior limit of the NMR device) and 220 MHz. The operating frequencies of many common nuclei are situated in this range, like phosphorus (^{31}P: 202.47 MHz), aluminum (^{27}Al: 130.31 MHz) and silicon (^{29}Si: 99.36 MHz). A picture of the NMR device and the installed probe are shown in Annex 2. The signal treatment and the device control were done by means of the program Bruker TopSpin 3.2 [24]. The reference frequency of the proton is

found due to the ^{1}H analysis on the tetramethylsilan (TMS). The reference frequencies of the other nuclei are calculated based on this result by TopSpin routine xiref, based on a IUPAC recommendation [4].

Before the analysis, the prepared rotor is cleaned with ethanol and dried, in order to prevent any foreign signal emanating from substances at the outer signal. This is of particular importance for the analysis of the proton. Then, a black half-circle is drawn with a permanent marker at the inclination at the bottom of the rotor. This line is necessary for the device in order to count the spinning frequency of the rotor. After inserting the rotor, it is tilted into the magic angle position and the spinning speed can be increased gradually but slowly. During the first analysis on the rotor after its filling, special attention has to be paid. As the product inside the rotor is not perfectly packed, the centrifugal force of the high-speed rotation is responsible for a compaction of the product on the walls of the rotor. Therefore, it is advised to keep the rotor turning at a speed of 5 kHz for about 1 minute to ensure that the product is well packed before increasing the rotation speed to higher values. The stability of the rotation can be supervised by the frequency line (wobble line). This line shows how strongly the signals at different frequencies are filtered inside the device. If the rotation tends to become unstable, vibrations start to appear in the line and the rotation potentially has to be stopped or increase more slowly. Rotational instabilities can be very dangerous and may cause damage to the probe, if they become too strong.

When the spinning speed has been increased to 15 kHz, the frequency line is tuned in such way that the operating frequency of the nucleus to be analyzed is filtered minimally. This is done mechanically with regulators at the bottom side of the device, for each entrance channel of the probe separately. For each channel, there are two regulators. One of them is called the *Matching* and adapts the general filtration intensity and the other one is called *Tuning* and is used to vary the minimum filtration frequency. Both regulators are not necessarily independent. Besides, if previously to an experiment a lot of variation had to be done, it is recommended to verify the frequency line after a few scans and to restart the data collection.

Having accomplished all these steps, the analysis can finally be launched. To do so, firstly the new experiment file has to be created and the experimental properties can be adapted if needed. Afterwards, different commands in TopSpin can be used to launch an analysis or multiple analyses simultaneously. When the signal collection is finished, the program is able to transform the signal into its spectrum by a Fourier transform and to do some basic operations, like multiplying by an exponential in order to vary the peak broadening and adjusting the phase of the spectrum.

4.5 Information about the different NMR experiments

In this section, more detailed information about the different experiments is provided. For the more basic experiments, the pulse sequences are given, as well as some important parameters of the experiment in general. It is important to note that only a very selective part of the parameters is shown in this report, for reasons of simplicity and because a lot of those parameters are not very significant.

4.5.1 ^{1}H MAS NMR

^{1}H MAS NMR analysis is carried out using an operating frequency of 500.13 MHz. The pulse program is similar to the one represented in **Figure 11**. The single 90° excitation pulse in the program has a power of 109.6 kHz and a pulse length (P1) of 2.3 μs. For a fixed power, the pulse length has been optimized in order to be sure to have an impulsion of 90°. Other important parameters are the recycle delay (D1), which is only 5 s due to the fast relaxation of the proton spins. The sweep width (SWH) is 0.1 MHz and in total only 16 scans (NS) are necessary.

4.5.2 ^{31}P MAS NMR

^{31}P MAS NMR analysis is carried out using an operating frequency of 202.46 MHz. The pulse program is similar to the one of the ^{1}H MAS NMR experiment represented in **Figure 11**. The single 90° pulse has a power of 68.1 kHz and a P1 of 3.7 μs. P1 has been optimized, in the same way as for ^{1}H in order to ensure that the pulse corresponds to a 90° impulsion of the ^{31}P nucleus. The SWH of the experiment equals 0.1 MHz and NS was set to 4096, but so many scans have rarely been performed. The S/N ratio increases with NS, but already with more than 256 scans, the S/N ratio was sufficient for the spectrum analysis. D1 was initially set to 30 s in order to be absolutely sure that the relaxation of the spins in the phosphorus nucleus is completed. After measuring the relaxation time of the ^{31}P nuclei by *cpxt1* experiments, it was found out that a D1 of 15 s is sufficient for the analysis of the nuclei found in the different samples. As a result, D1 was set to 15 s for further experiments.

4.5.3 ^{1}H − ^{31}P CP MAS NMR

This analysis is a cross-polarization experiment, similar to the one presented in the paragraph 2.2.2 and shown in **Figure 12**. The first pulse in the sequence is the pulse that rotates the magnetization of the protons by 90° and therefore is exactly the same as for the ^{1}H MAS NMR analysis: power of 109.6kHz and length of 2.3 μs. The next pulses are the two contact pulses of the proton and the next pulses are the two contact pulses of the proton and the ^{31}P nucleus. The contact pulse has RAMP shape (ramp10050.100). The contact pulse length is varied from 20 μs to 16000 μs. Afterwards the signal of the ^{31}P nucleus is detected with SPINAL64 decoupling of the 62.5 kHz proton power.

4.5.4 Pulse calibration experiment

The aim of this experiment is to adjust the pulse parameters, in order to have a pulse that rotates the magnetization by exactly 90°. The pulse time is varied for a given pulse intensity and the signal intensity is compared using the *parameter optimization* function of the Bruker TopSpin program. It is known that for a pulse corresponding to 90° the signal intensity is maximal, but as shown in **Figure 19**, the intensity around the maximum varies only slowly and the time corresponding exactly to a 90° pulse is therefore hard to determine. In contrast, the pulse length that gives a signal with an intensity equal to zero is easier to determine and corresponds to a 180° pulse. In consequence this pulse length is determined from the graph and the 90° pulse length is defined as half of this value.
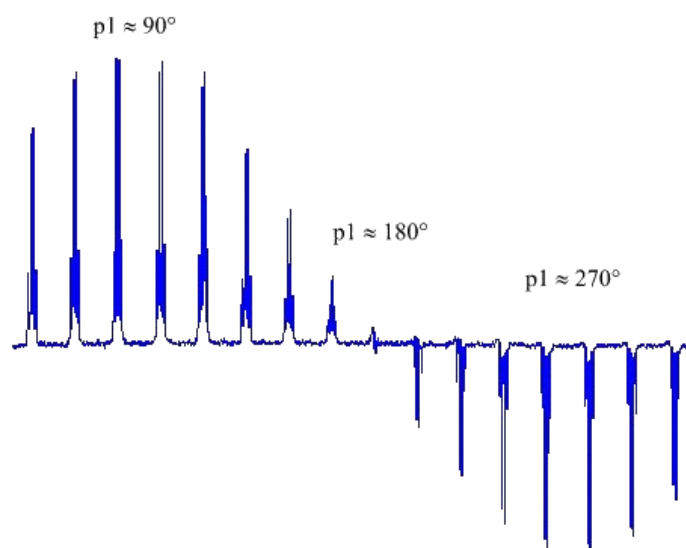
Figure 19. Example of a signal intensity vs pulse length graph of a pulse length calibration (taken from [25])

4.5.5 Inductively coupled plasma (ICP) elemental analysis

ICP elemental analysis of phosphorus has been used in order to verify the probe quantity added to the sample. In the first step, the sample is transferred into a digestion tubes and weighed, because due to the reaction with humidity, the sample mass increases during the hydration. The samples in the tubes are digested in duplicate in an HNO_3/HF environment with the help of a new generation microwave digester *Ultrawave* from *MILESTONE*.

The *Ultrawave* digestion system consists in heating up the samples, enclosed in a PTFE (Polytetrafluorethylene) reactor under pressure. The total is placed into a reactor made of steel, which is heated by a magnetron. Before the start of the digestion, the reactor is filled with nitrogen at 40 bar, in order to increase the boiling point of the solutions and to be able to close the sample tubes. This process

has several advantages compared to traditional microwaves. It allows the mineralization of bigger quantities and in a simpler acid environment and reduces the losses of volatile elements.

The digested solutions are analyzed directly by inductively coupled plasma atomic emission spectroscopy (ICP-AES). The ICP device *ARCOS* from the company *SPECTRO* is used, which is able to analyzed simultaneously different lines of the same element. The phosphorus line at 177 nm is analyzed, because it gives the best signal-to-noise ratio (SNR). Previously, a calibration for phosphorus contents from 0 to 10 ppm has been done to detect the P concentration in the sample.

5   Results

In the following, the results of the different NMR experiments are represented and analyzed. First of all, the experiments on each probe molecule and each zeolite are represented separately. Afterwards, the comparison of results is given to derive more information regarding the acidity of the zeolites and to derive a general model of the analysis.

5.1   TMPO probe molecule

According to the literature, TMPO is the most commonly used R_3PO probe molecule. For that reason, many different solid acids have been analyzed by means of this NMR method. Various properties of the molecule have been mentioned in section 4.2 and in **Table 2**. It is important to bear in mind that TMPO is the smallest of the used probe molecules and it is considered to enter into the supercages of Y type zeolites, but not the sodalities cages. However, due to hydrogen bonding even the smaller pores can be probed.

In order to have a reference spectrum, an NMR rotor is filled with pure TMPO, and the ^{31}P 15 kHz MAS NMR spectra are acquired. The TMPO is used as it is without any further treatment. Therefore, humidity can possibly influence the spectrum of TMPO due to its hygroscopic nature. The spectrum of this experiment including the fitting is demonstrated in **Figure 20**. As one can see, there are two peaks: the first one is centered at 41.5 ppm, the other one at 42.3 ppm. These results are in agreement with the data stated in the literature that claim the crystalline TMPO peak around 39 ppm and the crystalline TMPO in presence of a small amount of water, like the humidity in the air, to a peak around 41ppm [18][26]. Depending on the spectrum referencing, the chemical shift can be slightly different compared to the literature as in the this work we used a dilluted TMS in cloroform (0.1 %) as an external reference, and the chemical shifts for other nuclei were recalculated from it using Bruker macro *xiref*.
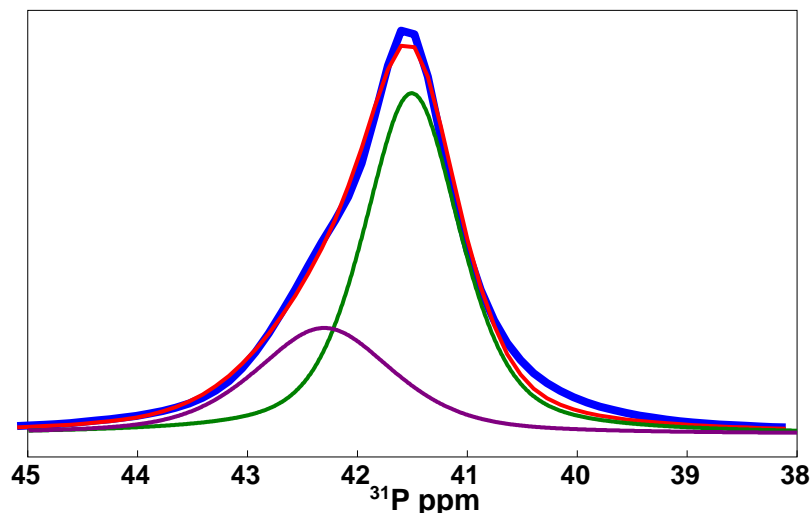
Figure 20: ^{31}P 15 kHz MAS NMR spectrum of pure TMPO, not dehydrated. Two distinct peaks can be observed. Both correspond to crystalline TMPO under the influence of humidity in a slightly different environment.

The main experiment used to determine the different acidic properties of the zeolites is ^{31}P 15 kHz MAS NMR analysis as well. All zeolites have been studied with TMPO as a probe molecule as a function of probe molecule masses, different equilibration temperatures, and with various durations of the heat treatments. The results are represented in the next chapters and the concentration of the different acid sites are calculated.

5.1.1 CBV720 analysis by TMPO

For this kind of analysis, the most distinct variations of probe molecule mass and heat treatments have been performed. An example of ^{31}P 15 kHz MAS NMR spectrum of CBV720 zeolite impregnated with TMPO probe shown in **Figure 21** (TMPO mass is 4.9 mg, zeolite mass is 43.8 mg, T is 200 °C during 2 h). In **Table 3**, the chemical shift and the peak width of the different peaks of the fitting shown in **Figure 21** are given, as well as the percentage of the total integral below the spectrum.

As one can see, there is one peak at a chemical shift of 39 ppm, filled in purple. This peak can unambiougsly be assigned to residual crystalline TMPO in the sample, as cited in many references [18][20][26]. The peak centered at a chemical shift of about 45 ppm, filled in blue, is assigned to physisorbed TMPO. This is in accordance with different refernces in the literature [18][19][27]. Moreover, the stronger the probe molecule interacts with an acid site on the zeolite, the larger the chemical shift in the ^{31}P MAS NMR spectrum. The physisorbed peak area increases remarkably with the quantity of probe molecule added to the sample, as shown further on in **Table 6**, due to the fact that physisorption does occur in multiple layers. The peak filled in green at a chemical shift around 50 ppm is attributed to TMPO

bonded to terminal silanol groups (SiOH) of the zeolite framework [20]. The bonding of TMPO to the SiOH groups is weaker compared to the bridging acid sites, shown afterwards. Accordingly, the peak is situated in between the physisorbed and the ones reacted with Brønsted acid sites. An evidence that this peak cannot be related to physisorbed TMPO is that its area is relatively independent of the quantity of TMPO added to the sample as shown in **Table 6**.
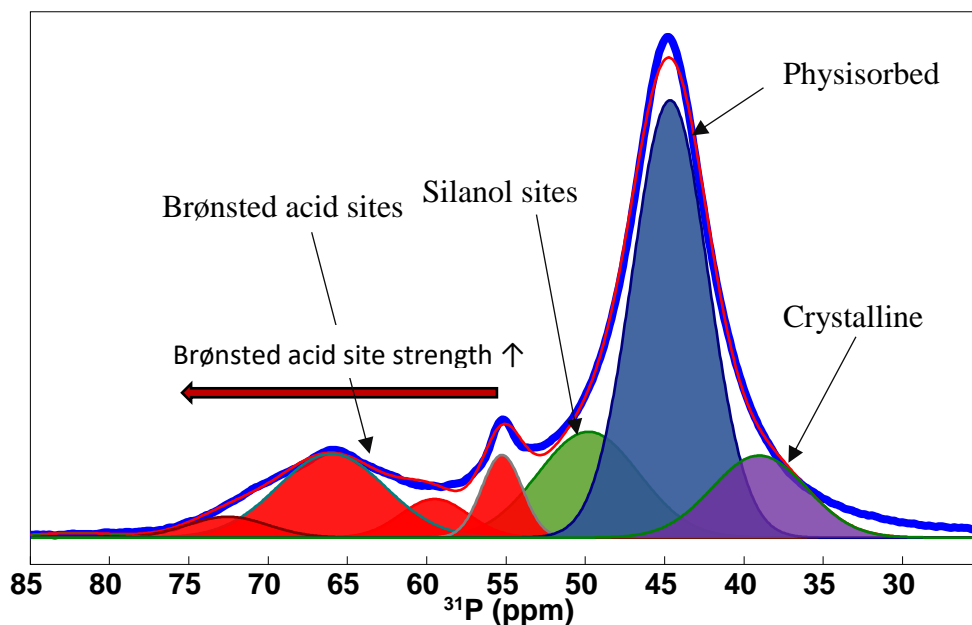
Figure 21: ^{31}P 15 kHz MAS NMR spectrum of 43.8 mg CBV720 zeolite impregnated with 4.9 mg TMPO, treated at 200 °C during 2 h. Seven peaks can be distinguished, 4 corresponding to TMPO bond to Brønsted acid sides of different strength (higher chemical shift = stronger site), one to TMPO bond to silanol groups and one each to physisorbed and bulk crystalline TMPO.

Table 3. ^{31}P 15 kHz MAS NMR chemical shift (δ), peak area and environment of the different peaks shown in **Figure 21** (sample: 4.9 mg TMPO with 43.8 mg of CBV720, treated at 200 °C during 2 h). Compared to the spectrum, one supplement peak at a high chemical shift can be seen in this table, assigned to TMPO bond to Lewis acid sites.

δ ^{31}P, ppm	Peak width, ppm	At. % peak area	Site type
39	7	11	Crystalline
44.7	5.6	48	Physisorbed
49.8	7.5	16	Silanol
55.2	3	5	Brønsted
59.5	5	4	Brønsted
66	8	13	Brønsted

72.5	6	2	Brønsted
82.1	7	1	Lewis

<center>* The type of line shape used is pure Gaussian for all fitting lines</center>

Finally, the remaining peaks, filled in read, are all attributed to TMPO bonded to acid sites of the zeolite. The four main visible peaks at chemical shifts around 55, 59.5, 66 and 72.5 ppm are all assigned to Brønsted acid sites, due to the presence of acid bridge SiOHAl groups according to reference [27]. The reaction mechanism between TMPO and those acid sites has already been presented in **Figure 16 (b)** and the different peaks correspond to acid bridge in a different environment and therefore has a different acid strength [19]. The higher the acid strength of the site, the higher is the interaction force with TMPO, leading to a higher chemical shift in the ^{31}P MAS NMR spectrum. It has been shown in ref. [18] that a linear relationship has been established between proton affinity (PA) of the acid site and the chemical shift in ppm of the peak corresponding to the Brønsted acid site.

The last peak at a very high chemical shift of about 82 ppm is less intensive. According to the literature, information pertaining to this peak is doubtful. However, using the approach explained in the paper [18] to assign the peak to the Lewis acid sites by verifying the peak dissappearence after the sample hydration, it is concluded that this peak corresponds to Lewis acid sites generated by EFAl, caused by an expulsion of Al from the framework during steaming, according to CBV sample treatment protocol [15]. The representation of the evolution of the spectrum after sample hydration at atmosphere and the analysis of the changes consists in the following. The sample shown in **Figure 21** is exposed to the atmosphere for four days at room temperature. The ^{31}P 15 kHz MAS MAS NMR spectrum of this sample, including the fitting is shown in **Figure 22** and compared to the non-hydrated spectrum. In **Table 4**, the chemical shift and the peak width of the different peaks of the fitting shown in **Figure 22** are given, as well as the percentage of the total integral below the spectrum. As one can see, the fitting is still composed of the same number of peaks, but some of them have slightly shifted in comparision with the non-hydrated spectrum due to water presence nearby the acid sites. A first thing that is observed, is the fact that the peak corresponding to residual bulk TMPO shifts from 39 ppm to around 41 ppm. This is in agreement with the experiments carried out in ref. [26] stating that after the addition of a small amount of water, the resonance peak of solid TMPO has shifted to 41 ppm. In addition, the experiments performed on crystalline TMPO, represented in **Figure 20**, also have demonstrated that crystalline, non-dehydrated TMPO has its peak at a chemical shift around 41 ppm. The peak of physisorbed TMPO is slightly shifted and the peak area of physisorbed peak has increased by 5 at.%. A first reason is purely technical due to a

fitting procedure as the shifting of the crystalline peak closer to the physisorbed eak can provoke the additional errors. Due to the fitting, the bigger physisorbed peak may take away some intensity of the smaller crystalline peak, which has diminished in comparison with the non hydrated case. Secondly, it may be possible that some of the crystalline TMPO or some of the one bonded to an acid site have dissociated and physisorbed during the hydration treatment.
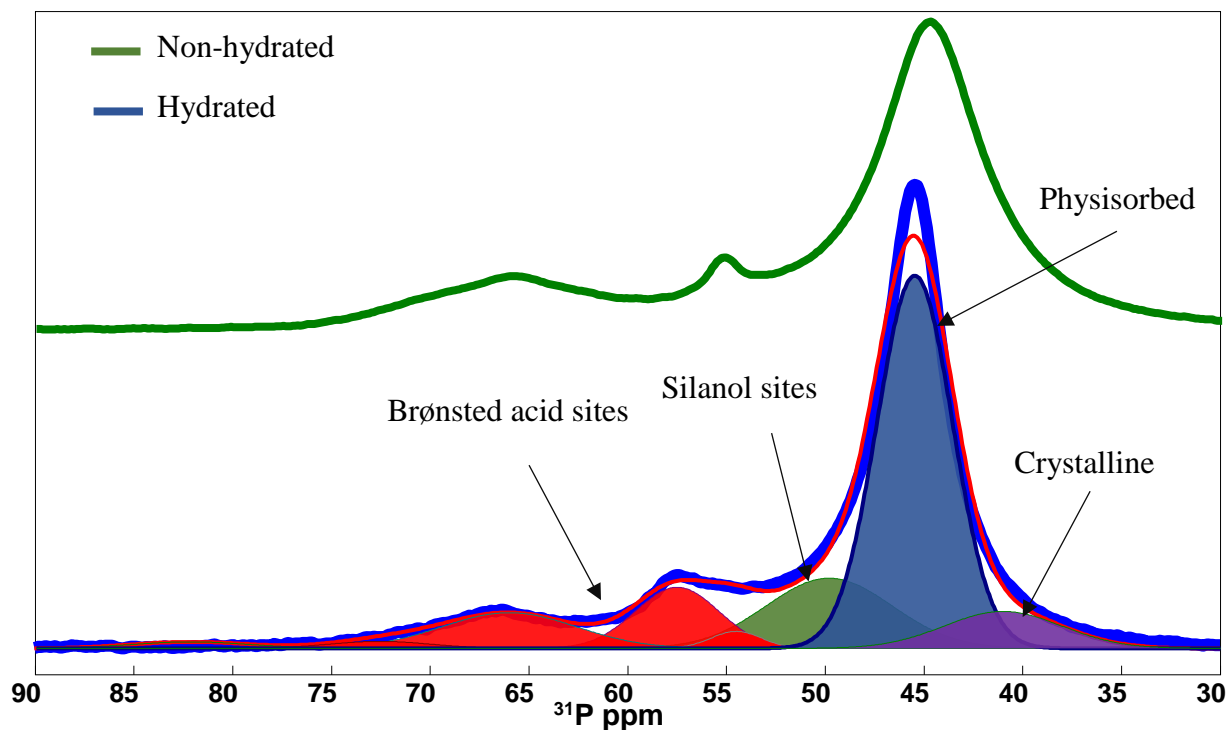
Figure 22: ^{31}P 15 kHz MAS NMR spectrum of 43.8 mg CBV720 zeolite impregnated with 4.9 mg TMPO, treated at 200 °C during 2 h, hydrated for 4 days at atmosphere (blue line); compared to the non-hydrated spectrum (green line). Observations: a) Increase of intensity of the physisorbed peak, b) Decrease of intensity of the peaks corresponding to Brønsted acid sites and silanol sites.

The remaining peaks are those of TMPO bonded to acid sites. Analyzing the sum of all acid sites, it becomes clear that it has decreased to about 22 at.%, compared to 25 at.% in the non-hydrated case. A first reason for this may be vanishment upon hydration of the peak corresponding to Lewis acid sites, situated at about 82 ppm, which is only present in a very small quantity after hydration. Another reason may be the slightly reduced amount of TMPO bonded to the four Brønsted acid sites, due to the influence of humidity. Due to the fact that the difference is quite small, it might also be possible to attribute this difference to experimental and fitting errors. Lastly, it is noticeable that the peak around 60 ppm has shifted downwards to 57.5 ppm and has increased quite a lot in intensity at the expense of the intensity

of the three others. The quite important movement during hydration from the two Brønsted peaks with the lowest chemical may be explained by their lower acid strength and a resulting stronger influence of water.

Table 4. ^{31}P 15 kHz MAS NMR chemical shift (δ), peak area and environment of the different peaks shown in **Figure 22** (sample: 4.9 mg TMPO with 43.8 mg of CBV720, treated at 200 °C for 2 h, hydrated during 4 days at atmosphere)

δ ^{31}P, ppm	Peak width, ppm	At. % peak area	Site type
41	7	8	Crystalline
45.5	4.5	53	Physisorbed
49.8	7.5	17	Silanol
54.5	3	2	Brønsted
57.5	5	10	Brønsted
66	8	9	Brønsted
72.5	6	1	Brønsted
82	7	<1	Lewis

* The type of line shape used is pure Gaussian for all fitting lines

As the different peaks have been attributed to the TMPO in different environments, the method for calculating the quantity of the TMPO in the different environments is presented. First of all, the assumptions that the whole quantity of TMPO added to the sample gives a signal in the ^{31}P MAS NMR spectrum and that the TMPO is distributed more or less homogeneously inside the rotor are done. The calculating method is based on the principle that the peak area in the spectrum is directly proportional to quantity of TMPO situated in the environment corresponding to this peak. First of all, the concentration of phosphorus C_P in mol/g$_{zeolite}$ inside the zeolite sample is calculated using the mass of the probe molecule and the zeolite added to the rotor. Afterwards, it needs to multiply by the fraction of the peak area or the peak areas, corresponding to the environment to be analyzed in order to find the desired concentration C_i, as shown in equation (19):

$$C_i = \underbrace{\frac{m_{probe}}{m_{zeolite}} * \frac{1}{M_{probe}}}_{C_P} * f_{area,i} \left(\frac{mol}{g}\right) \qquad (19)$$

with $m_{probe}, m_{zeolite}$ the mass of the probe and zeolite added to the sample, respectively, M_{probe} the molar mass of the probe (= 92 g/mol for TMPO) and $f_{area,i}$ the fraction of the peak area. According to this formula, primarily the number of acid sites is calculated, but also the quantity of silanol sites and the

amount of physisorbed and crystalline TMPO that remains in the sample can be derived. Those quantities for the sample represented in **Figure 21** and **Table 3** are shown in **Table 5** in order to estimate the order of magnitude.

Table 5. Calculation of the concentration of the different TMPO environments based on ^{31}P 15 kHz MAS NMR shown in **Figure 21** and **Table 3** (sample: 4.9 mg TMPO with 43.8 mg CBV720, treated at 200 °C during 2 h)

		Crystalline	$137\ \mu mol/g_{zeolite}$
		Physisorbed	$585\ \mu mol/g_{zeolite}$
C_P	$0.0012\ mol/g_{zeolite}$	Silanol	$189\ \mu mol/g_{zeolite}$
		Brønsted	$294\ \mu mol/g_{zeolite}$
		Lewis	$8\ \mu mol/g_{zeolite}$

The most interesting value is the concentration of acid sites of the zeolite. Due to the very small amount of Lewis acid sites, one can see that this value is almost equivalent to the number of Brønsted acid sites, which one is principally interested in. The evolution of the detected Brønsted acid site concentration as function of the quantity of the probe molecule, which changes the probe molecule to zeolite ratio, and the temperature and duration of the heat treatment is analyzed in the following. Experiments have been performed for a m_{TMPO}/m_{CBV720} ratio between 0.03 up to 0.29 and the samples have been treated at different temperatures from 150 °C up to 210 °C. Most of the time, a heat treatment of 2 h was estimated to be sufficient from the reference [22], but the influence of longer treatments has also been analyzed.

First of all, the influence of the treatment temperature is analyzed. The results for m_{TMPO}/m_{CBV720} ratios of 0.05 - 0.08, corresponding to around 2.5 mg TMPO added to the sample, and 0.11 - 0.14, corresponding to around 5 mg, are represented in **Figure 23**. A first observation is that the measured Brønsted acid site concentration is systematically superior for the cases with a higher m_{TMPO}/m_{CBV720} ratio. A second observation is the trend of observing an increased number of sites with an increasing treatment temperature. This can be explained due to the fact that with increasing temperature, the diffusion of the probe molecule is facilitated and the reactivity with the acid sites increases. The probe molecule is consequently able to access more sites. For temperatures above 210 °C, we suggest that the probe molecule is in the gaseous phase, because one is situated largely over the boiling point of TMPO. However, the pore confinement effect may influence the boiling point, especially in small micropores, which is not studied hereinafter. In addition, higher temperatures are not supported by most of the rotor

caps and there is a risk of burning the sample. One therefore considers the diffusion to be fast enough and the reactivity high enough to detect most of the sites. In the end, it is important to note that those observations are all affected by several sources of imprecisions. Errors can occur due to imprecisions during the different weightings or due to an inaccuracy of the fitting. For example, the unknown Gaussian-Lorentzian ratio of the shape of the peaks is only estimated during the fitting and can cause variations of around ±5 % of the results. Due to those imprecisions, error bars of ±5 % to each side of the measured concentration have been introduced in the graph and the tendencies may therefore be less remarkable than they seem on the first view.

Figure 23: Evolution of the measured Brønsted acid site concentration by ^{31}P 15 kHz MAS NMR for CBV720 samples impregnated with TMPO of two m_{TMPO}/m_{CBV720} ratio ranges (0.05-0.08; 0.11-0.14), as function of the treatment temperature of the sample (treatment duration 2 h). A steady increase of the detected concentration is observed for higher treatment temperatures due to enhanced diffusion and reaction with the acid sites

The next parameter to be analyzed is the influence of the heat treatment duration on the measured Brønsted acid site concentration. At temperatures of 200 °C and 210 °C and for m_{TMPO}/m_{CBV720} ratios between 0.11 and 0.13, the samples have been treated in the furnace during up to 17 h and the results are represented in **Figure 24**. Analyzing results for the samples treated at 200 °C, one can see that there is a major increase between the measured concentration for the treatment during 2 h and the one for the treatment during 4 h. Longer treatments do not seem to have an influence. The samples treated at 210 °C only have been tested for two different durations, 2 h and 4 h. A higher concentration is observed for a longer treatment duration, but considering the experimental errors, this difference is not significant.
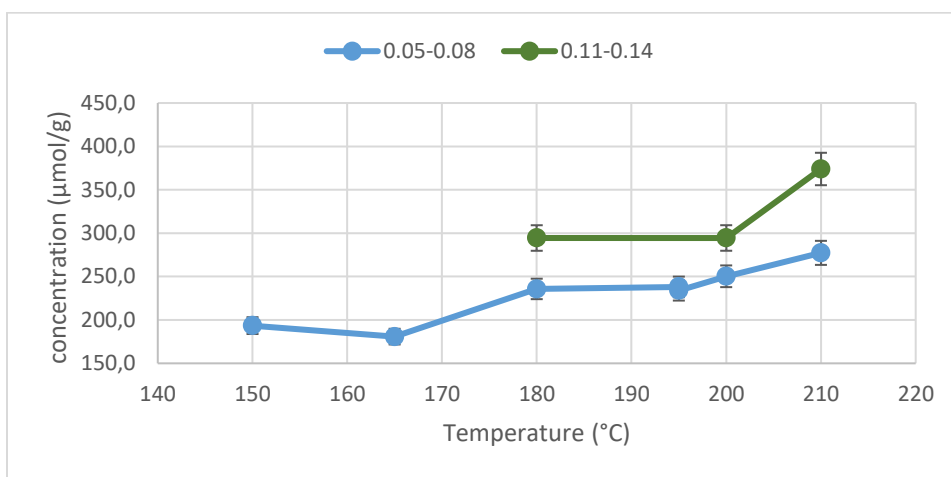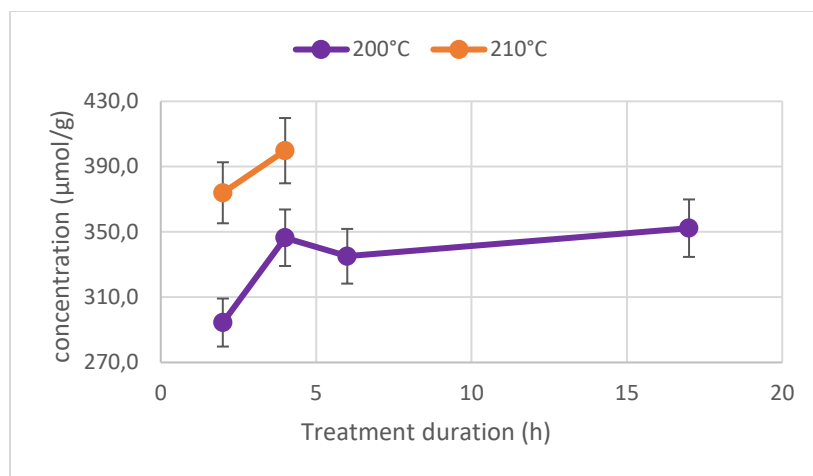
Figure 24: Evolution of the measured Brønsted acid site concentration by ^{31}P 15 kHz MAS NMR for CBV720 samples impregnated with TMPO and treated at 200 °C and 210 °C, as function of the treatment duration of the sample (m_{TMPO}/m_{CBV720} ratio of the samples: 0.11 - 0.13). Considering experimental errors: No difference is detected for treatments longer than a) 2 h at 210 °C, b) 4 h at 200 °C. Therefore, doing longer treatments is unnecessary.
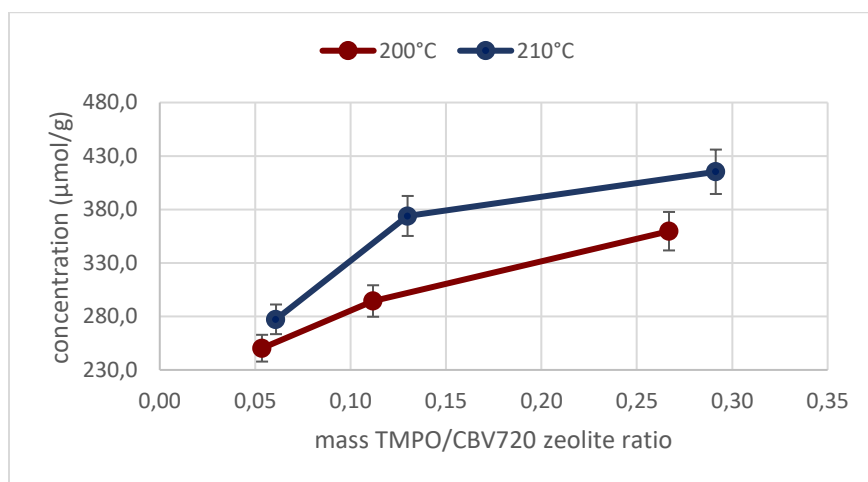
Figure 25: Evolution of the measured Brønsted acid site concentration by ^{31}P 15 kHz MAS NMR for CBV720 samples impregnated with TMPO treated at 200 °C and 210 °C, as function of the m_{TMPO}/m_{CBV720} ratio of the sample (treatment duration: 2 h). It can be seen that an increasing probe quantity results in a higher detected concentration, but the relative intensity of the Brønsted acid site peaks decreases. Therefore, an optimal value can be found.

The last factor to be analyzed is the influence of the TMPO quantity added to the sample and the resulting m_{TMPO}/m_{CBV720} ratio of the sample on the measured Brønsted acid site concentration. The influence of a m_{TMPO}/m_{CBV720} ratio varying between 0.05 and 0.29 is represented in **Figure 25**, for samples treated at 200 °C or 210 °C for 2 h. It can be seen that the measured concentration increases with the m_{TMPO}/m_{CBV720} ratio for both temperatures. The problem that occurs for too high ratios is the fact

that the signal corresponding to physisorbed and crystalline TMPO becomes more important than the signals corresponding to the Brønsted acid sites, which increases the fitting errors. Thus, an optimal probe quantity to be added can be found.

In **Figure 26**, the ^{31}P 15 kHz MAS NMR spectrum of 34.0 mg CBV720 zeolite impregnated with 9.9 mg TMPO, which corresponds to a m_{TMPO}/m_{CBV720} ratio of 0.29, treated at 210 °C during 2 h is shown including the fitting. The peak positions and widths of the peaks corresponding to the different acid sites and the silanol sites are almost the same as in the spectrum shown in **Figure 21**, corresponding to a sample with a m_{TMPO}/m_{CBV720} ratio of 0.11. However, no peak around a chemical shift of 45 ppm, previously assigned to physisorbed TMPO, can be found. On the other hand, a very tall peak can be seen at a chemical shift of 40 ppm. Due to the fact that this peak is close to the peak around 39 ppm in **Figure 21**, assigned to crystalline TMPO, it can be assumed that because of the large quantity of TMPO added to the sample, the TMPO is physisorbed in many layers and in a very large quantity. Therefore, the environment of the physisorbed TMPO gets close to the one of crystalline bulk TMPO and the peak shifts downwards. Analyzing the peak areas, it is calculated that the peak corresponding to crystalline/ physisorbed TMPO covers 78 at.% of the total integral below the spectrum, whereas the total area corresponding to Brønsted acid sites covers only 13 at.%. Due to its size, the fitting of the physisorbed peak can therefore easily influence the fitting of the Brønsted acid sites, which decreases its accuracy.
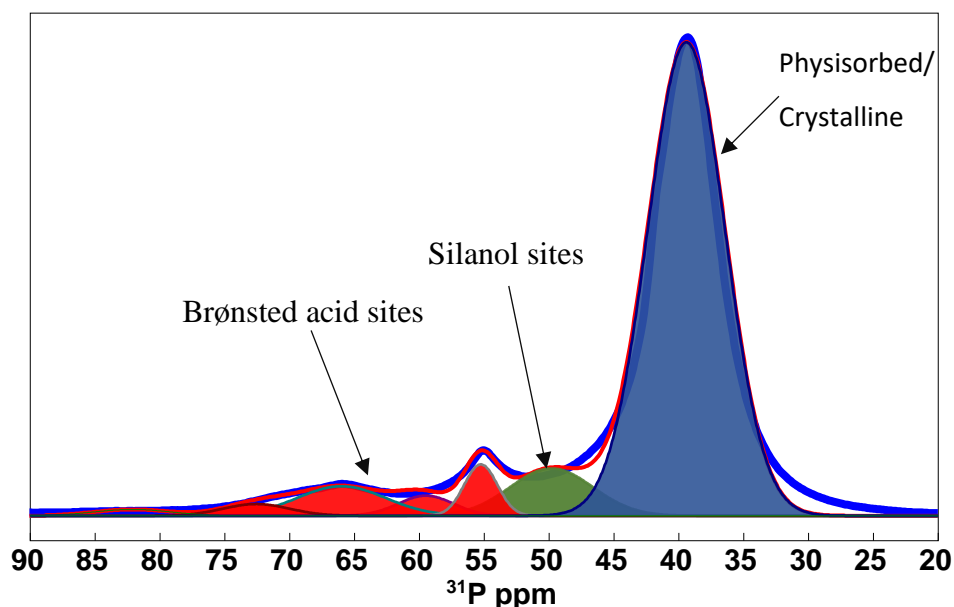

Figure 26: ^{31}P 15 kHz MAS NMR spectrum of 34.0 mg CBV720 zeolite impregnated with 9.9 mg TMPO, treated at 210 °C during 2 h. A very intense physisorbed peak justifies its attribution. In comparison, the Brønsted acid site peaks are small, which decreases their fitting accuracy.

In **Figure 27**, the ^{31}P 15 kHz MAS NMR spectrum of 41.0 mg CBV720 zeolite impregnated with 2.5 mg TMPO, which corresponds to a m_{TMPO}/m_{CBV720} ratio of 0.06, treated at 210 °C during 2 h is shown including the fitting. The peak positions and widths are almost the same for all peaks as the ones of the spectrum shown in **Figure 21**, corresponding to a sample with a m_{TMPO}/m_{CBV720} ratio of 0.11. In the spectrum, the main peak corresponds to a chemical shift of around 50 ppm (green), assigned to silanol sites. The peaks assigned to physisorbed and crystalline TMPO (blue and purple, respectively) are quite small in this spectrum, covering together only 16 at. % of the spectrum. In this case, the peaks corresponding to Brønsted acid sites (red) cover together 42 at. % of the spectrum and are therefore not all influenced by the fitting of the two previous ones. Due to the smaller intensity of the physisorbed peak, the small peak corresponding to Lewis acid sites around 82 ppm (yellow) has a higher relative intensity, too and can better be seen. The drawback of such a small m_{TMPO}/m_{CBV720} ratio is that there are only very few probe molecules in the sample and the diffusion is therefore limited. Thus, less acid sites are detected. In conclusion of the analysis of the spectra shown in **Figure 21**, **Figure 26** and **Figure 27**, a m_{TMPO}/m_{CBV720} ratio of around 0.11 was estimated to be the optimal quantity.
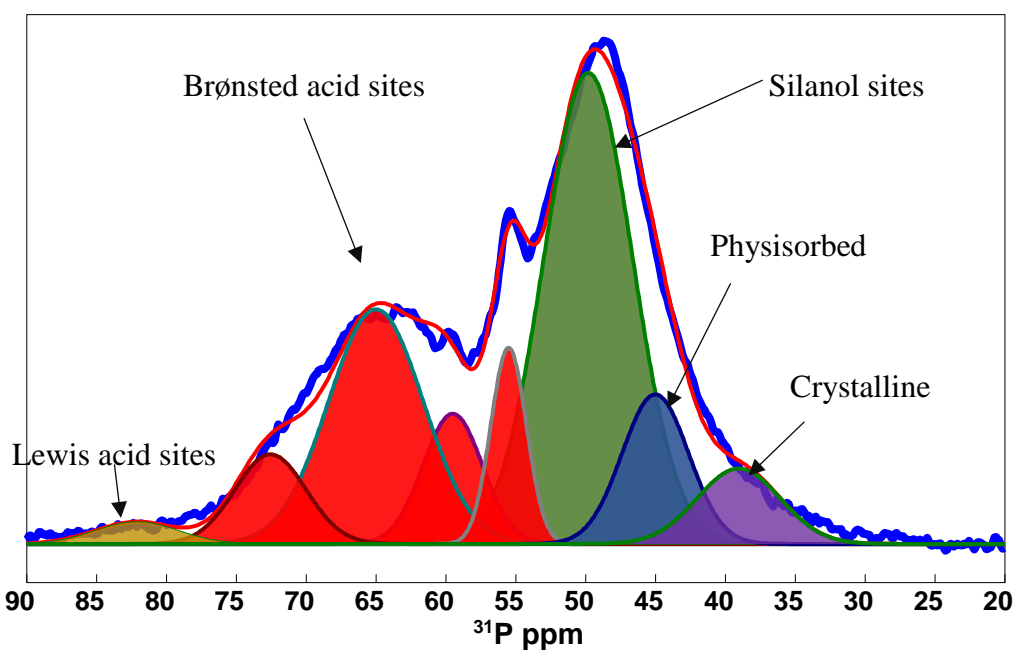

Figure 27: ^{31}P 15 kHz MAS NMR spectrum of 41.0 mg CBV720 zeolite impregnated with 2.5 mg TMPO, treated at 210 °C during 2 h. The very low intensity of the physisrobed and crystalline peaks justifies their attribution and they do not all influence the larger Brønsted acid site peaks. Their low concentration limits the probe molecule diffusion and reaction with the acid sites.

In order to quantify the effect of the m_{TMPO}/m_{CBV720} ratio in the sample on the observed concentration of all site types, the spectra shown **Figure 21**, **Figure 26** and **Figure 27** are compared in **Table 6**. As already observed in **Figure 25**, the observed concentration of Brønsted acid sites increases with an increasing m_{TMPO}/m_{CBV720} ratio. On the other hand, no global tendency of the observed concentration of silanol sites as function of the m_{TMPO}/m_{CBV720} ratio can be seen, which justifies that this peak does not correspond to physisorbed TMPO. The variations of the measured value can be explained by fitting errors due to the close proximity to the physisorbed peak, which varies very strongly in intensity. The strong increase in intensity of crystalline and physisorbed TMPO justifies the attribution of those peaks to these sites.

Table 6. Comparison of the concentration of the different TMPO sites observed by ^{31}P 15 kHz MAS NMR, represented in the spectra in **Figure 21**, **Figure 26** and **Figure 27** for different m_{TMPO}/m_{CBV720} ratios.

m_{TMPO}/m_{CBV720} ratio	0.06	0.11	0.29
Crystalline	40 $\mu mol/g_{zeolite}$	137 $\mu mol/g_{zeolite}$	2452 $\mu mol/g_{zeolite}$
Physisorbed	64 $\mu mol/g_{zeolite}$	585 $\mu mol/g_{zeolite}$	
Silanol	268 $\mu mol/g_{zeolite}$	189 $\mu mol/g_{zeolite}$	263 $\mu mol/g_{zeolite}$
Brønsted	277 $\mu mol/g_{zeolite}$	294 $\mu mol/g_{zeolite}$	415 $\mu mol/g_{zeolite}$
Lewis	12 $\mu mol/g_{zeolite}$	8 $\mu mol/g_{zeolite}$	32 $\mu mol/g_{zeolite}$

5.1.2   CBV712 analysis by TMPO

The zeolite CBV712 has a bulk Si/Al ratio of 6, whereas the previously analyzed CBV720 has a Si/Al ratio of 15. Due to this fact, CBV712 is less stable than CBV720, but should possess more Brønsted acid sites. Beside these differences, the structure of the micropores and therefore the strength of the different Brønsted acid sites and their corresponding chemical shifts should be similar [15]. Considering these facts and the different results of the CBV720 analysis by TMPO, the CBV712 has been analyzed with different m_{TMPO}/m_{CBV712} ratios.

In **Figure 28**, an example of a ^{31}P 15 kHz MAS NMR spectrum of CBV712 zeolite impregnated with TMPO probe is shown (TMPO mass is 11.7 mg, CBV712 mass is 42.2 mg, T is 210 °C during 2 h). In the left spectrum, the sample has not been hydrated, whereas the right spectrum corresponds to analysis of the same sample, hydrated for 52 h at amosphere. For the non-hydrated spectrum, the chemical shift and the peak width of the different peaks of the fitting are shown In **Table 7**, as well as the percentage of the total integral below the spectrum. For the hydrated spectrum, this deconvolution is shown in Annex 3 in **Table**

22. Comparing the non-hydrated spectrum and its fitting with the ones shown in **Figure 21** of the CBV720 zeolite analysis by TMPO, one can observe that almost all peaks are situated at a similar chemichal shift and have the same width. The only peak that is different is the peak around 42 ppm (blue), corresponding to physisorbed TMPO. This obsrevation is not extraordinary, because already when analyzing CBV720, it was found out that the position and width of this peak is quite variable as function of the m_{TMPO}/m_{CBV720} ratio. Further, the peaks assigned to crystalline TMPO have the same characteristics and the same holds for the peaks in both spectra corresponding to TMPO bond to silanol groups. On can conclude that no differences in the environment of the terminal SiOH groups in both zeolites are detected by TBPO. Finally, the different peaks assigned to Brønsted acid sites (red) are all situated within a range of ± 1 ppm in both cases. Assuming that this difference can be explained by the experimental accuracy of the NMR analysis and by imprecisions of the fitting, one can conclude that the TMPO does not detect a significant difference in the acid site strength in between both zeolites [18].
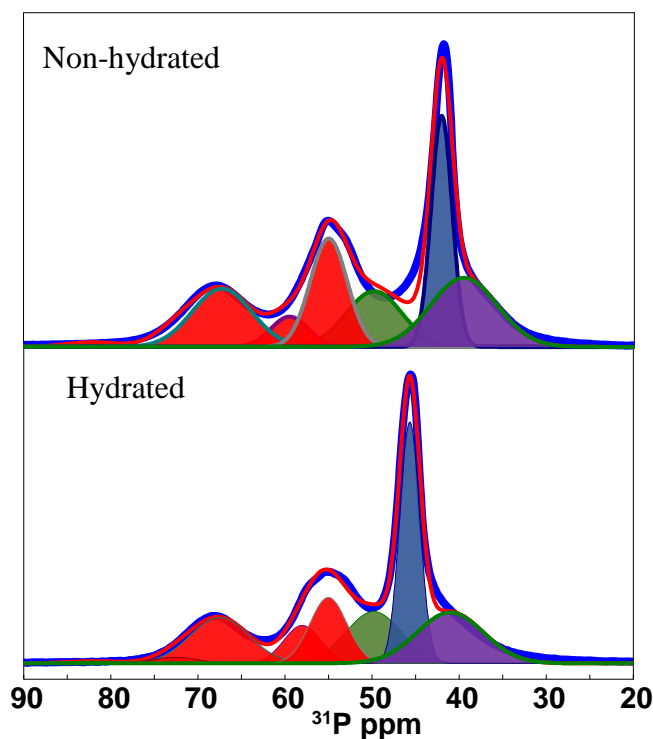
Figure 28: ^{31}P 15 kHz MAS NMR spectra of 42.2 mg CBV712 zeolite impregnated with 11.7 mg TMPO, treated at 210 °C during 2 h; Top: Non-hydrated, Bottom: Hydrated for 52 h at atmosphere. Red peaks: Brønsted acid sites, green: silanol terminal groups, blue: physisorbed TMPO, purple: crystalline bulk TMPO. The same kind of peaks can be observed as for its counterpart in the CBV720 analysis. A slight increase in intensity of physisorbed peak and decrease in intensity of Brønsted acid site peaks in the hydrated spectrum.

Table 7. ^{31}P 15 kHz MAS NMR chemical shift (δ), peak area and environment of the different peaks shown in **Figure 28**, non-hydrated (sample: 11.7 mg TMPO with 42.2 mg of CBV712, treated at 210 °C during 2 h). Compared to the spectrum, one supplement peak at a high chemical shift can be observed in this table, assigned to TMPO bond to Lewis acid sites.

δ ^{31}P, ppm	Peak width, ppm	At. % peak area	Site type
39.5	7	18	Crystalline
42.1	3	24	Physisorbed
50	7.5	15	Silanol
55	5	18	Brønsted
59.5	5	5	Brønsted
67.2	8	16	Brønsted
72.5	6	3	Brønsted
82.1	7	1	Lewis

* The type of line shape used is pure Gaussian for all fitting lines

When analyzing the ^{31}P 15 kHz MAS NMR spectrum in **Figure 28** of the hydrated sample and its fitting deconvolution shown in **Table 22** in Annex 3 and comparing them with the non-hydrated one, the observations are similar to the analysis of CBV720 impregnated with TMPO. In accordance with the literature, the peak corresponding to crystalline TMPO shifts upwards to 41 ppm [26], but remains relatively constant in intensity. Also the silanol peak keeps more or less its intensity over hydration. On the other hand, the total area of the different peaks assigned to Brønsted and Lewis acid sites have declined from 43 at. % to 38 at. %. The only acid peak that increased in intensity is the peak around 59.5ppm, which has shifted downwards during the hydration to about 58 ppm. During hydration, the probe molecules dissociated from these acid sites became physisorbed, because this peak has shifted upwards and increased in intensity.

Based on the formula (19), the data from **Table 7** can be used to calculate the concentration of the different TMPO environments that exist in the sample represented in **Figure 28**. The results are represented in **Table 8** and the main value one is interested in, is the detected concentration of the Brønsted acid sites. With 1267 $\mu mol/g_{zeolite}$, this concentration is much bigger than for the CBV720, which is in concordance with the literature [24].

Table 8. Calculation of the concentration of the different TMPO environments based on ^{31}P 15 kHz MAS NMR shown in **Figure 28** and **Table 7** (sample: 11.7 mg TMPO with 42.2 mg CBV712, treated at 210 °C during 2 h). A very high Brønsted acid site concentration can be observed.

C_P	$0.0030\ mol/g_{zeolite}$	Crystalline	$529\ \mu mol/g_{zeolite}$
		Physisorbed	$717\ \mu mol/g_{zeolite}$
		Silanol	$465\ \mu mol/g_{zeolite}$
		Brønsted	$1267\ \mu mol/g_{zeolite}$
		Lewis	$33\ \mu mol/g_{zeolite}$

In order to analyze the influence of the added probe molecule quantity, the detected Brønsted acid site concentration is compared for samples prepared with m_{TMPO}/m_{CBV712} ratios ranging from 0.12 to 0.29 and treated at a temperature around 210 °C during 2 h. As shown in **Figure 29**, the measured concentration increases systematically with increasing m_{TMPO}/m_{CBV720} ratio. This is caused by the higher TMPO content, which tends to accelerate the TMPO diffusion or increases its reactivity with the Brønsted acid site. Nevertheless, a too high TMPO quantity results in a bigger physisorbed peak, compared to the Brønsted acid site ones. This may introduce additional errors during the fitting and an optimum m_{TMPO}/m_{CBV720} ratio can be found.
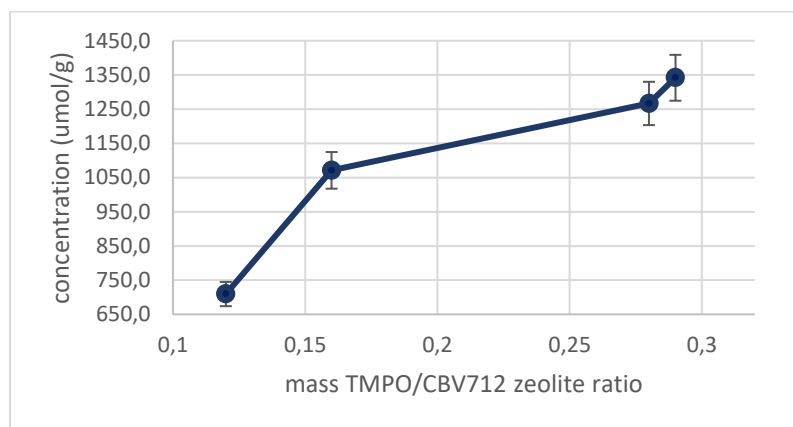
Figure 29: Evolution of the measured Brønsted acid site concentration by ^{31}P 15 kHz MAS NMR for CBV12 zeolite samples impregnated with TMPO treated at approximately 210 °C, as function of the m_{TMPO}/m_{CBV712} ratio of the sample (treatment duration: 2 h). It can be observed that an increasing probe quantity results in a higher detected Brønsted acid site concentration, due to its faster diffusion and reaction with the acid sites.

The next zeolite to be analyzed is the CBV760, which has a bulk Si/Al ratio of 30 due to its severe dealumination treatment. This makes this zeolite more stable than the two previous ones, but it should contain less Brønsted acid sites. As a reminder and as shown in the two previous paragraphs, the microporous structure of the zeolite does not change remarkably during the dealumination treatment and the Brønsted acid sites should give similar signals as for the two previous zeolites during ^{31}P 15 kHz MAS NMR analysis of 760 impregnated with TMPO [15].
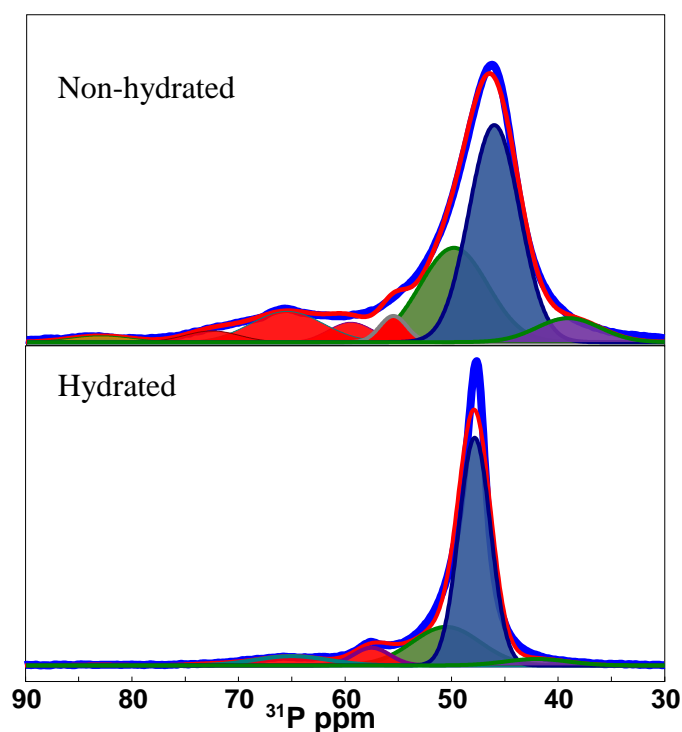
Figure 30: ^{31}P 15 kHz MAS NMR spectra of 41.9 mg CBV760 zeolite impregnated with 3.1 mg TMPO, treated at 210 °C during 2 h; Top: Non-hydrated, Bottom: Hydrated for 5 days at atmosphere. Red peaks: Brønsted acid sites, green: silanol terminal groups, blue: physisorbed TMPO, purple: crystalline bulk TMPO. The same kind of peaks can be observed as for its counterpart in the CBV720 analysis. An important increase in intensity of physisorbed peak and decrease in intensity of Brønsted acid site peaks in the hydrated spectrum.

An example of a ^{31}P 15 kHz MAS NMR spectrum of CBV760 zeolite impregnated with TMPO probe (TMPO mass is 3.1 mg, CBV760 mass is 41.9 mg, T is 210 °C during 2 h) is shown in **Figure 30**. In the same figure, this spectrum is compared to the ^{31}P 15 kHz MAS NMR spectrum of the same sample hydrated for

5 days at atmosphere. In **Table 9**, various peak properties of the spectrum the non-hydrated sample are presented, which is done in **Table 23** in Annex 3 for the hydrated one. When comparing the non-hydrated spectrum with the ones of the CBV712 and CBV720 analysis by TMPO, It can be observed that the different peaks are situated at a similar chemical shift and have a comparable width. Again, only the physisorbed peak (blue) around 46 ppm has changed considerably. The different peaks assigned to Brønsted acid sites (red) and terminal silanol groups (green) are all situated within a range of ±1.5 ppm in between the three cases. This difference can be explained by the experimental accuracy of the NMR analysis and by imprecisions of the fitting. One can conclude that the TMPO does not detect a difference in the acid site strength in between the three zeolites [18].

Table 9. ^{31}P 15 kHz MAS NMR chemical shift (δ), peak area and environment of the different peaks shown in **Figure 30** (sample: 3.1 mg TMPO with 41.9 mg of CBV760, treated at 210 °C during 2 h). Compared to the spectrum, one supplement peak at a high chemical shift can be observed in this table, assigned to TMPO bond to Lewis acid sites.

$\delta\ ^{31}P$, ppm	Peak width, ppm	At. % peak area	Site type
39	7	6	Crystalline
46	5.6	46	Physisorbed
49.8	7.5	27	Silanol
55.5	3	3	Brønsted
59.5	5	4	Brønsted
65.5	8	9	Brønsted
72.5	6	3	Brønsted
83	7	2	Lewis

* The type of line shape used is pure Gaussian for all fitting lines

When comparing the spectra of the sample before and after hydration and their peak deconvolution, it can be seen that a big part of the TMPO bond to Brønsted and Lewis acid sites has dissociated during the hydration. The result is a major increase in intensity of the peak corresponding to physisorbed TMPO. These phenomena already have been observed during the previous analyses of the other zeolites, but the effect of the hydration seems to be more severe. This may be explained by the longer hydration time but is more probably because of the better accessibility of the sites by the water due to the stronger dealumination and the resulting mesoporosity.

Table 10. Calculation of the concentration of the different types of TMPO in the sample: 3.1 mg TMPO with 41.9 mg CBV760, treated at 210 °C for 2 h. A lower Brønsted acid site concentration than of the other zeolites is observed.

		Crystalline	$52 \ \mu mol/g_{zeolite}$
C_P	$0.0008 \ mol/g_{zeolite}$	Physisorbed	$372 \ \mu mol/g_{zeolite}$
		Silanol	$217 \ \mu mol/g_{zeolite}$
		Brønsted	$150 \ \mu mol/g_{zeolite}$
		Lewis	$14 \ \mu mol/g_{zeolite}$
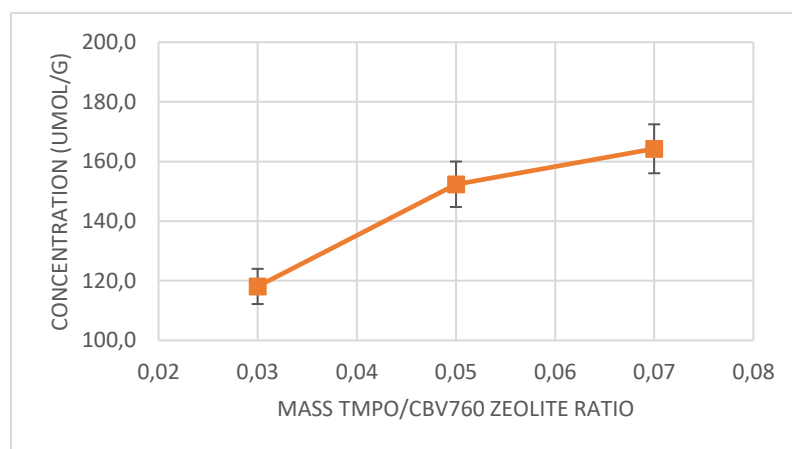
Figure 31: Evolution of the measured Brønsted acid site concentration by ^{31}P 15 kHz MAS NMR for CBV60 zeolite samples impregnated with TMPO treated at 210 °C, as function of the m_{TMPO}/m_{CBV760} ratio of the sample (treatment duration: 2 h). For lower probe quantities, an important raise in the detected acid site concentration is observed for an increasing probe content, due to an enhanced diffusion or reaction with the acid sites. For higher quantities this effect becomes insignificant.

The relative area of the different peaks shown in **Table 9** and formula (19) can be used to calculate the concentration of the different TMPO environments detected in the sample and the results are represented In **Table 10**. The main value one is interested in, is the detected concentration of the Brønsted acid sites. With $150 \ \mu mol/g_{zeolite}$, this concentration is smaller than for CBV712 and CBV720, which is in concordance with the literature. Due to the stronger dealumination, many Brønsted acid sites have disappeared from the initial zeolite [24]. In **Figure 31**, the influence on this value of the added probe molecules quantity in the sample is analyzed for m_{TMPO}/m_{CBV760} ratios ranging from 0.03 to 0.07 and treated at a temperature of 210 °C during 2 h. It can be seen that the detected Brønsted acid site concentration increases with a rising m_{TMPO}/m_{CBV760} ratio, for smaller ratios. For higher ratios, no significant difference can be observed due to the presence of the error bars. For lower ratios, the

increasing probe quantity accelerates the TMPO diffusion and the reaction with the Brønsted acid site. For higher ratios, this effect is reduced due to the relatively high porosity of the zeolite and the resulting good diffusion properties. In addition, the physisorbed peak becomes very intense compared to the ones corresponding to acid sites, which may introduce additional fitting errors. Therefore, an optimal m_{TMPO}/m_{CBV760} ratio can be found.

5.1.4 Summary and comparison of the analysis by TMPO

In this section, the concentrations of the Brønsted acid sites of diverse acid strength and of the silanol groups of the different zeolites that have been analyzed are compared. The goal of this analysis is to detect the influence of the dealumination treatment on the acidic properties of the zeolite detected by the TMPO probe molecules.

Table 11. Representation of the peak model (including tolerances) used for the determination of Brønsted acid sites and the silanol groups in USY zeolites by TMPO probe molecule. It can be seen that for some peaks quite important tolerances have to be introduced, whereas none are needed for some other peaks.

$\delta\ ^{31}P$, ppm	Peak width, ppm	Site type
49.9 ± 0.1	7.5	Silanol
55.5 ± 0.5	4 ± 1	Brønsted
59.5	5	Brønsted
66.3 ± 0.8	8	Brønsted
72.5	6	Brønsted

First of all, the peak model that has been used for the determination of Brønsted acid sites and the silanol groups in USY zeolites by TMPO probe molecule is represented in **Table 11**, including the tolerances. The model is relatively precise for some peaks and less precise for others. For example, quite big tolerances had to be introduced for the peaks arounds 55.5 ppm and 66.3 ppm for the analysis of the three different zeolites. As already cited in the beginning of this section, Zheng et al. [18]have developed a linear correlation between the ^{31}P chemical shift in a MAS NMR spectrum of TMPO absorbed on a Brønsted acid site and the proton affinity (PA) of this acid site, representing the strength of this acid site:

$$\delta^{31}P = 182.866\ (\pm 5.314) - 0.3902\ (\pm 0.020) * PA;\ R^2 = 0.9913\ (20)$$

with PA in kcal/mol. This correlation has been obtained using DFT calculation of TMPO adsorbed onto 8T aluminosilicate clusters with different bond length and therefore different acid site strength. This

correlation is assumed to be valid for the three zeolites used in this work, as it has been applied in different publications for different types of zeolites [18][19][20]. Applying this formula to the peaks assigned to Brønsted acid sites in the previous model, the PA of the different sites can be calculated. The results are represented in **Table 12**. It can be seen that the PA of the different Brønsted acid sites varies from 326 kcal/mol to 283 kcal/mol, corresponding to acid site strengths from weak, to medium and strong [21].

Table 12. Calculation of the PA of the different Brønsted acid sites, based on their chemical shift in the MAS NMR spectrum (15kHz ^{31}P): 4.9 mg TMPO with 43.8 mg CBV720, treated at 200 °C for 2 h.

$\delta\ ^{31}P$ (ppm)	PA (kcal/mol)
55.5	326
59.5	316
66.3	299
72.5	283

Table 13. Comparison of the detected concentration of the different Brønsted acid sites and the silanol groups by ^{31}P 15kHz MAS NMR for the different zeolites with TEPO as probe, treated at 210 °C for 2 h.

		Concentration of the site in the zeolite , $\mu mol/g_{zeolite}$		
$\delta\ ^{31}P$, ppm	Site type	CBV712	CBV720	CBV760
49.9 ± 0.1	Silanol	465	230	216
55.5 ± 0.5	Brønsted	142 (17)	72 (19)	24 (14)
59.5	Brønsted	46 (6)	60 (16)	31 (19)
66.3 ± 0.8	Brønsted	550 (66)	195 (52)	75 (46)
72.5	Brønsted	90 (11)	47 (13)	20 (13)
Total Brønsted acid site concentration		827	374	164

* The value in the parentheses represents the percentage of the total acidity contributed by this site

In **Table 13**, an overview of the detected concentration by ^{31}P 15kHz MAS NMR of the different Brønsted acid sites and of the terminal silanol groups is given for the different zeolites with TMPO as probe, treated at 210 °C for 2 h. It is important to remember that the detected concentrations vary in function of the added probe quantity, as shown in **Figure 25**, **Figure 29** and **Figure 31** for the detected Brønsted acid site concentration. Nevertheless, the order of magnitude remains the same and the results are sufficient in order to analyze the global tendencies. It can be observed that the detected Brønsted

acid site concentration reduces with increasing severity of the dealumination treatment and therefore with an increasing Si/Al ratio, which is in accordance with the literature [15][24]. In [24], a higher silanol terminal group concentration was detected for less dealuminated zeolites. This tendency is also observed in **Table 13**, even if the values of CBV720 and CBV760 are very close compared to the one of CBV712. One has to mention that those values are very likely to be influenced by fitting errors, due to the close proximity of the peak to the strong intensity peak assigned to physisorbed TMPO.

5.2   TEPO probe molecule

In the literature, TEPO is not commonly used as probe molecule and thus only few solid acids have been analyzed by means of this NMR method. Various properties of the molecule have been mentioned in section 4.2 and in **Table 2**. It is important to remind that TEPO is the second smallest of the used probe molecules and it is considered to enter into the supercages of Y type zeolites, but not the sodalities cages. However, due to hydrogen bonding even the smaller pores can be probed.
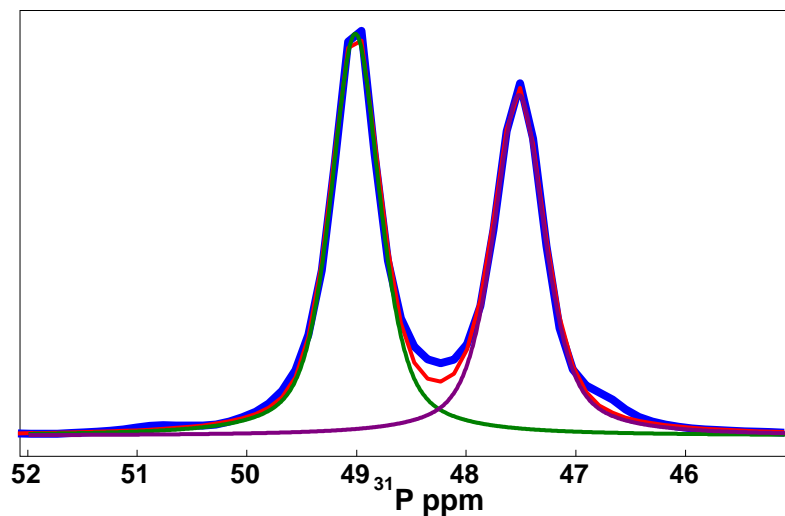
Figure 32: ^{31}P 15kHz MAS NMR spectrum of pure TEPO, partly dehydrated. The two peks correspond to crystalline TEPO, but one of them is shifted due to the influence of humidity

In order to have a reference spectrum, an NMR rotor is filled with pure TEPO, and the ^{31}P 15 kHz MAS NMR spectra are acquired. Due to its very hygroscopic nature, TEPO cannot be used at atmosphere and without any further treatment, it liquefies when pushed into the rotor. Therefore, the probe molecule has been dehydrated under vacuum at 25 °C for 2 h. Due to the fact that TEPO was in the form of large agglomerates, humidity possibly influences the spectrum. In order to reduce further the influence of humidity, the TEPO is kept under nitrogen atmosphere before performing the experiments. The spectrum

of the ^{31}P 15 kHz MAS NMR experiment including the fitting is demonstrated in **Figure 32**. As one can see, there are two peaks: the first one is centered at 47.5 ppm, the other one at 49.0 ppm. These results are in agreement with literature data that claim the crystalline TEPO peak around 48 ppm [20]. One of both peaks is probably due to the remaining influence of humidity. Depending on spectrum referencing, the chemical shift can be slightly different compared to the literature as in this work we used a dilluted TMS in cloroform (0.1 %) as an external reference, and the chemical shifts for other nuclei were recalculated from it using Bruker macro *xiref*.

The main experiment used to determine the different acidic properties of the zeolites is ^{31}P 15 kHz MAS NMR analysis as well. All zeolites have been studied with TEPO as a probe molecule and at different equilibration temperatures. The results are represented in the next chapters and the concentration of the different acid sites are calculated.

5.2.1   CBV720 analysis by TEPO
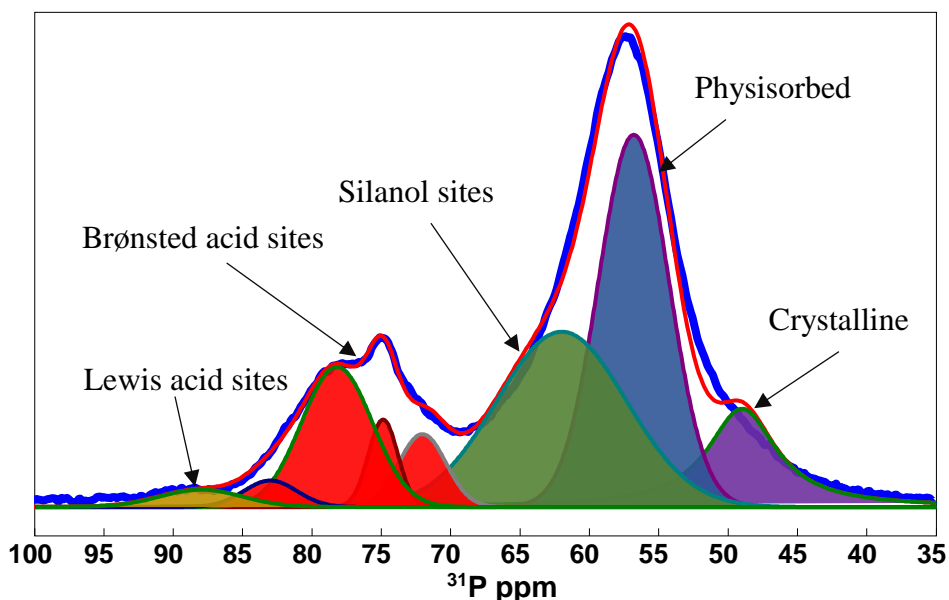
Figure 33: ^{31}P 15 kHz MAS NMR spectrum of 39.8 mg CBV720 zeolite impregnated with 5.1 mg TEPO, treated at 210 °C during 2 h. Eight peaks can be distinguished, 4 corresponding to TEPO bond to Brønsted acid sides of different strength (higher chemical shift = stronger site), one each to TEPO bond to silanol groups and Lewis acid sites and to physisorbed and bulk crystalline TEPO.

In order to attribute the different peaks that can be observed during the analysis of zeolites impregnated with TEPO, an example of ^{31}P 15 kHz MAS NMR spectrum of CBV720 zeolite impregnated

with TEPO probe shown in **Figure 33** (TEPO mass is 5.1 mg, zeolite mass is 39.8 mg, T is 210 °C during 2 h).

In **Table 14**, the chemical shift and the peak width of the different peaks of the fitting shown in **Figure 33** are given, as well as the percentage of the total integral below the spectrum.

As one can see, there is one peak at a chemical shift of 49 ppm, filled in purple. This peak can be assigned to residual crystalline TEPO in the sample, as cited in the reference [20] and as observed in **Figure 32**. The peak centered at a chemical shift of 56.8 ppm, filled in blue, is assigned to physisorbed TEPO. This attribution is made due to the fact that a stronger interaction of the probe molecule with an acid site on the zeolite results in a larger the chemical shift in the ^{31}P MAS NMR spectrum, similar to the observations of the analysis with TMPO. In addition, this peak area deceases with increasing treatment temperature, as shown further on in **Figure 34**, due to the fact that at higher temperature the probe diffusion and reaction with the acid sites is enhanced. The peak filled in green at a chemical shift around 62 ppm is attributed to TEPO bonded to terminal silanol groups (SiOH) of the zeolite framework. . The bonding of TEPO to the SiOH groups is less strong compared to the bridging acid sites. Similarly to TMPO, the peak is situated in between the physisorbed and the ones reacted with Brønsted acid sites. As cited in [24], two different types of silanol groups exist in the CBV zeolites, bonded to different Si sites. Analyzing the spectrum, it can be argued that the single silanol peak can be replaced by two different ones around this peak. Nevertheless, in order to comply with the analysis by TMPO and because the precise determination of the silanol sites is not required, just a single peak is used in the fitting.

Table 14. ^{31}P 15 kHz MAS NMR chemical shift (δ), peak area and environment of the different peaks shown in **Figure 33** (sample: 5.1 mg TEPO with 39.8 mg of CBV720, treated at 210 °C during 2 h).

δ ^{31}P, ppm	Peak width, ppm	At. % peak area	Site type
49	6	13	Crystalline
56.8	6	34	Physisorbed
62	11	29	Silanol
72	4	4	Brønsted
74.9	2.5	3	Brønsted
78.2	6	13	Brønsted
83	4.5	2	Brønsted
88	7	2	Lewis

* The type of line shape used is pure Lorentzaian for the crystalline fitting line an pure Gaussian for the others

Finally, the remaining peaks, filled in red, are all attributed to TEPO bonded to acid sites of the zeolite. The four main visible peaks at chemical shifts around 72, 74.9, 78.2 and 83 ppm are assigned to Brønsted acid sites, due to the presence of acid bridge SiOHAl groups. The reaction mechanism between TEPO and those acid sites is the same as for TMPO, represented in **Figure 16 (b)**. The different peaks correspond to acid bridges in a different environment, which gives them a different acid site strength [19]. The higher the acid strength of the site, the higher the interaction force with TEPO, which leads to a higher chemical shift in the ^{31}P MAS NMR spectrum. It has been mentioned in ref. [18] that a linear relationship has been established between proton affinity (PA) of the acid site and the chemical shift in ppm of the peak corresponding to the Brønsted acid site.

The attribution of the less intensive peak at a very high chemical shift of about 88 ppm is conducted using the observations made in chapter 5.1.1 about the CBV720 analysis by TMPO, because no information about this peak could be found in literature. By verifying the peak dissappearence after the sample hydration as explained in the paper [18], it is concluded that this peak corresponds to Lewis acid sites generated by EFAl, caused by expulsion of Al from the framework during steaming, according to CBV sample treatment protocol [15]. The ^{31}P 15 kHz MAS MAS NMR spectrum including the fitting of the sample shown in **Figure 33** after hydration at atmosphere for eight days at room temperature is shown in Annex 3 in **Figure 50**, as well as the infromation about the peaks of the fitting in **Table 24**. The most important observation is the almost complete disappeareance of the Lewis acid site peak, which justifies its attribution. Also the other variations that can be observed in between the spectra before and after hydration are similar to the ones that have been made during the analysis with TMPO as probe. The main observations are an important overall decrease in intesity of the peaks assigned to TEPO bond to the different acid sites and the terminal silanol groups. The dissociation of these TEPO molecules has caused a major increase in intensity of the physisorbed peak, which also has shifted upwards. Globally seen, one can say that the effect of hydration is more severe than in the case of the CBV720 analysis by TMPO. This may be due to the longer hydration time, but also due to the higher hygroscopy of the TEPO molecules, as observed during the sample preparation.

Now that he different peaks have been attributed to the TEPO in different environments, equation (19) can be used to calculate the concentration of TEPO in the different environments. In this case, the molar mass of the probe equals M_{TEPO} = 134 g/mol. Using the relative peak areas given in **Table 14** of the different peaks shown in **Figure 33**, primarily the number of acid sites is calculated, but also the quantity of silanol sites and the amount of physisorbed and crystalline TEPO that remains in the sample are shown in **Table 15**.

Table 15. Calculation of the concentration of the different TEPO environments based on ^{31}P 15 kHz MAS NMR shown in **Figure 33** and **Table 14** (sample: 5.1 mg TEPO with 39.8 mg CBV720, treated at 210 °C during 2 h). A lower Brønsted acid site concentration is observed, compared to the CBV720 analysis by TMPO.

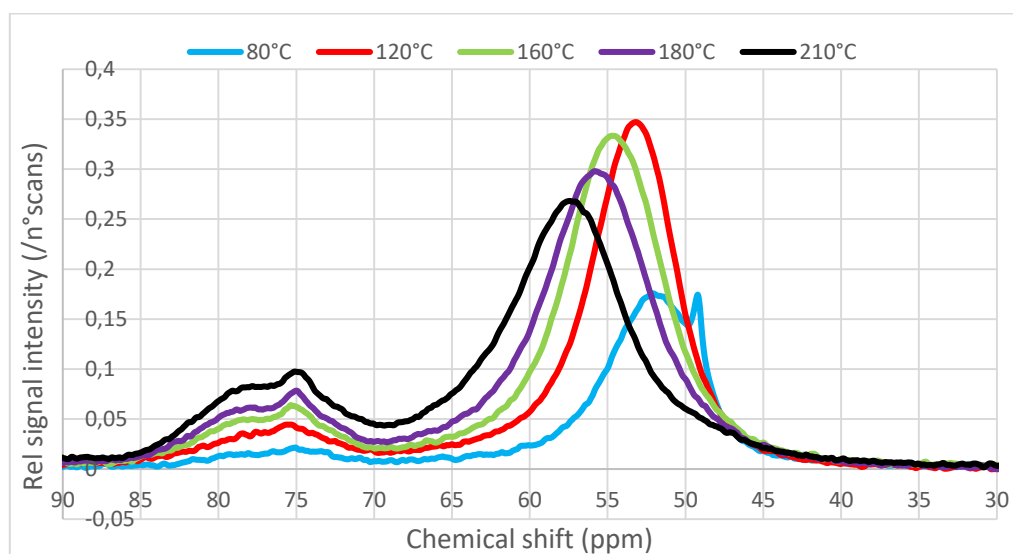|		Crystalline	$124 \; \mu mol/g_{zeolite}$
		Physisorbed	$325 \; \mu mol/g_{zeolite}$
C_P	$0.0010 \; mol/g_{zeolite}$	Silanol	$277 \; \mu mol/g_{zeolite}$
		Brønsted	$210 \; \mu mol/g_{zeolite}$
		Lewis	$20 \; \mu mol/g_{zeolite}$

Figure 34: Evolution of the measured Brønsted acid site concentration by ^{31}P 15 kHz MAS NMR for a sample of 39.8 mg CBV720 impregnated with 5.1 mg TEPO as function of the treatment temperature of the sample (treatment duration 2 h at each temperature). The peaks corresponding to Brønsted acid sites and silanol terminal groups increase steadily with the treatment temperature, due to the faster diffusion and reaction with the acid sites at higher temperatures. The peak of physisorbed TEPO shifts upwards and decreases in intensity.

The value one is primarily interested in is the detected concentration of Brønsted acid sites, namely 210 $\mu mol/g_{zeolite}$. The evolution of this value, detected by ^{31}P 15 kHz MAS NMR of 39.8 mg CBV720 impregnated with 5.1 mg TEPO, as function of the treatment temperature is analyzed in **Figure 34** for temperatures ranging from 80 °C to up to 210 °C. No temperatures above 210 °C have been tested due to the limitations of the rotor caps and the risk of burning the sample. First of all, it has to be mentioned that the total signal intensity for a treatment at 80 °C is visibly much lower than for higher treatment

temperatures. This can be explained by residual TEPO in the bottom of the rotor due to slow diffusion at such a low temperature that only gives a less intense signal during the NMR analysis. For the other spectra a steady increase of the detected Brønsted acid site concentration can be observed, which can be explained by faster diffusion and reaction with the acid sites at higher temperatures. The same applies for the peak attributed to silanol around 62 ppm. On the other hand, the peak assigned to physisorbed TEPO moves from about 53 ppm to 57 ppm with higher treatment temperatures and decreases in intensity. Those phenomena are an additional evidence for the attribution of those two peaks.

By analyzing the absolute integral value evolution of the lines associated with Brønsted acid sites, one can draw some conclusions on diffusion limitations. In this part, it is assumed that a 2 h treatment is enough to equilibrate the sample. The Arrhenius plot of the absolute integral of Brønsted acid sites is displayed in **Figure 35**: On the X axis is inverse absolute temperature (1/K) and on the Y axis is the natural logarithm of the absolute intensity in a.u. A linear dependency is observed and the activation energy can simply be recalculated from the slope of the curve by multiplying its modulus by the universal gas constant R = 8.314 J/(mol*K). This operation provide a value of 4.5 ± 0.4 kcal/mol, which corresponds to microporous materials with pore sizes less than 1 nm, according to [28].
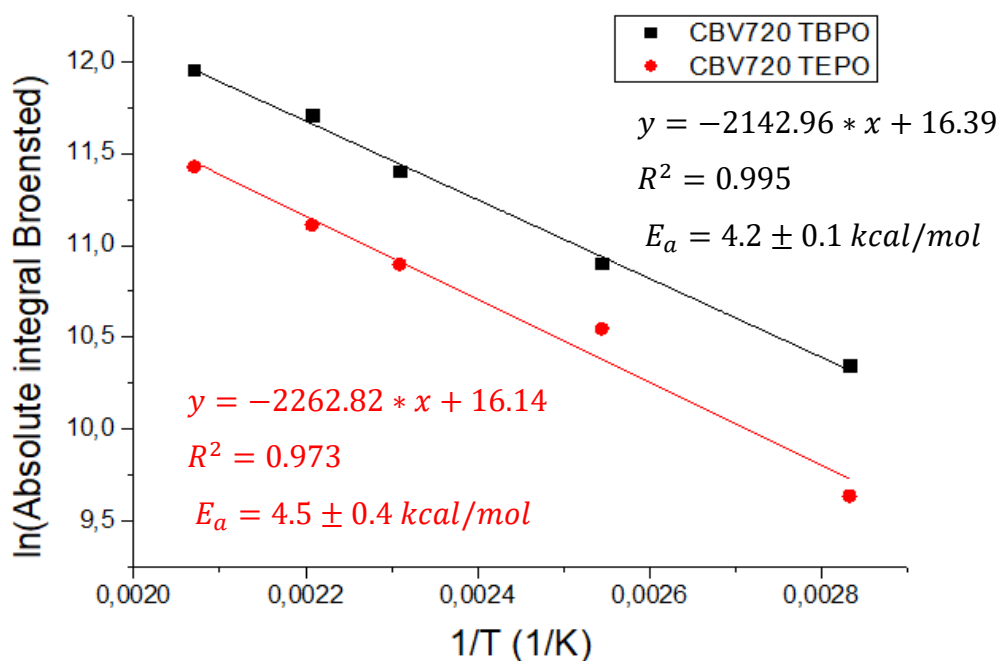

Figure 35: Arrhenius plot of the absolute integral of Brønsted acid sites in **Figure 34** (CBV720 impregnated with TEPO) and **Figure 39** (CBV720 impregnated with TEPO). X axis: inverse absolute temperature (1/K); Y axis: natural logarithm of the absolute intensity in a.u. A linear correlation is found and the activation energy is calculated.

5.2.2   Summary and comparison of the CBV720, CBV712 and CBV760 analysis by TEPO

In **Figure 36**, the ^{31}P 15 kHz MAS NMR spectra of the analysis of the three different zeolites impregnated with TEPO are shown. The spectrum of CBV720 with the fitting has already been shown in the previous paragraph, whereas the spectra of the two other zeolites impregnated with TEPO can be found in Annex 3 including the detailed fitting.
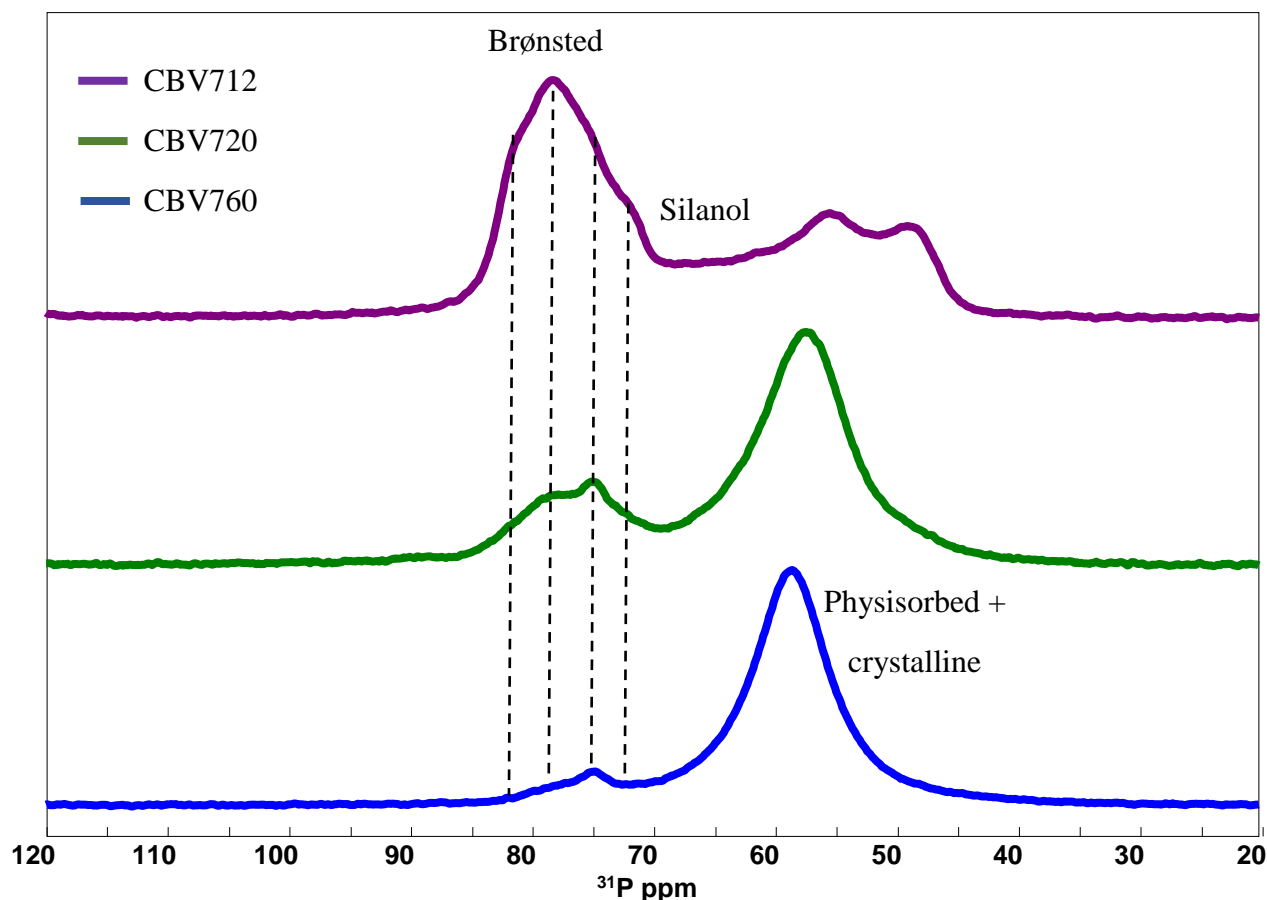
Figure 36: Comparison of the ^{31}P 15 kHz MAS NMR spectra of three different zeolites impregnated with TEPO. Purple: 44.0 mg CBV712, 8.8 mg TEPO; Green: 39.8 mg CBV720, 5.1 mg TEPO; Blue: 44.4 mg CBV760, 3.0 mg TEPO. Brønsted acid site peak intensity (72 ppm – 83 ppm): CBV712 > CBV720 > CBV760. The spectra are normalized on maximal intensity.

When analyzing the different spectra shown in **Figure 36**, it can be seen that the different peaks are all situated at a similar chemical shift and seem to have the same shape. The most important observation that can be made is the variation in intensity of the peaks in between 72 ppm and 83 ppm, corresponding to TEPO bond to Brønsted acid sites. The intensity of the peaks increases with decreasing Si/Al ratio of the

zeolites, which has already been observed during the analysis of the zeolites impregnated with TMPO. On the other hand, the intensity of the peak corresponding to terminal silanol groups around 62.5 ppm remains relatively constant. Conclusions about the peaks corresponding to physisorbed and crystalline TEPO are difficult to make, because their intensities strongly depend on the added amount of probe molecule. The samples of CBV712 and CBV760 impregnated with TEPO have also been analyzed after hydration at atmosphere and the spectra are represented in Annex 3. The observations are very similar to the ones of CBV720 impregnated with TEPO, except that the dissociation of TEPO bond to the acid sites is more severe for CBV760 and less severe for CBV712. This can be explained by the higher mesoporosity in the zeolites with a higher Si/Al ratio, which gives a better accessibility of the sites by water [15]. As for CBV720 in **Figure 34**, also for CBV712 and CBV760 the influecne of an increasing treatment temperature has been tested. The evolution of those spectra is shown in **Figure 53** and **Figure 56** in Annex 3 and the observations are similar to the analysis of CBV720.

As seen in **Figure 36**, the peaks corresponding to TEPO bond to Brønsted acid sites and terminal silanol groups have similar characteristics, which is verified by the peak deconvolution of those spectra. Therefore, a peak model for the analysis of USY zeolites with TEPO as probe molecule can be set up and is represented in **Table 16** including the tolerances. The model seems to be very precise and only for one peak a relatively big tolerance of 0.5 ppm was introduced for the analysis of the three different zeolites. Considering the linear relationship between the chemical shift of TEPO bond to a Brønsted acid site and the proton affinity of this acid site introduced in [18], one can conclude that the TEPO does not detect a difference in the acid site strength as function of the dealumination treatment of the USY zeolites. Unfortunately, only one experiment has been performed per zeolite, which means that the reproducibility of the model cannot been verified. From a graph shown in ref. [18], an approximative equation of this linear correlation can be derived:

$$\delta^{31}P = 214.22 - 0.47 * PA \qquad (21),$$

with PA in kcal/mol and $\delta^{31}P$ in ppm. The results are represented in **Table 16**. It can be seen that the PA of the different Brønsted acid sites varies from 303 kcal/mol to 278 kcal/mol, corresponding to acid site strengths from medium to strong [21].Comparing these results with the ones of TMPO, it can be seen that TEPO detects the acids sites to be slightly stronger. This difference can arise from the basicity of the molecules or it can be due to the fact that those correlations give only an approximation of the PA and are not totally correct for Y zeolites.

Table 16. Representation of the peak model (including tolerances) used for the determination of Brønsted acid sites and the silanol groups in USY zeolites by TEPO probe molecule

$\delta\ ^{31}P$, ppm	Peak width, ppm	PA, kcal/mol	Site type
62.5	11	/	Silanol
72	4	303	Brønsted
74.9	2.5	296	Brønsted
78.1 ± 0.1	6	290	Brønsted
83.5 ± 0.5	4.5	278	Brønsted

In order to numerically quantify the measured concentration of the different Brønsted acid sites and the silanol groups, equation (19) and the relative area of the different peaks are used to calculate those concentrations. The results are represented in **Table 32** for the ^{31}P 15kHz MAS NMR analysis of the different zeolites with TEPO as probe, treated at 210 °C for 2 h. As already observed during the analysis with TMPO as probe, the detected Brønsted acid site concentration reduces with increasing severity of the dealumination treatment and therefore with an increasing Si/Al ratio, which is in accordance with the literature [15][24]. During the analysis with TMPO as probe molecule and in [24], a higher silanol terminal group concentration was detected for less dealuminated zeolites. This tendency cannot be observed for the CBV712 zeolite in **Table 32**. However, only a single sample has been tested and when analyzing the results of the same samples treated at 180 °C and 160 °C, a silanol site concentration of about 380 $\mu mol/g_{zeolite}$ was detected. This tendency therefore has to be tested with further experiments in order to be verified. It is important to remember that the detected concentrations vary as according to different parameters, such as the added probe quantity and the heat treatment. Nevertheless, it is assumed that the orders of magnitude remain the same and the results are sufficient in order to analyze the global tendencies.

Table 17. Comparison of the detected concentration of the different Brønsted acid sites and the silanol groups by ^{31}P 15kHz MAS NMR for the different zeolites with TEPO as probe, treated at 210 °C for 2 h.

$\delta\ ^{31}P$, ppm	Site type	Concentration of the site in the zeolite , $\mu mol/g_{zeolite}$		
		CBV712	CBV720	CBV760
62.5	Silanol	266	278	166
72	Brønsted	142 (17)	42 (20)	10 (21)
74.9	Brønsted	46 (6)	32 (15)	11 (24)

78.1 ± 0.1	Brønsted	550 (66)	121 (57)	23 (52)
83.5 ± 0.5	Brønsted	90 (11)	17 (8)	1 (3)
Total Brønsted acid site concentration		827	212	45

* The value in the parentheses represent the percentage of the total acidity contributed by this site

5.3   TBPO probe molecule

In literature, TBPO is the second most used R_3PO probe molecule. Various properties of the molecule have been cited in section 4.2 and in **Table 2**. It is important to remember that TBPO has a kinetic diameter of 0.82 nm and is therefore considered not to enter either the supercages or the sodalite cages of the zeolite as shown in **Figure 14**. However, due to hydrogen bonding even the smaller pores can be probed.

In order to have a reference spectrum, an NMR rotor is filled with pure TBPO, and the ^{31}P 15 kHz MAS NMR spectra are acquired. The TBPO is used as it is without any further treatment. Therefore, there is a possible influence of humidity on the spectrum of TBPO hygroscopic nature. The spectrum of this experiment including the fitting is demonstrated in **Figure 37**. As one can see, there are two peaks: the first one is centered at 44.8 ppm, the other one at 45.4 ppm. In literature, crystalline TBPO is associated to a peak around 47 ppm [18][20][29]. This difference of about 2 ppm is quite important and may partially depend on spectrum referencing, as in this work we used a dilluted TMS in cloroform (0.1 %) as an external reference, and the chemical shifts for other nuclei were recalculated from it using Bruker macro *xiref*.
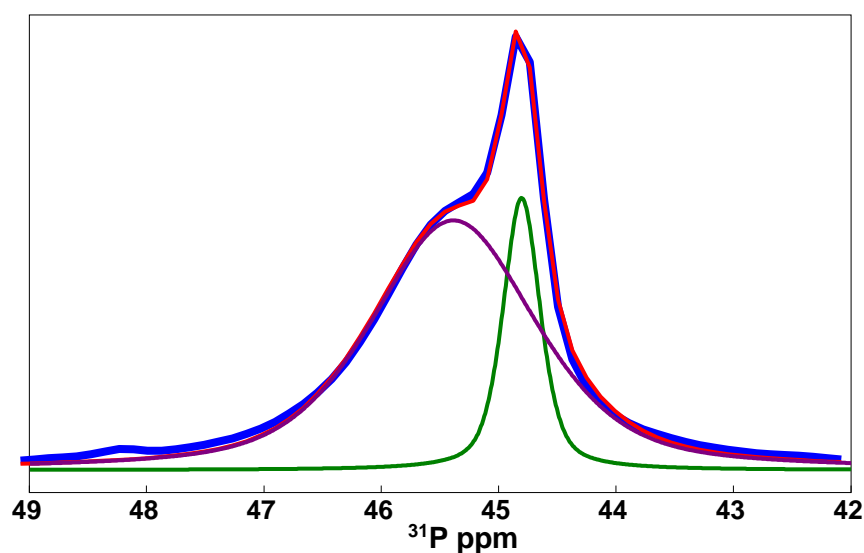

Figure 37: ^{31}P 15kHz MAS NMR spectrum of pure TBPO, not dehydrated. Two peaks can be observed, one corresponds to crystalline TBPO and the other one to TBPO under the influence of humidity.

All different zeolites have been analyzed with TBPO as probe molecule for various probe molecule masses and treated in the furnance at different temperatures and with different durations of the heat treatments. The results are represented in the next chapters and the concentration of the different acid sites are calculated using ^{31}P 15kHz MAS NMR analysis.

5.3.1 Summary and comparison of the analysis by TBPO of CBV712, CBV720 and CBV760

In this section, the ^{31}P 15 kHz MAS NMR spectra of the different zeolites impregnated with TBPO as probe and the detected concentration Brønsted acid sites of diverse acid strength and of the silanol groups are compared. The goal of this analysis is to detect the influence of the dealumination treatment on the acidic properties of the zeolite detected by the TBPO probe molecules.

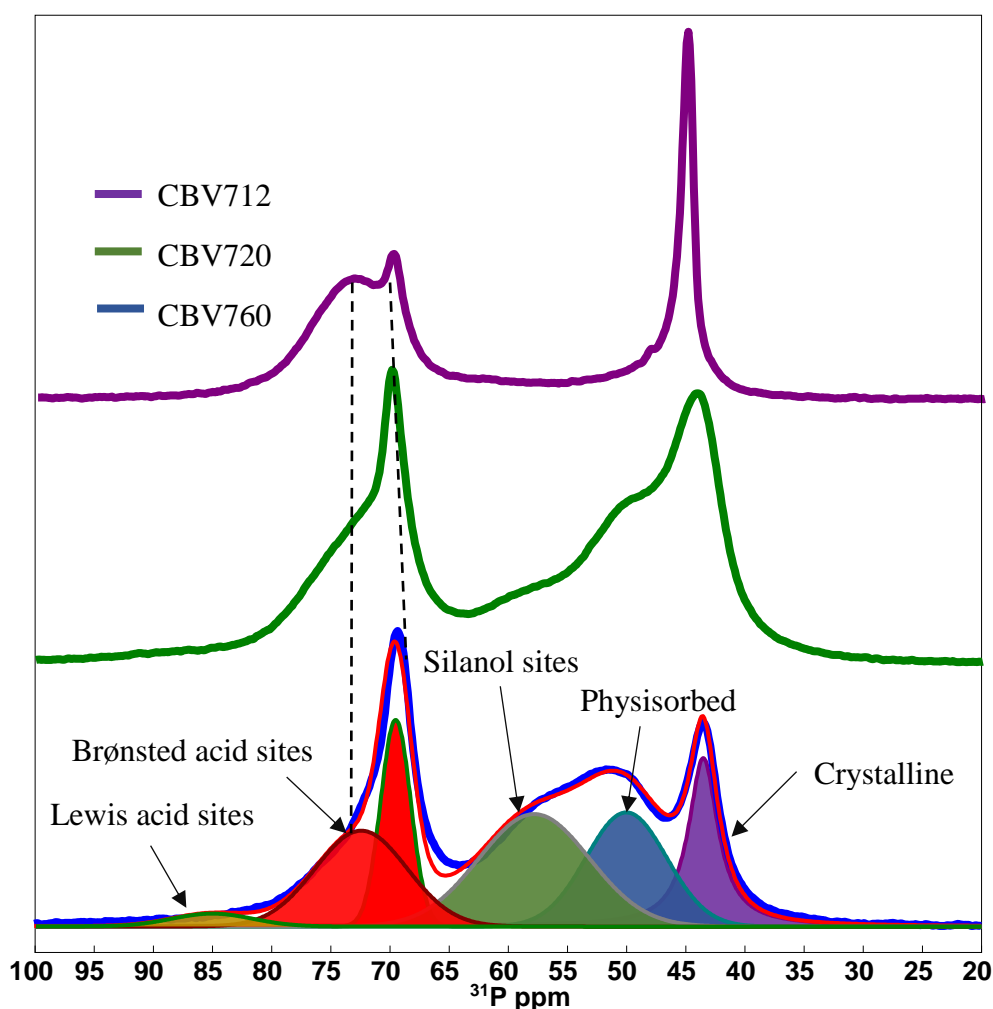**Figure 38:** Comparison of the ^{31}P 15 kHz MAS NMR spectra of CBV712, CBV720 and CBV760 impregnated with TBPO. Blue: 37.0 mg CBV760, 6.9 mg TBPO, including the fitting with its different peaks; green: 36.2 mg CBV720, 9.7 mg TBPO; purple: 40.4 mg CBV712, 10.2 mg TBPO. For CBV760, only two Brønsted acid site peaks are detected and also the other spectra seem to be made of the same number of peaks at a similar chemical shift.

In **Figure 38**, the ^{31}P 15 kHz MAS NMR spectra of the analysis of CBV712, CBV720 and CBV760 impregnated with TBPO are illustrated. For the spectrum of CBV760 (blue), also the fitting including its different peaks is shown. A total of 6 peaks can be observed, whose characteristics are represented in **Table 18** The peak at at a chemical shift of about 43.5 ppm (filled in purple) is attributed to crystalline bulk TBPO, based on the observation of **Figure 37**. The peaks around 50 ppm (blue) and 57.8 ppm (green) are attributed to physisorbed TBPO and to TBPO bond to silanol groups, respectively, due to the stronger interaction energy between the zeolite and TBPO, when its bond to the terminal silanol groups. In addition, the intensity of the physisorbed peak decreases with increasing treatment temperature and the silanol peak remains relatively constant, as shown further on **Figure 39**. The two peaks at chemical shifts of 69.5 ppm and 72.4 ppm are assigned to Brønsted acid sites with different acid site strengths, due to the presence of acid bridge SiOHAl groups in a different environment. It has been mentioned in ref. [18] that a linear relationship has been established between proton affinity (PA) of the acid site and the chemical shift in ppm of the peak corresponding to the Brønsted acid site. The presence of only two peaks in this case, compared to the presence of four peaks when analyzing CBV720 with TMPO or TEPO as probe, can be due to the size of TBPO. With a kinetic diameter of 0.82 nm, TBPO is considered not to enter the supercages with an entrance size of 0.72 nm, but still can probe them due to hydrogen bonding without entering the probe, differently from what is shown in **Figure 16 (b)**. Due to this bonding, the differentiation of various sites is therefore less precise and only a single peak can be distinguished. The peak with the highest chemical shift of about 86.5 ppm is attributed to TBPO bond to Lewis acid sites generated by EFAl, like during the analyses of the zeolites with TMPO and TEPO as probe.

Table 18. ^{31}P 15 kHz MAS NMR chemical shift (δ), peak area and environment of the different peaks of the CBV760 spectra (blue) shown in **Figure 38** (sample: 6.9 mg TBPO with 37.0 mg of CBV760, treated at 210 °C during 2 h). The most surprising observation is the presence of only two Brønsted acid site peaks

δ ^{31}P, ppm	Peak width, ppm	At. % peak area	Site type
43.5	3	18	Crystalline
50	8	20	Physisorbed
57.8	11	27	Silanol
69.5	3	14	Brønsted
72.4	9.1	19	Brønsted
85	8	2	Lewis

* The type of line shape used is pure Lorentzaian for the crystalline fitting line an pure Gaussian for the others

Comparing the different spectra of the three zeolites in **Figure 38**, it can be observed that they seem to be composed of the same number of peaks, located at a similar chemical shift and possessing the same width. These observations are justified, when analyzing the fitting with its different peaks of the CBV712 and CBV720 spectra shown in Annex 3. Some small variations can be observed for the peaks corresponding to crystalline, physisorbed TBPO and the one corresponding to Lewis acid sites. The most interesting peaks correspond to TBPO bonded to Brønsted acid sites and to the silanol terminal groups. Therefore, the peak model for the determination of those sites in USY zeolites is represented in **Table 19** including the tolerances. For all three peaks tolerances had to be included for the analysis of the three different zeolites, especially for the peak position of the silanol peak. The position of the two Brønsted peaks is relatively constant, even if the peak width of the peak around a chemical shift of 69.7 ppm varies quite a lot. Considering the linear relationship between the chemical shift of TBPO bond to a Brønsted acid site and the proton affinity of this acid site mentioned in [18], one can conclude that the TBPO does not detect a difference in the acid site strength as function of the dealumination treatment of the USY zeolites. From a graph shown in ref. [18], an approximative equation of this linear correlation can be derived

$$\delta^{31}P = 211.77 - 0.46 * PA \qquad (22),$$

The results are represented in **Table 19**. It can be seen that the PA of the different Brønsted acid sites varies from 306 kcal/mol to 300 kcal/mol, corresponding to medium acid site strengths [21]. Comparing these results with the ones of TEPO of TMPO, it can be seen that TBPO does not detect any strong and weak acid sites. The reason is probably the size of TBPO. It is not considered to enter the supercages and may probe their acid sites from outside due to hydrogen bonding, which is not taken into account in the correlation. Another reason is the large linewidth of the peak around 72.3 ppm of TBPO. Therefore, probably all stronger sites contribute to the same line, but they cannot be distinguished. The fact that TBPO measures for more "mesoporous" CBV760 and CBV720 zeolites a higher number of acid site supports the assumption that strong acid sites contribute to broad low field (higher ppm) line.

In Annex 3, also the spectra of the different samples hydrated at atmosphere are shown. The observations are similar to the ones made during the analysis with TEPO and TMPO as probe but the dissociation of TBPO bond to the acid sites is less severe. This can be explained by the strong basicity of TBPO compared to the two other probes, and the resulting stronger bonding to the acid sites.

Table 19. Representation of the peak model (including tolerances) used for determining the Brønsted acid sites and the silanol groups in USY zeolites by TBPO probe molecule.

$\delta\ ^{31}P$, ppm	Peak width, ppm	PA, kcal/mol	Site type
57.5 ± 1	11	/	Silanol
69.7 ± 0.3	2.2 ± 0.7	306	Brønsted
72.3 ± 0.3	9.0 ± 0.1	300	Brønsted

In **Table 20**, an overview of the detected concentration by ^{31}P 15kHz MAS NMR of the different Brønsted acid sites and of the terminal silanol groups is given for the different zeolites with TBPO as probe, treated at 210 °C for 2 h. As mentioned in the previous sections, the detected Brønsted acid site concentration reduces with increasing severity of the dealumination treatment and therefore with an increasing Si/Al ratio, which is in accordance with the literature [15][24]. During the analysis with TMPO as probe molecule and in [24], a higher silanol terminal group concentration was detected for less dealuminated zeolites. For the analysis with TBPO as probe, this tendency is not observed for CBV712. This can be explained by the less severe dealumination treatment of this zeolite, which gives raise to only few mesopores. The relatively big TBPO therefore only has a limited access to the terminal silanol groups in small pores and does not probe them. It is important to remind that the detected concentrations vary as function of different parameters, like the added probe quantity and the heat treatment. Nevertheless, it is assumed that the orders of magnitude remain the same and the results are sufficient in order to analyze the global tendencies.

Table 20. Comparison of the detected concentration of the different Brønsted acid sites and the silanol groups by ^{31}P 15kHz MAS NMR for the different zeolites with TBPO as probe, treated at 210 °C for 2 h.

		Concentration of the site in the zeolite , $\mu mol/g_{zeolite}$		
$\delta\ ^{31}P$, ppm	Site type	CBV712	CBV720	CBV760
57.5 ± 1	Silanol	110	308	231
69.7 ± 0.3	Brønsted	38 (6)	67 (18)	116 (41)
72.3 ± 0.3	Brønsted	555 (94)	302 (82)	164 (59)
Total Brønsted acid site concentration		593	369	280

* The value in the parentheses represent the percentage of the total acidity contributed by this site

Finally, the influence on the ^{31}P 15 kHz MAS NMR spectra and the detected Brønsted acid site concentration of the treatment temperature of the different zeolites impregnated with TBPO is tested. In **Figure 39**, the different spectra of 36.5 mg CBV720 impregnated with 7.9 mg TBPO are compared for temperatures ranging from 80 °C to up to 210 °C. No temperatures above 210 °C have been tested due to the limitations of the rotor caps and the risk of burning the sample. A steady growth of the detected Brønsted acid site concentration can be observed, which can be explained by the faster diffusion and reaction with the acid sites at higher temperatures. Also, the intensity of the silanol peak around 58 ppm increases slightly. The crystalline peak moves downwards and decreases in intensity, at the expense of the physisorbed one, which becomes slightly more important.
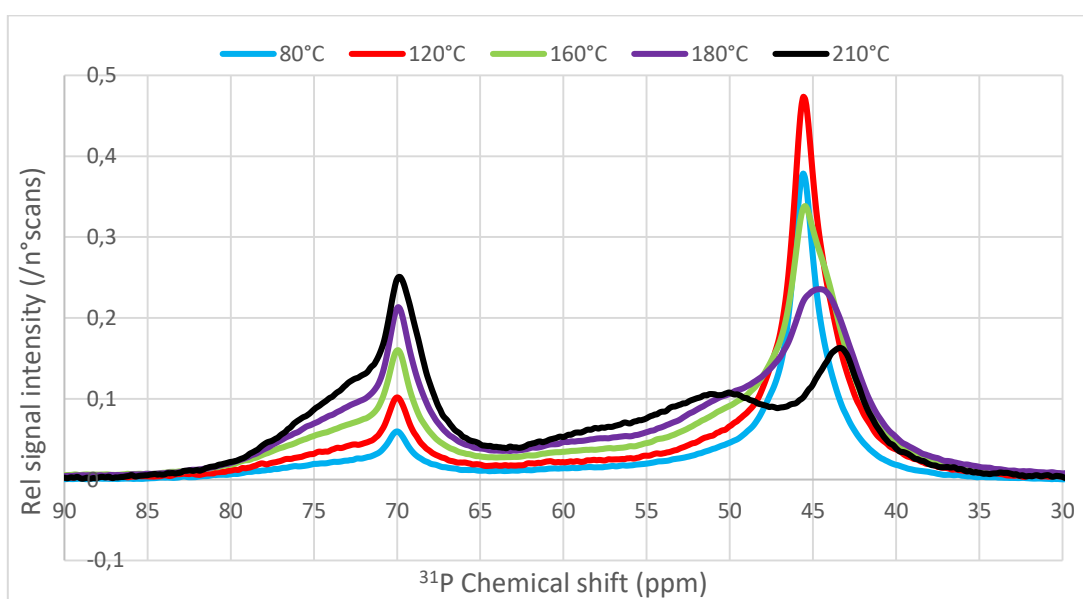

Figure 39: Evolution of the measured Brønsted acid site concentration by ^{31}P 15 kHz MAS NMR for a sample of 36.5 mg CBV720 impregnated with 7.9 mg TBPO as function of the treatment temperature of the sample (treatment duration 2 h at each temperature).

The analysis of the absolute integral value evolution of the lines associated with Brønsted acid sites as function of the treatment temperature of the sample shown in **Figure 39** is represented in **Figure 35**. The results are very similar to the analysis with TEPO as probe and an activation energy of $E_a = 4.2 \pm 0.1 \ kcal/mol$ is found. This corresponds to microporous materials with pore sizes less than 1 nm [28].

5.4 Results of the ICP elemental analysis

For all kind of zeolite-probe combination, at least one sample has been tested using ICP elemental analysis. The results of the ICP analysis are compared with the estimated phosphorus concentration in the

sample, calculated based of the sample mass after hydration, the added probe quantity and the molar mass of the probe. This comparison is represented in **Figure 40** including error bars of 5% in each direction, due to weighing errors and errors of the ICP analysis. A linear behavior can be observed with a slope close to unity and almost passing the origin. This justifies the estimated phosphorus amount in the sample and no probe is lost during the experiments.
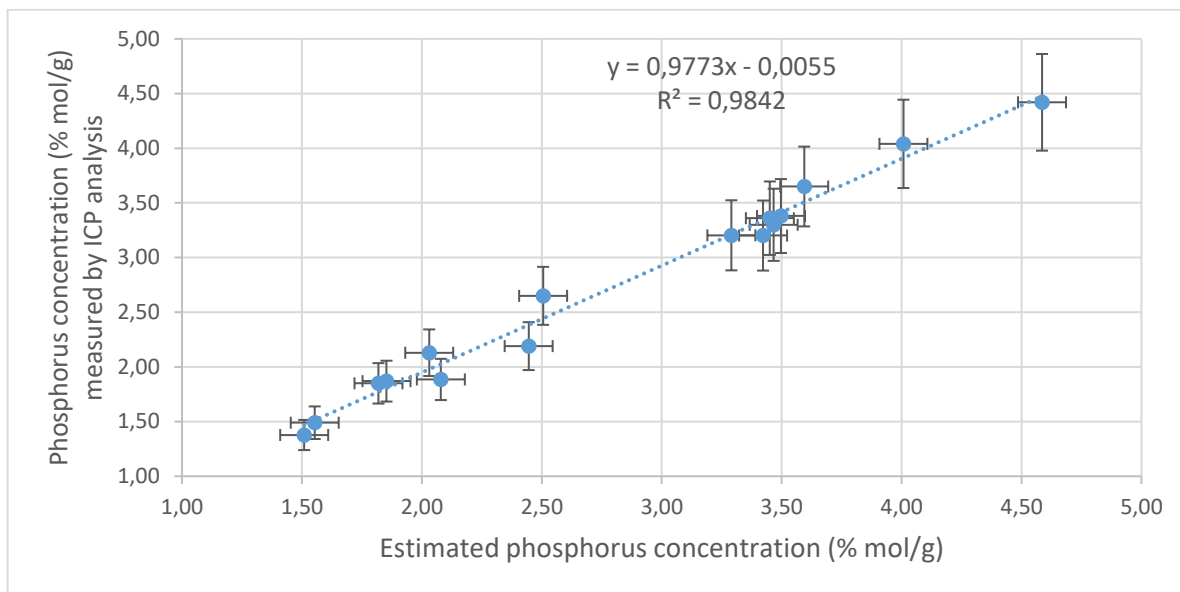

Figure 40: Comparison of the P concentration in the sample measured by ICP analysis and the one estimated based on the added probe quantity and the sample mass after hydration. A linear behavior with a slope close to unity and passing almost the origin is observed.

6 Discussion of the analyses of CBV712, CBV720 and CBV760 with TMPO, TEPO and TBPO as probe molecules

In the previous sections, the results of the analysis of all three zeolites with the three different probe molecules have been presented. In this section, the most important results are presented and the distinct cases are compared.

The zeolite properties one is mainly interested in are the concentration, the strength and the location of the Brønsted acid sites, which are responsible for the catalytic performance of the zeolite. The concentrations for all three zeolites impregnated with the three different probe molecules, treated at 210 °C for 2 h and detected by ^{31}P 15 kHz MAS NMR are represented in **Table 21** and **Figure 42**. It is important to mention that for different probe quantities added to the sample and for other heat treatments,

different concentrations are detected than the ones represented in **Table 21**. Those differences can be quite important, although the observed trends remain the same. For all three probes, more Brønsted acid sites are detected for less dealuminated zeolites, which is in accordance with the literature [15][24]. When analyzing the same zeolite with different R_3PO probes molecules with different sizes, it can be observed that TEPO detects less acidity than TMPO. This observation can be explained by the larger kinetic diameter of TEPO, which therefore is hindered more in its diffusion and reaction with the acid sites due to steric effects. This explanation seems to be invalid when analyzing the values with TBPO as probe. For CBV720 and CBV760 it detects the most acid sites of all probes. Due to its size, this observation is surprising, especially when taking into account that its kinetic diameter (0.82 nm) is bigger than the entrance of the supercages (0.72 nm) and is considered not to enter inside them. An explication of this phenomenon is the higher basicity of TBPO, which results in stronger interactions with the acid sites and seems to overcome the steric effects during the analysis of those two zeolites. In addition, even if TBPO does not enter the supercages it can still probe them from outside due to hydrogen bonding. Another possibility is that at the high temperature during the heat treatment, the probe deforms and is able to enter the supercages. When analyzing CBV712 impregnated with TBPO it can be seen that the fewest acid sites are observed with this probe molecule. Despite the stronger basicity of TBPO, the steric effects seem to have the larger influence in this case. Due to the weak dealumination treatment of this zeolite, only few mesopores are created and there is less large channel for the diffusion of such a large probe [15][24]. Unfortunately, an unambiguous distinction between external and internal Brønsted acid site, like done in [18] for example, cannot be made with these probe molecules. Except from CBV712, even TBPO is very mobile inside the mesopores of the zeolites, created by dealumination, and can probe the acid sites inside smaller pores from outside. The existing linear correlations between the PA and the chemical shift of a Brønsted acid site show similar results on TMPO and TEPO molecules. In general, TEPO tends to measure lower values of PA. TBPO is supposed not to enter the supercages and is therefore not able to distinguish some strong sites, as shown experimentally. Nevertheless, the hydrogen bonding from outside the pores with the acid sites enable a proper quantification of the number of acid sites, but not of their strength. As a conclusion for the further analysis of different zeolites, it can be said that TBPO is adapted the best for the analysis of zeolites with bigger pores due to its strong basic characteristic. TMPO and TEPO on the other hand are better for the analysis of smaller pores because of their small kinetic diameter.

Table 21. Comparison of the detected Brønsted acid site concentration by ^{31}P 15kHz MAS NMR of three USY zeolites impregnated with different R_3PO probe molecules and treated at 210 °C for 2 h

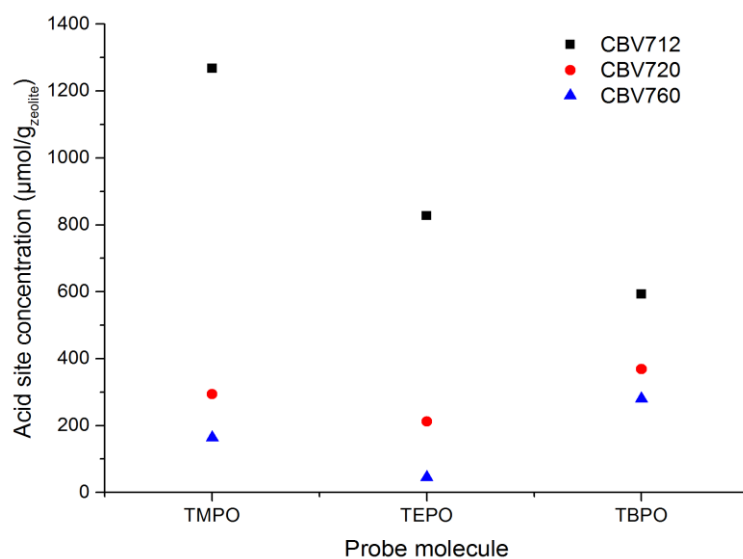| Zeolite Probe	Brønsted acid site concentration, $\mu mol/g_{zeolite}$		
	CBV712	CBV720	CBV760
TMPO	1267	294	164
TEPO	827	212	45
TBPO	593	369	280

Figure 41: Graphical representation of the evolution of the detected Brønsted acid site concentration by ^{31}P 15kHz MAS NMR of three USY zeolites as function of the used probe molecule (treated at 210 °C for 2 h)

During the different analyses, the influence of some sample preparation parameters on the detected Brønsted acid site concentration has been analyzed, namely the treatment temperature and duration and the relative amount of probe molecule in the sample. The tendencies are always the same and some parameters have been optimized. The influence of the treatment temperature is obvious, a higher treatment temperature leads to more detected Brønsted acid sites, since it tends to accelerate the probe diffusion or increases its reactivity with the sites. During the analysis, the treatment temperature was limited to 210 °C by the resistance of the rotor caps and the risk of burning the sample. A longer heat treatment gives the probe molecules more time to diffuse and react with the acid sites. Nevertheless, no significant changes in the detected Brønsted acid site concentration were observed after a certain time, function of the treatment temperature. Therefore, longer treatment simply waste time and energy and

provide no benefit. Also, for a higher relative amount of probe molecule in the sample, more Brønsted acid sites are detected, due to an enhanced diffusion or reactivity of the probe. However, a too high content leads to a very important peak of non-bonded probe molecules, which is likely to introduce errors to the fitting of the Brønsted acid site peaks.
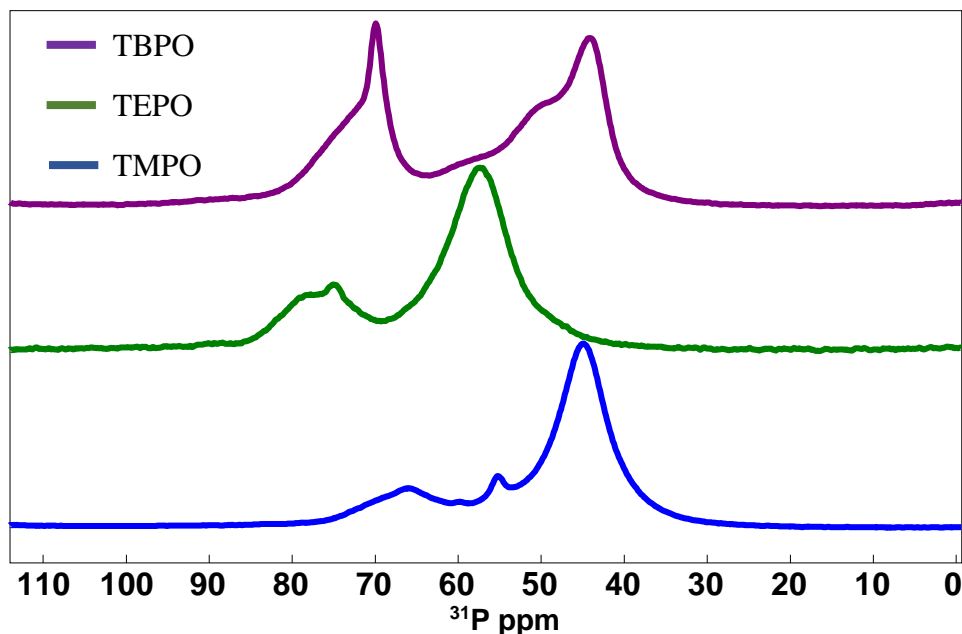

Figure 42: Comparison of the spectra of CBV20 impregnated with TBPO, TEPO and TMPO. The shape of the spectra is similar in the three cases. The most significant difference is the presence of only two Brønsted acid site peaks in the case of TBPO. It can also be observed that the distance between the physisorbed peak and the acid site peaks is larger, the bigger the probe molecule gets.

Apart from the detected amount of Brønsted acidity, there are other criteria that influence the choice of the probe molecule. An example is the available treatment temperature. As shown in **Table 2** in section 3.2, TEPO has the lowest melting point of all three probe molecules with around 60 °C, whereas the evaporation temperature of TMPO is the lowest with 194 °C. Therefore, TEPO is the best choice, if only a very low temperature is available, whereas TMPO is the best choice if treatment temperatures around 200 °C can be reached. Unfortunately, TEPO is very hygroscopic and therefore difficult to manipulate outside of a glovebox. Another point is the resolution of the different Brønsted acid sites, as shown in **Figure 42**. For the analysis by TMPO, the distance between the 4 peaks corresponding to Brønsted acid sites are separated by a distance of about 17 ppm in the peak model, compared to only 11.5 ppm in the case of TEPO. With TBPO as probe, only two different Brønsted acid site peaks can be distinguished, separated by a distance of about only 2.6 ppm. As a result, TMPO is the best probe, if the different acid

sites need to be distinguished. On the other hand, an advantage of the larger probe molecules is the spectral distance between the physisorbed peak and the different Brønsted acid site peaks in the spectra. It can be seen in **Figure 42** that the bigger the diameter of the probe molecule is, the larger the distance between those peaks. This reduces the risk of a fitting error in case of a high intensity physisorbed peak.

7 Conclusion

In conclusion, it can be said that the method of acid site analysis by R_3PO probe molecule ^{31}P MAS NMR was successfully developed on different USY zeolites and with different probe molecules. The solid route preparation has been found out to be a simple method, which avoids the use of toxic and dangerous products. The calculated amount of phosphorus added to the sample with the probe molecules corroborated with the data of the ICP elemental analysis performed on several samples.

It has been found out that the method provides qualitative and quantitative results of the acid site concentration and the influence of different sample preparation parameters on the results has been evaluated. The detected acid site concentrations strongly depend on those parameters and the used probe molecule, but the observed tendencies are in accordance with different references in the literature. It has been observed that for a zeolite with a higher Si/Al ratio, less Brønsted acid sites are detected, due to the stronger dealumination. However, no significant influence of the dealumination treatment on the acid site strength could be identified.

The analysis with the different R_3PO probes has brought to light that they all have advantages and disadvantages. The most suitable choice of probe molecule depends on various parameters such as the available treatment temperature, the porous structure of the zeolite and the exact information that needs to be collected from the analysis. It was found out that TBPO is adapted the best for the analysis of zeolites with bigger pores due to its strong basic characteristic, whereas TMPO and TEPO are better for the analysis of smaller pores because of their small kinetic diameter. In addition, TMPO gives the best resolution for the distinction of Brønsted acid sites with different strength.

There are some perspectives of research that will be done in the future based this work. The measured values and the observed tendencies are compared with the results of different other methods, like IR analysis with probe molecules and TPD of ammoniac. The method has been developed for the analysis of three different USY zeolites but can also be adapted for the acidity analysis of plenty other zeolites.

8 Bibliography

[1]   J. Keeler, *Comprendre la RMN*, 2nd ed. Lausanne, 2015.

[2]   National Institute of Standards and Technology, "Lab 8. NMR Spectroscopy. Introduction.," 2010. [Online]. Available: https://web.nmsu.edu/~snsm/classes/chem435/Lab8/intro.html. [Accessed: 07-Jun-2018].

[3]   Hamburg_University, "Gyromagnetic ratio." [Online]. Available: https://www.chemie.uni-hamburg.de/nmr/insensitive/tutorial/en.lproj/gyromagnetic_ratio.html. [Accessed: 18-Apr-2018].

[4]   "The Unified Scale for Referencing in NMR: New IUPAC Recommendations," *Work*, no. July, pp. 1–5, 2010.

[5]   S. Denis-Quanquin, "Cours de Résonance Magnétique Nucléaire." Ecole normale Supérieure de Lyon, Lyon, 2014.

[6]   C. Coillot, R. Sidiboulenouar, E. Nativel, M. Zanca, E. Alibert, M. Cardoso, G. Saintmartin, H. Noristani, N. Lonjon, M. Lecorre, F. Perrin, and C. Goze-Bac, "Signal modeling of an MRI ribbon solenoid coil dedicated to spinal cord injury investigations," *J. Sensors Sens. Syst.*, vol. 5, no. 1, pp. 137–145, 2016.

[7]   C. A. Fyfe, "Solid state NMR for chemists." C.F.C press, Ontario, 1983.

[8]   H. Tariq and A. Burney, "Brain MRI literature review for interdisciplinary studies," *J. Biomed. Graph. Comput.*, vol. 4, no. 4, 2014.

[9]   J. Ďurkovič, F. Kačík, and D. Olčák, "An evaluation of cellulose degradation affected by Dutch elm disease," *Bio-protocol*, vol. 5, no. 2003, p. e1535, 2015.

[10]   M. J. Duer, *Solid-State NMR spectroscopy, principles and applications.* Oxford: Blackwell Science Ltd., 2002.

[11]   G. A. Morag O, Sgourakis NG, Abramov G, "Filamentous Bacteriophage Viruses: Preparation, Magic-Angle Spinning Solid-State NMR Experiments, and Structure Determination.," *Methods Mol. Biol.*, vol. 1688, pp. 67–97, 2017.

[12]   "Magic Angle Spinning.," 2016. [Online]. Available: https://de.wikipedia.org/wiki/Magic-Angle-Spinning. [Accessed: 03-May-2018].

[13]   R. J. Davis, "New perspectives on basic zeolites as catalysts and catalyst supports," *J. Catal.*, vol. 216, no. 1–2, pp. 396–405, 2003.

[14]   J.-C. Legrand, "File: Reseau cavités zéolithe NaY.," 2014. [Online]. Available:

https://commons.wikimedia.org/wiki/File:Reseau-cavites-zeolithe-NaY.png. [Accessed: 29-Mar-2018].

[15]   D. Verboekend, N. Nuttens, R. Locus, J. Van Aelst, P. Verolme, J. Perez-Ramirez, and B. F. Sels, "Synthesis, characterisation, and catalityc evaluation of hierarchical faujasite zeolites: molestones, challenges, and future directions," *Chem. Soc. Rev.*, vol. 45, no. 12, p. 3331, 2016.

[16]   Zeolyst_International, "Zeolyte Y." [Online]. Available: https://www.zeolyst.com/our-products/standard-zeolite-powders/zeolite-y.html. [Accessed: 29-Mar-2018].

[17]   J. L. Agudelo, E. J. M. Hensen, S. A. Giraldo, and L. J. Hoyos, "Influence of steam-calcination and acid leaching treatment on the VGO hydrocracking performance of faujasite zeolite," *Fuel Process. Technol.*, vol. 133, pp. 89–96, 2015.

[18]   A. Zheng, S.-J. Huang, S.-B. Liu, and F. Deng, "Acid properties of solid acid catalysts characterized by solid-state 31P NMR of adsorbed phosphorous probe molecules," *Phys. Chem. Chem. Phys.*, vol. 13, no. 33, p. 14889, 2011.

[19]   Q. Zhao, W. H. Chen, S. J. Huang, Y. C. Wu, H. K. Lee, and S. Bin Liu, "Discernment and quantification of internal and external acid sites on zeolites," *J. Phys. Chem. B*, vol. 106, no. 17, pp. 4462–4469, 2002.

[20]   A. Zheng, S.-J. Huang, W.-H. Chen, P.-H. Wu, H. Zhang, H.-K. Lee, L.-C. de Ménorval, F. Deng, and S.-B. Liu, "31P Chemical Shift of Adsorbed Trialkylphosphine Oxides for Acidity Characterization of Solid Acids Catalysts," *J. Phys. Chem. A*, vol. 112, no. 32, pp. 7349–7356, Aug. 2008.

[21]   P. V. Wiper, J. Amelse, and L. Mafra, "Multinuclear solid-state NMR characterization of the Brønsted/Lewis acid properties in the BP HAMS-1B (H-[B]-ZSM-5) borosilicate molecular sieve using adsorbed TMPO and TBPO probe molecules," *J. Catal.*, vol. 316, pp. 240–250, 2014.

[22]   S. Lang, M. Benz, U. Obenaus, R. Himmelmann, and M. Hunger, "Novel Approach for the Characterization of Lewis Acidic Solid Catalysts by Solid-State NMR Spectroscopy," *ChemCatChem*, vol. 8, no. 12, pp. 2031–2036, 2016.

[23]   Sigma-Aldrich, "Dichloromethane Safety Data Sheet," 2015. [Online]. Available: https://www.sigmaaldrich.com/MSDS/MSDS/DisplayMSDSPage.do?country=BE&language=EN-generic&productNumber=02575&brand=SIAL&PageToGoToURL=https%3A%2F%2Fwww.sigmaaldrich.com%2Fcatalog%2Fproduct%2Fsial%2F02575%3Flang%3Dfr. [Accessed: 03-May-2018].

[24]   A. S. Andreev and V. Livadaris, "Characterization of Catalytic Materials through a Facile Approach to Probe OH Groups by Solid-State NMR," *J. Phys. Chem. C*, vol. 121, no. 26, pp. 14108–14119, 2017.

[25]   T. Parella, "AVANCE Tutorials - High-Power 90° 1H Observe Pulse Calibration.," 2003. [Online]. Available: http://triton.iqfr.csic.es/guide/tutorials/calib/90pulseh1.html. [Accessed: 04-May-2018].

[26]   E. F. Rakiewicz, A. W. Peters, R. F. Wormsbecher, K. J. Sutovich, and K. T. Mueller, "Characterization of Acid Sites in Zeolitic and Other Inorganic Systems Using Solid-State [31] P NMR of the Probe Molecule Trimethylphosphine Oxide," *J. Phys. Chem. B*, vol. 102, no. 16, pp. 2890–2896, 1998.

[27]   Q. Zhao, W.-H. Chen, S.-J. Huang, and S.-B. Liu, "39 Qualitative and quantitative determination of acid sites on solid acid catalysts," in *Science and Technology in Catalysis 2002*, vol. 145, M. Anpo, M. Onaka, and H. B. T.-S. in S. S. and C. Yamashita, Eds. Elsevier, 2003, pp. 205–209.

[28]   D. M. Ruthven and M. F. M. Post, "Chapter 12 Diffusion in zeolite molecular sieves," in *Introduction to Zeolite Science and Practice*, vol. 137, H. van Bekkum, E. M. Flanigen, P. A. Jacobs, and J. C. B. T.-S. in S. S. and C. Jansen, Eds. Elsevier, 2001, pp. 525–577.

[29]   A. Zheng, F. Deng, and S. Bin Liu, *Acidity Characterization of Solid Acid Catalysts by Solid-State 31P NMR of Adsorbed Phosphorus-Containing Probe Molecules*, 1st ed., vol. 81. Elsevier Ltd., 2014.

9 Annex

9.1 Annex 1: Complementary theoretical background

9.1.1 Fourier transformation of the FID

The FID signal in the time domain is given by equation (14):

$$S(t) = \left(S_x(t) + S_y(t)\right) * \exp\left(-\frac{t}{T_2}\right) = S_0 \exp(i\Omega t)\, exp\left(-\frac{t}{T_2}\right)$$

$$= S_0 \exp(i\Omega t)\, exp(-R_2 t) \qquad (14).$$

The signal in the frequency domain is obtained by the Fourier transformation:

$$S(\omega) = \int_0^{+\infty} S(t)e^{-i\omega t}dt = \int_0^{+\infty} S_0\, e^{i\Omega t - R_2 t - i\omega t}dt = S_0 \int_0^{+\infty} e^{[-i(\omega-\Omega)-R_2]t}dt$$

$$=> S(\omega) = \frac{S_0\, e^{[-i(\omega-\Omega)-R_2]t}}{[-i(\omega-\Omega)-R_2]}\Bigg\{_0^{+\infty} = -\frac{S_0}{[-i(\omega-\Omega)-R_2]} = \frac{S_0}{[i(\omega-\Omega)+R_2]}\frac{[-i(\omega-\Omega)+R_2]}{[-i(\omega-\Omega)+R_2]}$$

$$= \frac{S_0[-i(\omega-\Omega)+R_2]}{(\omega-\Omega)^2+R_2^2} = \frac{S_0 R_2}{(\omega-\Omega)^2+R_2^2} + i\frac{-S_0(\omega-\Omega)}{(\omega-\Omega)^2+R_2^2} = S_0[A(\omega)+i(D\omega)],$$

with $A(\omega)$ the real part and $D(\omega)$ the imaginary part of the spectrum. When plotting the real part, a spectrum with the so-called *absorption mode Lorentzian* lineshape is obtained. It has its maximum for $\omega = \Omega$ of an intensity equal to $S_0 A(\omega = \Omega)\frac{S_0 R_2}{(\Omega-\Omega)^2+R_2^2} = \frac{S_0}{R_2}$. In order to know how good the resolution of the spectrum is, the width at half maximum has to be calculated:

$$A\left(\omega_{\frac{1}{2}}\right) = \frac{S_0 R_2}{\left(\omega_{\frac{1}{2}}-\Omega\right)^2 + R_2^2} = \frac{1}{2R_2}$$

$$=> \left(\omega_{\frac{1}{2}}-\Omega\right)^2 = R_2^2$$

$$=> \left(\omega_{\frac{1}{2}}-\Omega\right) = \pm R_2$$

$$=> \omega_{\frac{1}{2}} = \Omega \pm R_2$$

This gives a width at half height of $2R_2$ rad/s. Because $\omega = 2\pi\nu$, the width at half height of the absorption mode lineshape is $\frac{R_2}{\pi}$ or $\frac{1}{\pi T_2}$ Hz.

9.1.2 A *Spin Echo* experiment

The second experiment to be analyzed is the so-called *spin echo* experiment. Analyzing the typical pulse sequence of such an experiment as shown in **Figure 43**, one can see that there are two different

pulses in the sequence, a first pulse of 90° and a second one of 180° after a time τ. The FID signal collection starts after a time τ after the second pulse. The objective of this pulse sequence is to refocus the evolution of the magnetization. As shown in **Figure 44**, the 90° pulse along the x axis tilts the magnetization vector along the $-$ y axis. When the pulse intensity is turned off, the magnetization vector starts the precession with a frequency Ω and after a time τ, the angle with the $-$y axis has become $\Omega\tau$. At this point, a pulse along the x axis of 180° is applied, rotating the magnetization vector by 180° around the x-axis. After the pulse, the magnetization vector is again in the x-y plane, but with an angle of $\pi - \Omega\tau$ to the $-$y axis, which means an angle $\Omega\tau$ with the y axis and restarts the precession. When the acquisition starts a time τ after the 180° pulse, the magnetization vector is perfectly aligned with the y-axis. The *spin echo* is used in order to avoid the problem of the dead time between a pulse and the moment the detection can start. This is valid especially for nuclei with a small T_2. Another goal is to eliminate the interactions of the sample nuclei if the amorphous rotor, because amorphous phase is less influenced by the 180° pulse [1].
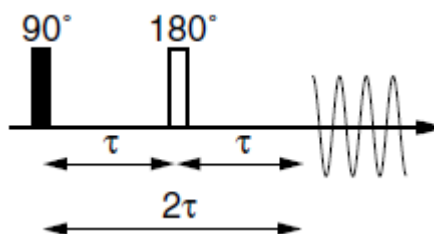

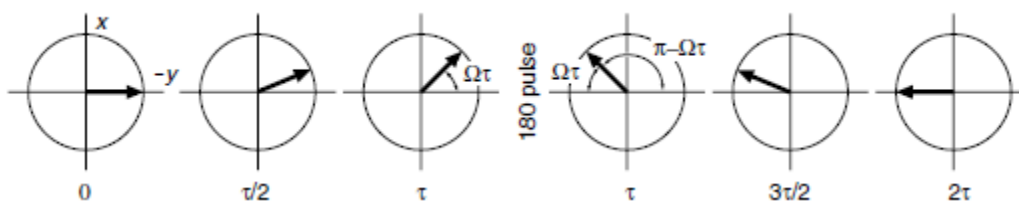**Figure 43.** Pulse sequence of the *spin echo* experiment (adapted from [1])

Figure 44. Vector representation how the pulse sequence of the *spin echo* experiments helps to refocus the magnetization (taken from [1])
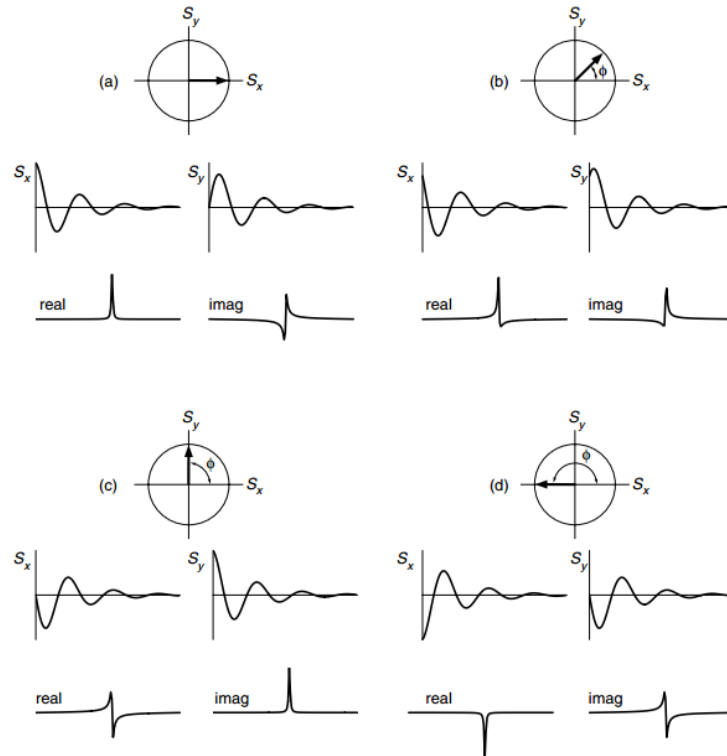
9.1.3 Phasing

Figure 45: The effect of a phase shift on the real and the imaginary signal in the time domain and the resulting spectra (adapted from [1])

In the case of an impulsion, where the magnetization is tilted in the xy-plane with an angle ϕ to the x-axis, the measured signal is dephased. The effect on the FID signal in the time domain and on the spectra in the frequency domain is represented in **Figure 45**. This effect can be represented mathematically in the time domain by multiplying the formula (14) of the FID signal by a factor $\exp(i\phi(\Omega))$, with $\phi(\Omega)$ also called the phase shift. One can see in **Figure 45** that the phase shift has the effect of modifying the absorption mode character of the real spectrum and the dispersion mode character of the imaginary spectrum and that it even can cause the inversion of the spectrum. Due to the fact that a perfectly absorption mode lineshape is of interest in the spectrum, this phase shift has to be corrected. Two different types of phase shifts are distinguished, the frequency independent and the frequency dependent phase shift. In the first one is simply due to a wrong association of the axis system where the signal is measured in. It can be corrected by multiplying the FID signal by the term $\exp(i\phi_{corr})$ to perform a frame rotation:

$$\exp(i\phi_{corr}) * S(t) = \exp(i\phi_{corr}) * S_0\exp(i\phi)\exp(i\Omega t)\,exp\left(-\frac{t}{T_2}\right) \quad (23)$$

When $\phi_{corr} = -\phi$, the phase shift is annulated and the real part of the spectrum becomes perfectly an absorption mode line. Unfortunately, the phase shift does depend on the frequency, because with increasing offset more magnetization is generated alongside the y-axis. In this case a frequency dependant pahse correction is necessary. Often, a first order correction with $\phi_{corr} = k * \Omega$ is sufficient in order to eliminate this imprecision. In both cases, the phase shift is not known and ϕ_{corr} has to be found empirically by adjusting the lineshpapes until they seem to be correct. The phase correction is a very crucial step, which has to be done very often during the post-aqcusition data treament [1].

9.2   Annex 2: Additional pictures of different devices used in the laboratory

Figure 46: The different filling devices used during this work, adapted to 4 mm rotors and caps

Figure 47: Another device, designed for the cap removal of 4 mm and 2.5 mm rotors

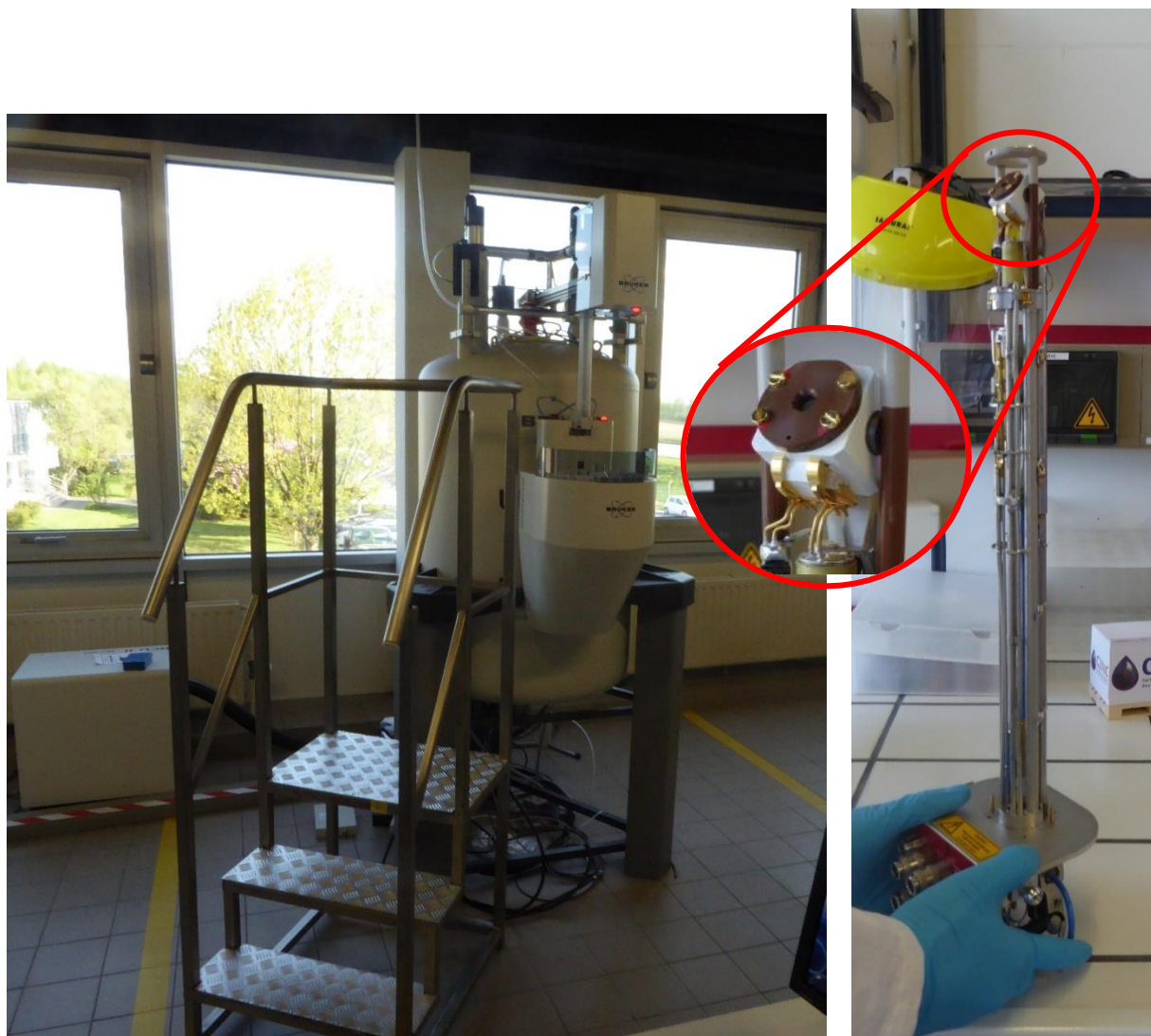**Figure 48:** Two types devices, designed for the cap removal of 4 mm rotors

Figure 49: A picture of the Bruker Avance III HD 500 MHz (11.7 T) device (left) and the installed 4 mm MAS probe, without its case (right) A the interior of the yellow lines, the magnetic field is higher than 10 times the magnetic field of the earth and no magnetic objects should be taken inside. The zoomed part encircled in red is resposible for tilting the sample into the magic angle and the high-frequency rotation.

9.3 Annex 3: Complementary experimental results

9.3.1 CBV712 analysis by TMPO

Table 22. ^{31}P 15 kHz MAS NMR chemical shift (δ), peak area and environment of the different peaks shown in **Figure 28**, hydrated (sample: 11.7 mg TMPO with 42.2 mg of CBV712, treated at 210 °C during 2 h, hydrated for 52 h at atmosphere)

$\delta\ ^{31}P$, ppm	Peak width, ppm	At. % peak area	Site type
41	9	19	Crystalline
45.6	2.7	27	Physisorbed
49.8	7.5	16	Silanol
55	5	14	Brønsted
58	5	8	Brønsted
67.5	8	15	Brønsted
72.5	6	1	Brønsted
82.1	7	<1	Lewis

* The type of line shape used is pure Gaussian for all fitting lines

9.3.2 CBV760 analysis by TMPO

Table 23. ^{31}P 15 kHz MAS NMR chemical shift (δ), peak area and environment of the different peaks shown in **Figure 30**, hydrated (sample: 3.1 mg TMPO with 41.9 mg of CBV760, treated at 210 °C during 2 h, hydrated for 5 days at atmosphere)

$\delta\ ^{31}P$, ppm	Peak width, ppm	At. % peak area	Site type
42	7	3	Crystalline
47.8	3.5	62	Physisorbed
50.5	7.5	22	Silanol
55.5	3	<1	Brønsted
57.5	4	5	Brønsted
65	8	6	Brønsted
72.5	6	1	Brønsted
82.5	7	<1	Lewis

* The type of line shape used is pure Gaussian for all fitting lines
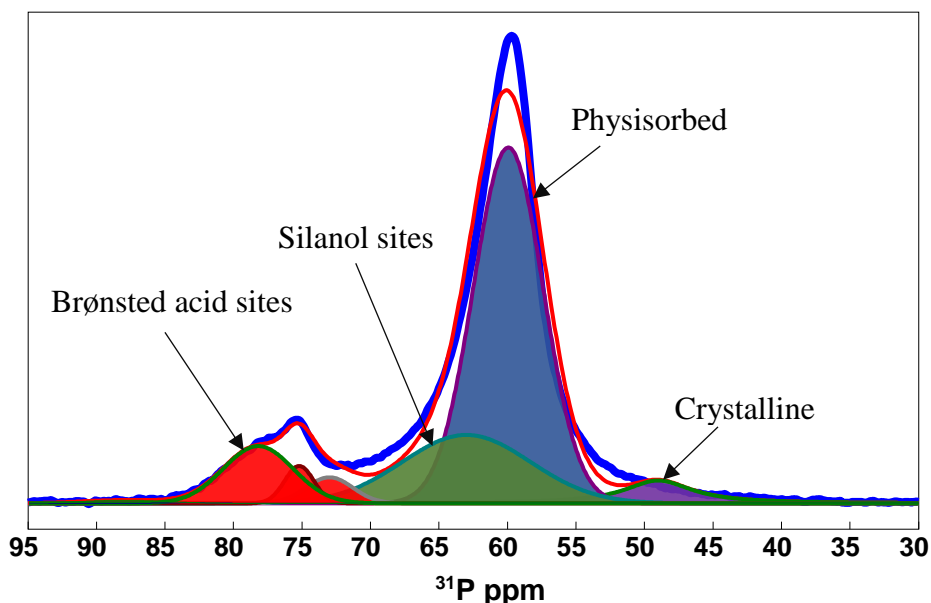
9.3.3 CBV720 analysis by TEPO

Figure 50: ^{31}P 15 kHz MAS NMR spectrum of 39.8 mg CBV720 zeolite impregnated with 5.1 mg TEPO, treated at 210 °C during 2 h, hydrated for 8 days at atmosphere. A decrease in intensity of the peaks corresponding to TEPO bond to Brønsted and Lewis acid sites and terminal silanol groups and crystalline TEPO can be observed. The peak assigned to physisorbed TEPO has shifted upwards and increased in intensity. The effect of the hydration seems to be more severe than for the analysis with TMPO as probe. This may be due to the longer hydration time, but also due to the higher hygroscopy of the TEPO molecules, as observed during the sample preparation.

Table 24. ^{31}P 15 kHz MAS NMR chemical shift (δ), peak area and environment of the different peaks shown in **Figure 50** (sample: 5.1 mg TEPO with 39.8 mg of CBV720, treated at 210 °C during 2 h, hydrated for 8 days at atmosphere)

δ ^{31}P, ppm	Peak width, ppm	At. % peak area	Site type
49	6	5	Crystalline
60	6	58	Physisorbed
63	11	21	Silanol
73	4	3	Brønsted
75.2	2.5	3	Brønsted
78.2	6	9	Brønsted
83	4.5	<1	Brønsted
88	7	<1	Lewis

* The type of line shape used is pure Lorentzaian for the crystalline fitting line an pure Gaussian for the others
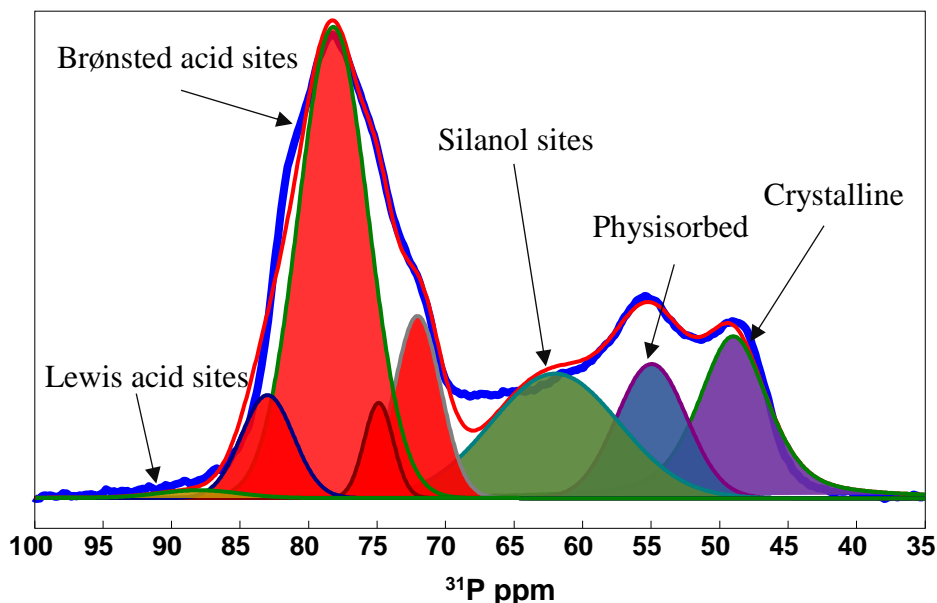
Figure 51: ^{31}P 15 kHz MAS NMR spectrum of 44.0 mg CBV712 zeolite impregnated with 8.8 mg TEPO, treated at 210 °C during 2 h. Similar peak parameters as for CBV720: Eight peaks can be distinguished, 4 corresponding to TEPO bond to Brønsted acid sides of different strength (higher chemical shift = stronger site), one corresponding to TEPO bond to Lewis acid sites, one to TEPO bond to silanol groups, one to physisorbed and one to bulk crystalline TEPO.

Table 25. ^{31}P 15 kHz MAS NMR chemical shift (δ), peak area and environment of the different peaks shown in **Figure 51** (sample: 8.8 mg TEPO with 44.0 mg of CBV712, treated at 210 °C during 2 h)

δ ^{31}P, ppm	Peak width, ppm	At. % peak area	Site type
49	6	15	Crystalline
55	6	10.5	Physisorbed
62	11	18	Silanol
72	4	9.5	Brønsted
74.9	2.5	3	Brønsted
78.2	6	37	Brønsted
83	4.5	6	Brønsted
88	7	1	Lewis

* The type of line shape used is pure Lorentzaian for the crystalline fitting line an pure Gaussian for the others
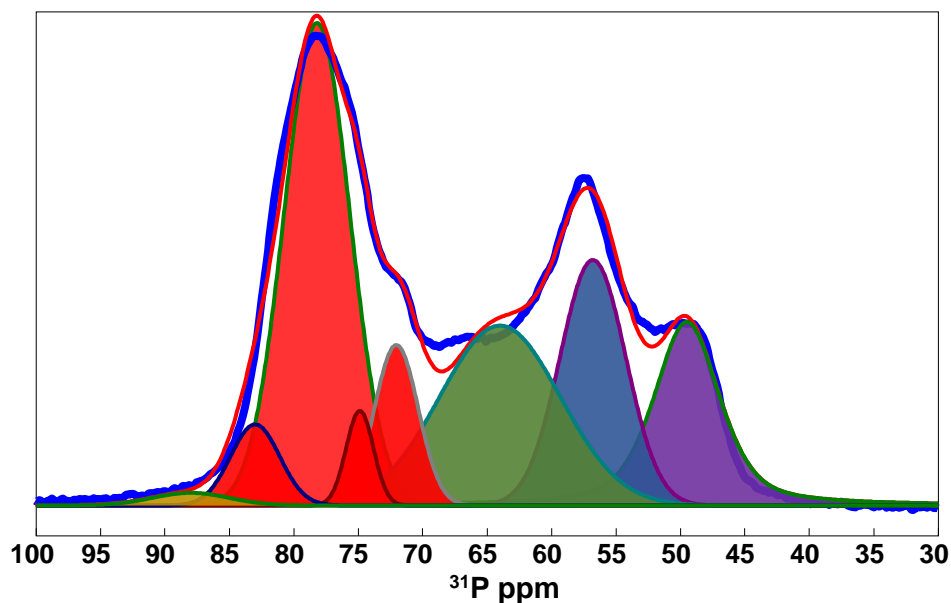
Figure 52: ^{31}P 15 kHz MAS NMR spectrum of 44.0 mg CBV712 zeolite impregnated with 8.8 mg TEPO, treated at 210 °C during 2 h, hydrated for 65 h. A slight decrease in intensity of the peaks corresponding to the different acid sites, but increase of the ones corresponding to physisorbed TEPO and silanol site. The hydration effect is quite low due to the low mesoporosity and low accessibility of the sites by water.

Table 26. ^{31}P 15 kHz MAS NMR chemical shift (δ), peak area and environment of the different peaks shown in **Figure 52** (sample: 8.8 mg TEPO with 44.0 mg of CBV712, treated at 210 °C during 2 h, hydrated for 65 h)

δ ^{31}P, ppm	Peak width, ppm	At. % peak area	Site type
49.5	6	15	Crystalline
56.8	6	16	Physisorbed
64	11	22	Silanol
72	4	7	Brønsted
74.9	2.5	3	Brønsted
78.2	6	32	Brønsted
83	4.5	4	Brønsted
88	7	1	Lewis

* The type of line shape used is pure Lorentzaian for the crystalline fitting line an pure Gaussian for the others

Table 27. Calculation of the concentration of the different TEPO environments by equation (19), based on the ^{31}P 15 kHz MAS NMR spectrum shown in **Figure 51** and **Table 25** (sample: 8.8 mg TEPO with 44.0 mg CBV712, treated at 210 °C during 2 h). A high Brønsted acid site concentration can be measured due to weak dealumination/ high Si/Al ratio of the CBV712.

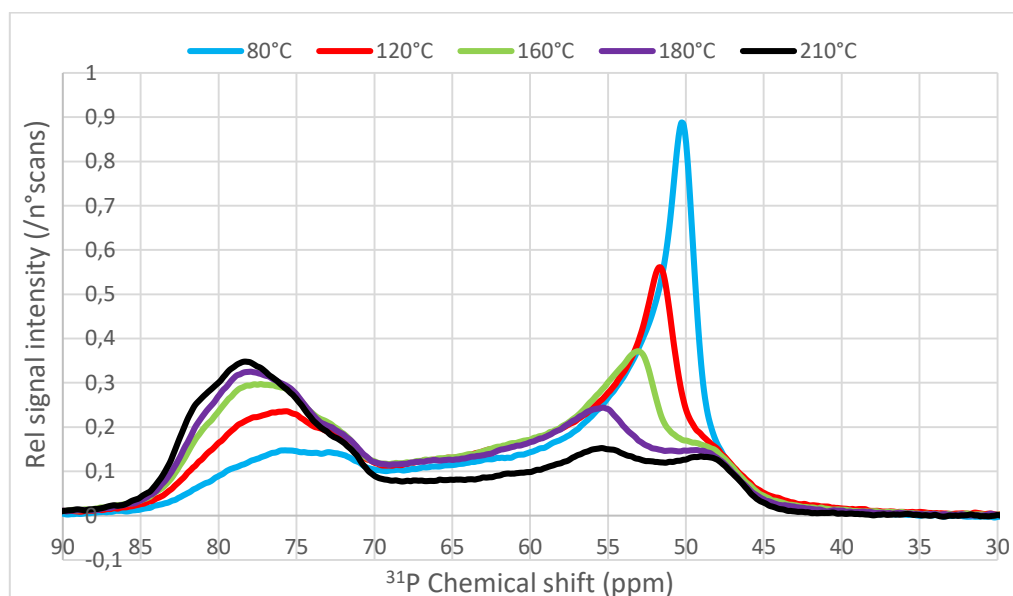|			
C_P	$0.0015\ mol/g_{zeolite}$	Crystalline	$228\ \mu mol/g_{zeolite}$
		Physisorbed	$156\ \mu mol/g_{zeolite}$
		Silanol	$266\ \ \mu mol/g_{zeolite}$
		Brønsted	$827\ \mu mol/g_{zeolite}$
		Lewis	$11\ \mu mol/g_{zeolite}$

Figure 53: Evolution of the measured Brønsted acid site concentration by ^{31}P 15 kHz MAS NMR for a sample of 44.0 mg CBV712 impregnated with 8.8 mg TEPO as function of the treatment temperature of the sample (treatment duration 2 h at each temperature). A steady increase of the detected Brønsted acid site concentration can be observed, which can be explained by faster diffusion and reaction with the acid sites at higher temperatures. The silanol peak around 62 ppm seems to have a quite constant intensity, the physisorbed peak moves from about 51 ppm to 55 ppm with higher treatment temperatures and decreases in intensity.
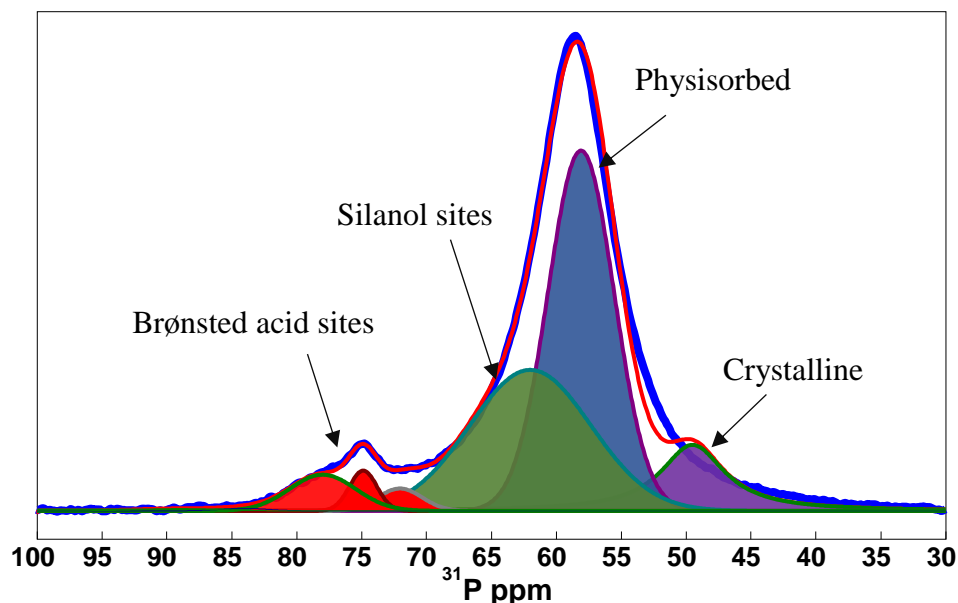
9.3.5 CBV760 analysis by TEPO

Figure 54: ^{31}P 15 kHz MAS NMR spectrum of 44.4 mg CBV760 zeolite impregnated with 3.0 mg TEPO, treated at 210 °C during 2 h. Similar peak positions and widths as for CBV720 and CBV712: Eight peaks can be distinguished, 4 corresponding to TEPO bond to Brønsted acid sides of different strength (higher chemical shift = stronger site), one to TEPO bond to silanol groups, one to physisorbed and one to bulk crystalline TEPO, but none corresponding to TEPO bond to Lewis acid sites

Table 28. ^{31}P 15 kHz MAS NMR chemical shift (δ), peak area and environment of the different peaks shown in **Figure 54** (sample: 3.0 mg TEPO with 44.0 mg of CBV760, treated at 210 °C during 2 h)

δ ^{31}P, ppm	Peak width, ppm	At. % peak area	Site type
49.5	6	12	Crystalline
58.1	6	46	Physisorbed
62	11	33	Silanol
72	4	2	Brønsted
74.9	2.5	2	Brønsted
78	6	5	Brønsted
84	4.5	1	Brønsted
89	7	1	Lewis

* The type of line shape used is pure Lorentzaian for the crystalline fitting line an pure Gaussian for the others
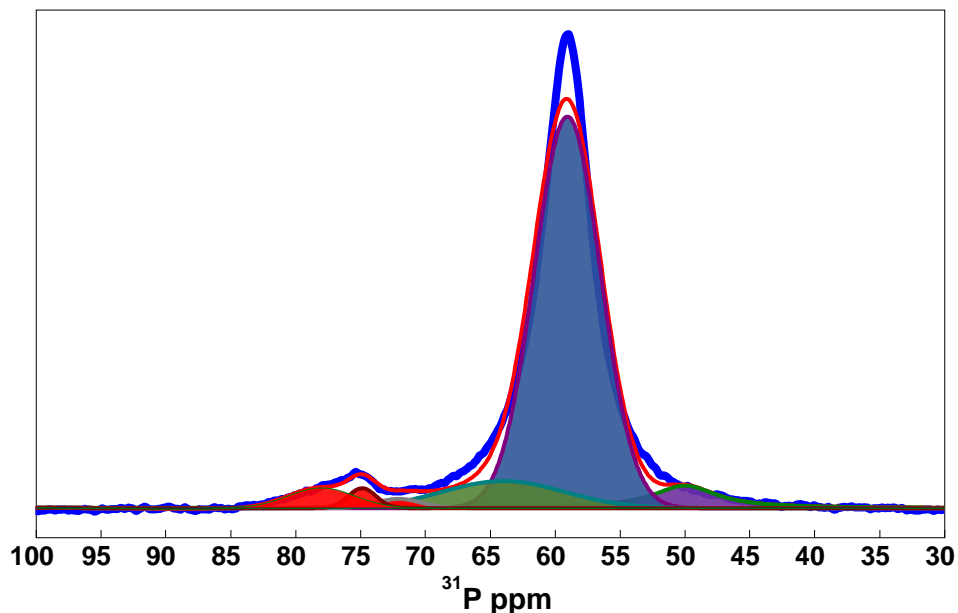
Figure 55: ^{31}P 15 kHz MAS NMR spectrum of 44.4 mg CBV760 zeolite impregnated with 3.0 mg TEPO, treated at 210 °C during 2 h, hydrated for 50 h. An important decrease in intensity of the peaks corresponding to the different acid sites, but increase of the ones corresponding to physisorbed TEPO and silanol site. The hydration effects are quite Important, due to the high mesoporosity and good accessibility of the sites by water.

Table 29. ^{31}P 15 kHz MAS NMR chemical shift (δ), peak area and environment of the different peaks shown in **Figure 55** (sample: 3.0 mg TEPO with 44.0 mg of CBV760, treated at 210 °C during 2 h, hydrated for 50 h at atmosphere).

$\delta\ ^{31}P$, ppm	Peak width, ppm	At. % peak area	Site type
50	6	6	Crystalline
59.1	6	77	Physisorbed
64	11	10	Silanol
72	4	1	Brønsted
74.9	2.5	2	Brønsted
78	6	4	Brønsted
84	4.5	<1	Brønsted
89	7	<1	Lewis

* The type of line shape used is pure Lorentzaian for the crystalline fitting line an pure Gaussian for the others

Table 30. Calculation of the concentration of the different TEPO environments based on ^{31}P 15 kHz MAS NMR shown in **Figure 54** and **Table 28** (sample: 3.0 mg TEPO with 44.4 mg CBV760, treated at 210 °C during 2 h). A low Brønsted acid site concentration is measured due to strong dealumination/ low Si/Al ratio of the CBV760

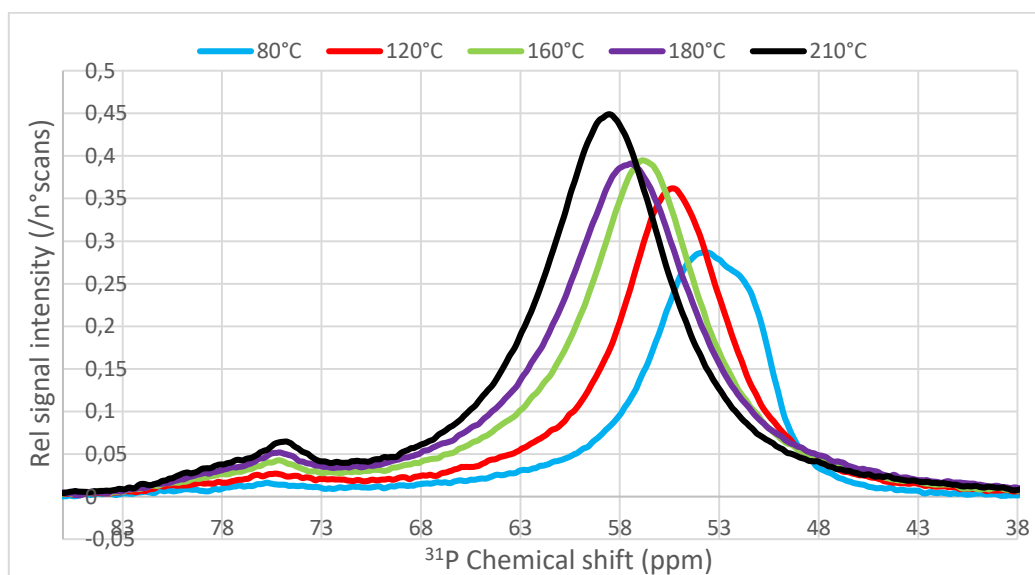|		Crystalline	228 $\mu mol/g_{zeolite}$
C_P	0.0015 $mol/g_{zeolite}$	Physisorbed	232 $\mu mol/g_{zeolite}$
		Silanol	166 $\mu mol/g_{zeolite}$
		Brønsted	45 $\mu mol/g_{zeolite}$
		Lewis	4 $\mu mol/g_{zeolite}$

Figure 56: Evolution of the measured Brønsted acid site concentration by ^{31}P 15 kHz MAS NMR for a sample of 44.4 mg CBV760 impregnated with 3.0 mg TEPO as function of the treatment temperature of the sample (treatment duration 2 h at each temperature). A steady increase of the detected Brønsted acid site concentration can be observed, which can be explained by faster diffusion and reaction with the acid sites at higher temperatures. The same effect can be seen for the silanol peak around 62 ppm. The physisorbed peak moves from about 54 ppm to 58 ppm with higher treatment temperatures and decreases in intensity.
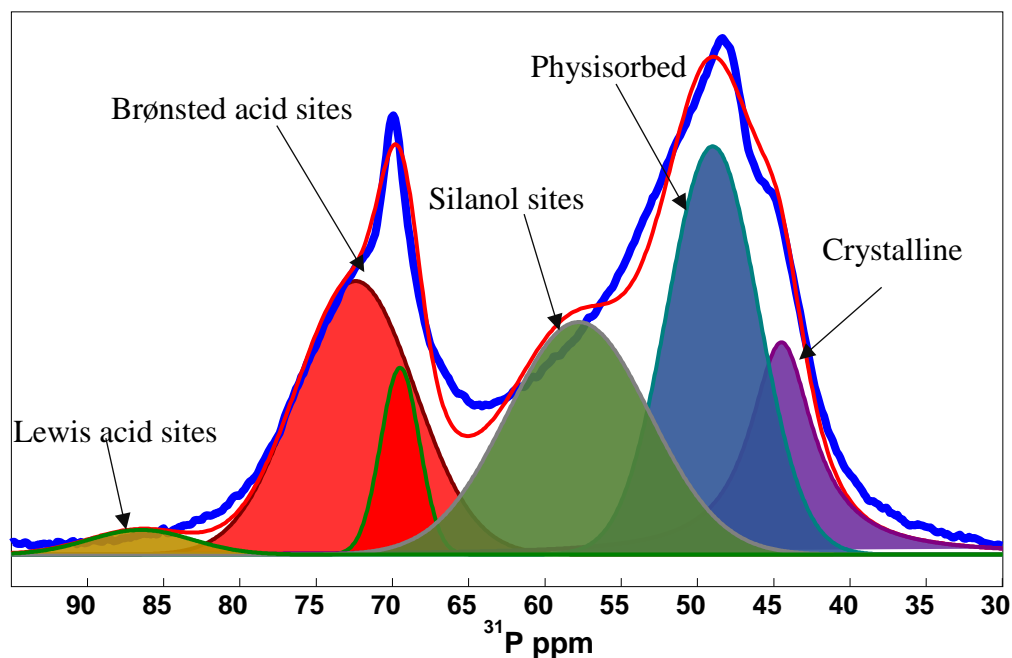
9.3.6 CBV720 analysis by TBPO

Figure 57: ^{31}P 15 kHz MAS NMR spectrum of 36.2 mg CBV720 zeolite impregnated with 9.7 mg TBPO, treated at 210 °C during 2 h. Similar peak positions and widths as for CBV760 and CBV712: Six peaks can be distinguished, 2 of them correspond to TBPO bond to Brønsted acid sides of different strength (higher chemical shift = stronger site) and one each to TBPO bond to Lewis acid sites, TBPO bond to silanol groups, physisorbed and bulk crystalline TEPO.

Table 31. ^{31}P 15 kHz MAS NMR chemical shift (δ), peak area and environment of the different peaks shown in **Figure 57** (sample: 9.7 mg TBPO with 36.2 mg of CBV720, treated at 210 °C during 2 h)

$\delta\ ^{31}P$, ppm	Peak width, ppm	At. % peak area	Site type
44.5	5	15	Crystalline
49	7	28	Physisorbed
57.8	11	25	Silanol
69.5	3	5	Brønsted
72.4	9.1	25	Brønsted
86.5	8	2	Lewis

* The type of line shape used is pure Lorentzaian for the crystalline fitting line an pure Gaussian for the others
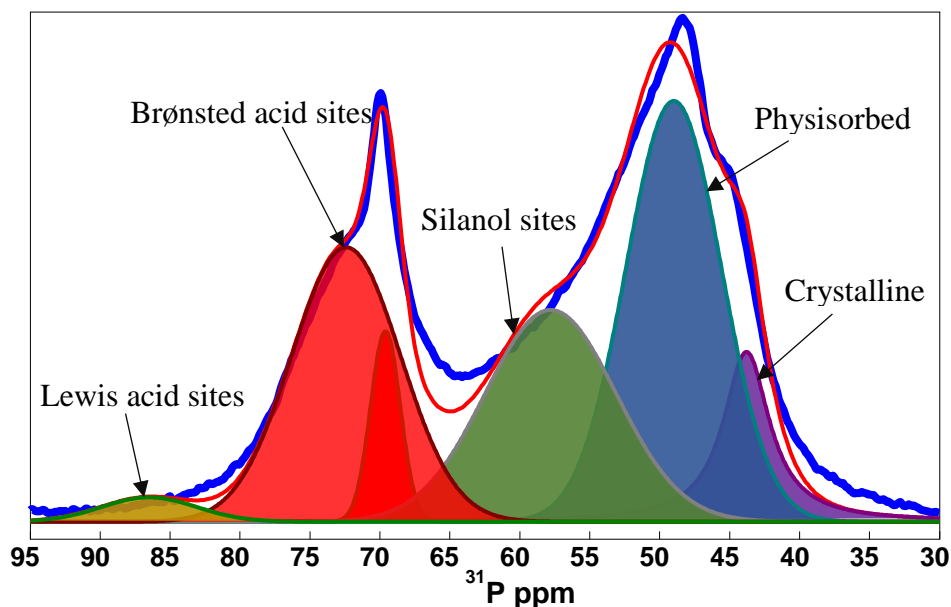
Figure 58: ^{31}P 15 kHz MAS NMR spectrum of 36.2 mg CBV720 zeolite impregnated with 9.7 mg TBPO, treated at 210 °C during 2 h, hydrated for 100 h at atmosphere. Only minor changes can be observed between the hydrated and the non-hydrated sample. The only significant difference is the increase of the physisorbed peak at the expense of the crystalline one.

Table 32. ^{31}P 15 kHz MAS NMR chemical shift (δ), peak area and environment of the different peaks shown in **Figure 58** (sample: 9.7 mg TBPO with 36.2 mg of CBV720, treated at 210 °C during 2 h, hydrated for 100 h at atmosphere)

$\delta\ ^{31}P$, ppm	Peak width, ppm	At. % peak area	Site type
43.8	4	10	Crystalline
49	8	34	Physisorbed
57.8	11	24	Silanol
69.6	2.5	5	Brønsted
72.4	9.1	25	Brønsted
86.5	8	2	Lewis

* The type of line shape used is pure Lorentzaian for the crystalline fitting line an pure Gaussian for the others

Table 33. Calculation of the concentration of the different TBPO environments by equation (19), based on ^{31}P 15 kHz MAS NMR shown in **Figure 57** and **Table 31** (sample: 9.7 mg TBPO with 36.2 mg CBV720, treated at 210 °C during 2 h). Despite the big size of the TBPO probe, a quite high Brønsted acid site concentration is observed, due to the strong basicity of TBPO.

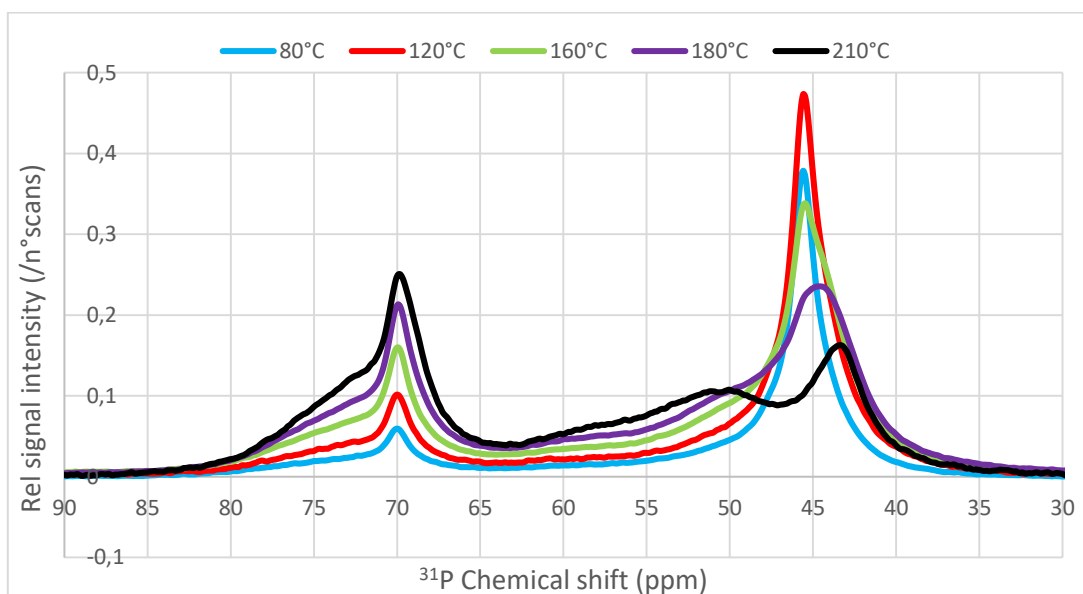|		Crystalline	$182\ \mu mol/g_{zeolite}$
		Physisorbed	$344\ \mu mol/g_{zeolite}$
C_P	$0.0012\ mol/g_{zeolite}$	Silanol	$308\ \mu mol/g_{zeolite}$
		Brønsted	$369\ \mu mol/g_{zeolite}$
		Lewis	$24\ \mu mol/g_{zeolite}$

Figure 59: Evolution of the measured Brønsted acid site concentration by ^{31}P 15 kHz MAS NMR for a sample of 36.5 mg CBV720 impregnated with 7.9 mg TBPO as function of the treatment temperature of the sample (treatment duration 2 h at each temperature). A steady growth of the detected Brønsted acid site concentration can be observed, which can be explained by faster diffusion and reaction with the acid sites at higher temperatures. Also, the intensity of the silanol peak around 58 ppm increases slightly. The crystalline peak moves downwards and decreases in intensity, at the expense of the physisorbed one, which becomes slightly more important.
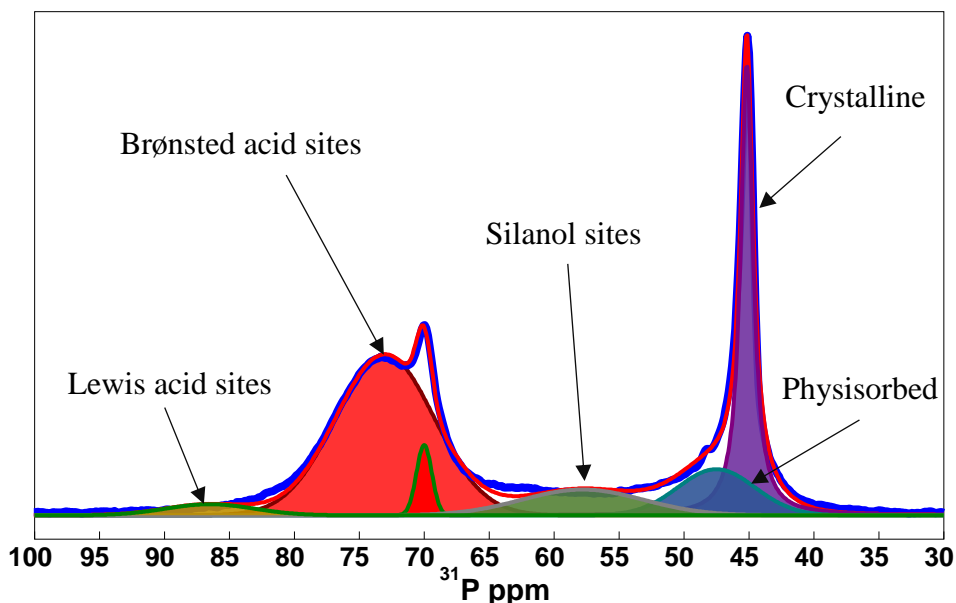
9.3.7 CBV712 analysis by TBPO

Figure 60: ^{31}P 15 kHz MAS NMR spectrum of 40.4 mg CBV712 zeolite impregnated with 10.2 mg TBPO, treated at 210 °C during 2 h. Similar peak positions and widths as for CBV760 and CBV720: Six peaks can be distinguished, 2 of them correspond to TBPO bond to Brønsted acid sides of different strength (higher chemical shift = stronger site) and one each to TBPO bond to Lewis acid sites, TBPO bond to silanol groups, physisorbed and bulk crystalline TEPO.

Table 34. ^{31}P 15 kHz MAS NMR chemical shift (δ), peak area and environment of the different peaks shown in **Figure 60** (sample: 10.2 mg TBPO with 40.4 mg of CBV712, treated at 210 °C during 2 h)

δ ^{31}P, ppm	Peak width, ppm	At. % peak area	Site type
45.1	1.2	26	Crystalline
47.5	7	11	Physisorbed
57.8	11	9	Silanol
70	1.4	3	Brønsted
73	8.9	48	Brønsted
86.5	8	3	Lewis

* The type of line shape used is pure Lorentzaian for the crystalline fitting line an pure Gaussian for the others
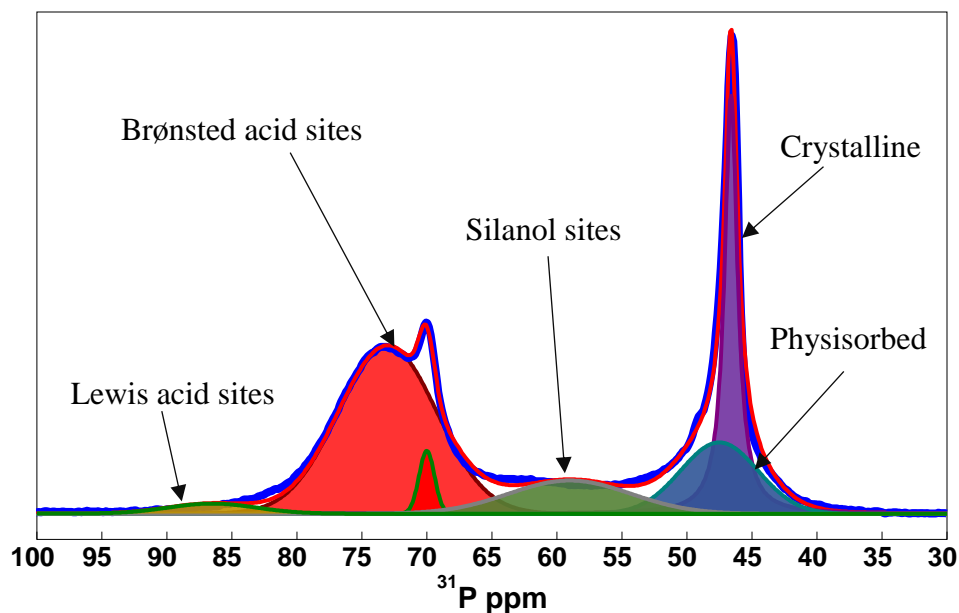
Figure 61: ^{31}P 15 kHz MAS NMR spectrum of 40.4 mg CBV712 zeolite impregnated with 10.2 mg TBPO, treated at 210 °C during 2 h, hydrated for 78 h at atmosphere. No significant changes can be observed between the hydrated and the non-hydrated sample.

Table 35. ^{31}P 15 kHz MAS NMR chemical shift (δ), peak area and environment of the different peaks shown in **Figure 61** (sample: 10.2 mg TBPO with 40.4 mg of CBV712, treated at 210 °C during 2 h, hydrated for 78 h at atmosphere)

$\delta\ ^{31}P$, ppm	Peak width, ppm	At. % peak area	Site type
46.6	1.2	23	Crystalline
47.5	7	15	Physisorbed
59	11	11	Silanol
70	1.4	3	Brønsted
73	8.9	46	Brønsted
86.5	8	2	Lewis

* The type of line shape used is pure Lorentzaian for the crystalline fitting line an pure Gaussian for the others

Table 36. Calculation of the concentration of the different TBPO environments based on ^{31}P 15 kHz MAS NMR shown in **Figure 60** and **Table 34** (sample: 10.2 mg TBPO with 40.4 mg CBV712, treated at 210 °C during 2 h). A relatively low Brønsted acid site concentration is measured, despite the weak dealumination/ high Si/Al ratio of the CBV712. This may can be explained by the low mesoporosity of the zeolite, which gives less space for diffusion and reaction of the bulky TBPO.

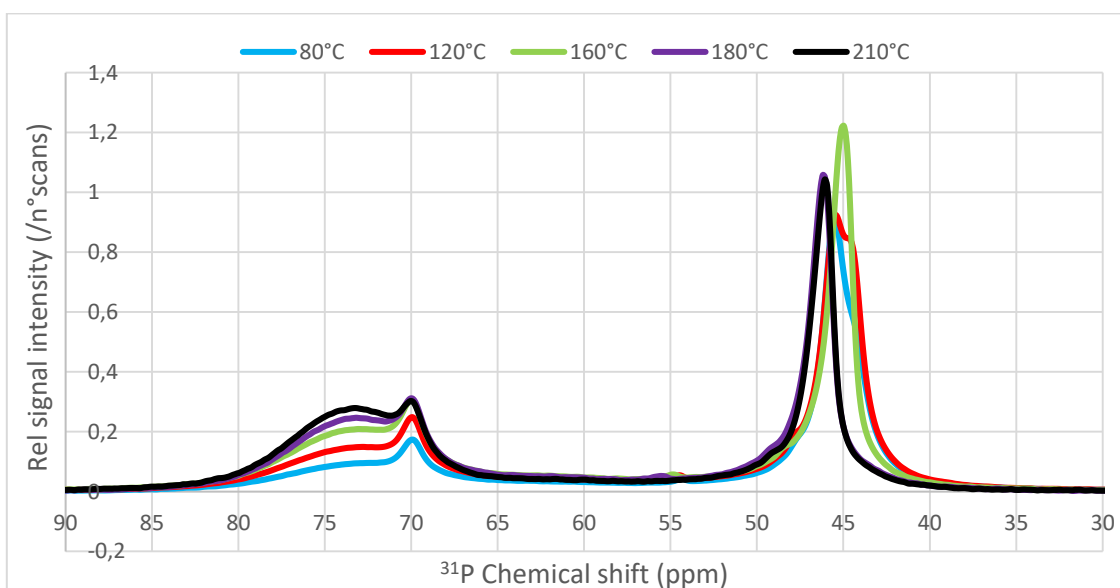|		Crystalline	296 $\mu mol/g_{zeolite}$
		Physisorbed	125 $\mu mol/g_{zeolite}$
C_P	0.0015 $mol/g_{zeolite}$	Silanol	110 $\mu mol/g_{zeolite}$
		Brønsted	593 $\mu mol/g_{zeolite}$
		Lewis	34 $\mu mol/g_{zeolite}$

Figure 62: Evolution of the measured Brønsted acid site concentration by ^{31}P 15 kHz MAS NMR for a sample of 37.7 mg CBV712 impregnated with 12.0 mg TBPO as function of the treatment temperature of the sample (treatment duration 2 h at each temperature). A steady raise of the detected Brønsted acid site concentration at the expense of the crystalline peak can be observed, which can be explained by faster diffusion and reaction with the acid sites at higher temperatures. The detected silanol concentration remains almost constant and only a very small physisorbed peak is observed.
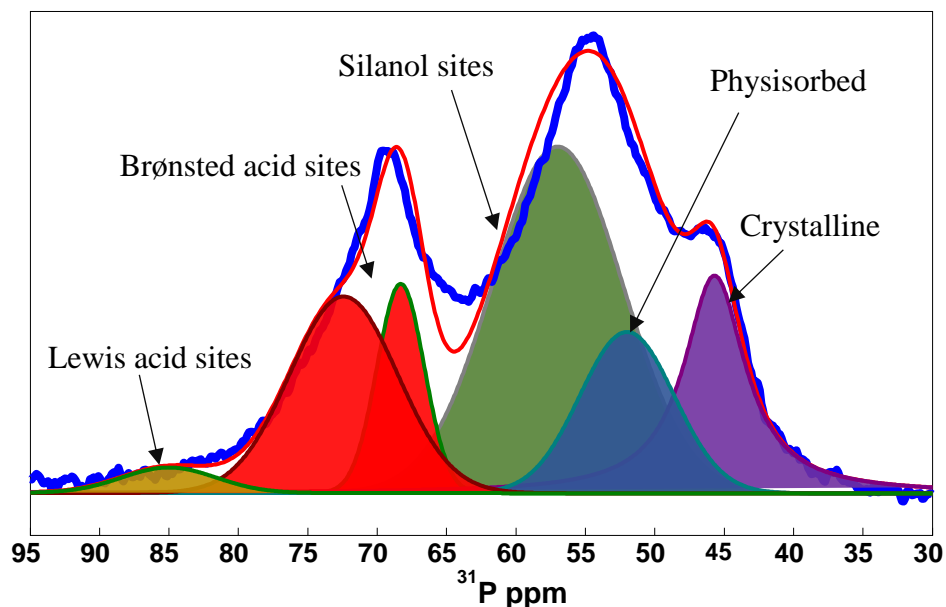
9.3.8 CBV760 analysis by TBPO

Figure 63: ^{31}P 15 kHz MAS NMR spectrum of 37.0 mg CBV760 zeolite impregnated with 6.9 mg TBPO, treated at 210 °C during 2 h, hydrated for 55 h at atmosphere. The observations are quite different to the previous cases. The detected acid site quantity decreases due to the good accessibility of the sites by the water. The silanol peak gains remarkably in intensity at the expense of the physisorbed one.

Table 37. ^{31}P 15 kHz MAS NMR chemical shift (δ), peak area and environment of the different peaks shown in **Figure 63** (sample: 6.9 mg TBPO with 37.0 mg of CBV760, treated at 210 °C during 2 h, hydrated for 55 h at atmosphere)

δ ^{31}P, ppm	Peak width, ppm	At. % peak area	Site type
45.7	5.3	18	Crystalline
52	8	13	Physisorbed
57	11	40	Silanol
68.3	4	9	Brønsted
72.4	9.1	19	Brønsted
85	8	2	Lewis

* The type of line shape used is pure Lorentzaian for the crystalline fitting line an pure Gaussian for the others

Table 38. Calculation of the concentration of the different TBPO environments based on ^{31}P 15 kHz MAS NMR shown in **Figure 38** and in **Table 18** (sample: 6.9 mg TBPO with 37.0 mg CBV760, treated at 210 °C during 2 h). A quite high Brønsted acid site concentration is measured for such a strongly dealuminated zeolite. This can be explained by the strong basicity of the probe and the

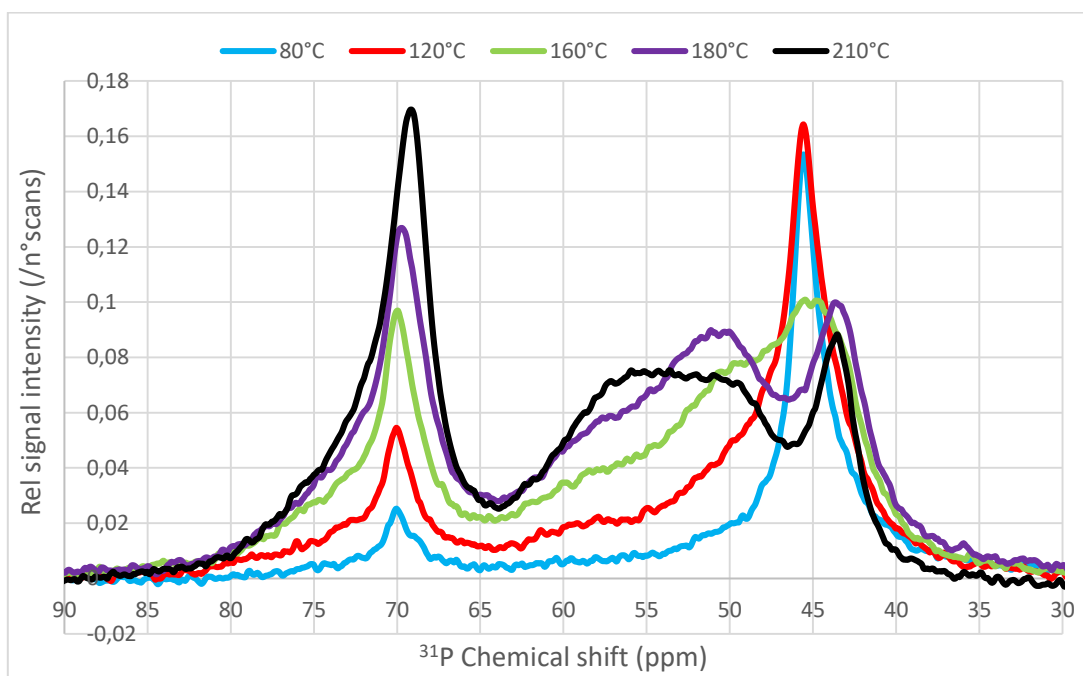|		Crystalline	$155\ \mu mol/g_{zeolite}$
		Physisorbed	$171\ \mu mol/g_{zeolite}$
C_P	$0.0015\ mol/g_{zeolite}$	Silanol	$231\ \mu mol/g_{zeolite}$
		Brønsted	$280\ \mu mol/g_{zeolite}$
		Lewis	$18\ \mu mol/g_{zeolite}$

Figure 64: Evolution of the measured Brønsted acid site concentration by ^{31}P 15 kHz MAS NMR for a sample of 37.7 mg CBV760 impregnated with 6.2 mg TBPO as function of the treatment temperature of the sample (treatment duration 2 h at each temperature). The peaks corresponding to Brønsted acid sites and silanol terminal groups increase steadily with the treatment temperature, due to the faster diffusion or increased reaction with the acid sites at higher temperatures. Also, the physisorbed peak around 49 ppm gains slightly in intensity, all at the expense of the quantity of crystalline TBPO.